2023

Steady-State Regulation of Secretory Cargo Export and ER Homeostasis by Inositol Trisphosphate Receptors and Penta-EF-Hand Proteins

Aaron J. Held
University of Montana, Missoula

STEADY-STATE REGULATION OF SECRETORY CARGO EXPORT AND ER HOMEOSTASIS BY INOSITOL TRISPHOSPHATE RECEPTORS AND PENTA-EF-HAND PROTEINS

Aaron Jeffrey Held

Bachelor of Science, University of Montana, Missoula, MT, 2017
Bachelor of Arts, University of Montana, Missoula, MT, 2017

Dissertation

presented in partial fulfillment of the requirements
for the degree of

Doctor of Philosophy
in Cellular, Molecular, and Microbial Biology

The University of Montana
Missoula, MT

Official Graduation Date August 2023

Approved by:

Ashby Kinch,
Graduate School Dean

Jesse Hay
Division of Biological Sciences

Mark Grimes
Division of Biological Sciences

Ekaterina Voronina
Division of Biological Sciences

Richard Bridges
Division of Biological Sciences

Scott Wetzel
Division of Biological Sciences

John Quindry
Integrative Physiology and Athletic Training

TABLE OF CONTENTS

Aaron J. Held, Ph.D., Spring 2023 *Cellular, Molecular, and Microbial Biology*

Steady-State Regulation of Secretory Cargo Export and ER Homeostasis by Inositol Trisphosphate Receptors and Penta-EF-Hand Proteins

Chairperson: Jesse Hay

ABSTRACT

Constant protein degradation and turnover necessitates constitutive secretion that delivers the correct mix of nascent proteins to their appropriate subcellular destinations. Cells thus exhibit steady-state secretion and the additional ability to adjust secretory flux, though we lack a clear understanding of this critical process. During secretion, the COPII coat is responsible for providing a balance of actively and passively selected ER cargos to enter the secretory pathway. Furthermore, Ca^{2+}-binding proteins have been implicated in regulating this process in response to Ca^{2+} signals. In **Chapter 1**, we review the secretory pathway and vesicular trafficking, with a focus on ER-to-Golgi transport. We then examine the known roles of Ca^{2+} in ER proteostasis and trafficking with a particular emphasis on the Inositol 1,4,5-Trisphosphate Receptors (IP3Rs) and the Penta-EF-Hand (PEF) proteins ALG-2 and Peflin. **Chapter 2** describes experimental procedures while **Chapter 3** examines the roles of Ca^{2+} and the PEF proteins in determining steady-state trafficking flux. We find that in Normal Rat Kidney (NRK) epithelial cells, depletion of the IP3R-3 isoform augments Ca^{2+} signaling, including spontaneous Ca^{2+} oscillations. This shift in Ca^{2+} signaling drove an 'activated' ALG-2 phenotype in which ER-to-Golgi transport of the model cargo VSV-G is accelerated. Additionally, we find that ALG-2 activation augments COPII cargo sorting stringency, concentrating COPII client cargo at ER Exit Sites (ERES) at the expense of bulk flow cargos. These findings suggest that the steady-state transport and cargo sorting capacity of a given cell may be influenced by its spontaneous Ca^{2+} signaling characteristics via ALG-2 regulation of COPII function. **Chapter 4** details a set of preliminary experiments exploring the role that IP3R-3 and Mitochondria-ER Contact Sites (MERCs or MAMs) may play in the maintenance of ER proteostasis. Depletion of IP3R-1 from NRK cells–a condition which favors function of the IP3R-3 channel–causes partial depletion of ER Ca^{2+}, yet cells are protected from ER stress. This is of interest since Ca^{2+} is traditionally thought of as a rate-limiting component for protein folding in the ER. Since IP3R-3 is known to be the IP3R at MAMs, this data highlights the protective effects of MAMs on ER proteostasis.

ACKNOWLEDGEMENTS

I would like to say thank you to:

Jesse Hay – for your supportive mentorship and guidance. You inspired my passion for research in this field and molded me into the scientist I am today. You provide the example that I aspire to, and I cannot thank you enough for your belief in me all these years.

My Committee Members – for your time and energy challenging me and encouraging my development as a student and as a scientist.

John Sargeant and Lauren Foltz – for sharing your lives and showing me the ropes. We'll strike it big with one of our business ideas one of these days. If not, we'll just start our farm.

Jacob Lapka and Nagashree Avabhrath – for the friendship and laughter. Our wasted time was always time well spent.

Danette Seiler, Sam Galindo, Alaa Shaheen, Tucker Costain, and Colin Bingham – for your companionship and teamwork in the lab. It was a blast working with each of you.

Mariah Rayl, Caleb Schwartzkopf, Chris Trolinder, Michelle Nemetchek, Valery Román-Cruz, Jessica Bailey, Adam Drobish, Emily Gagliano, and all other past and present MBS graduate students – for your companionship on the rollercoaster that is graduate school.

Past and present DBS faculty and staff – for guiding me through the hoops of graduate school and putting up with my constant questions.

Jaming Chang, Eden Racket, Andy Bustos, and Levi Hall – I couldn't have asked for better lifelong friends.

The Finch, Fichtner, Edelstein, and Gardner families – for being the most loving and supporting in-laws a man could ask for.

Karlie Peltomaa, Wesley Rigler, and Lacie Sramek – for your unwavering support of me and my family.

My parents and siblings – for your unconditional love and support. You encouraged me to pursue my passions, supported me through the difficult times, and inspired me when I lost my spark. I can only hope to build a family as loving as the one I grew up with.

Bentley and Layla – for your unconditional love and licks.

Eleanora Rae Held – My daughter, my reason, my meaning. Everything I do in this life; I do for you.

Kelcie Peltomaa – The love of my life and my center of gravity. You make me a better man and I couldn't have done any of this without you.

ABBREVIATIONS	
Acronym	**Description**
AXER	ATP/ADP exchanger in ER membrane
Ca^{2+}	Calcium
ER	Endoplasmic reticulum
ERES	ER exits site
ERGIC	ER Golgi intermediate compartment
GAP	GTPase Activating Protein
GEF	Guanine Nucleotide Exchange Factor
IBC	IP3 binding core
ICW	Intercellular Ca^{2+} waves
IP3	Inositol 1,4,5-trisphosphate
MAM	Mitochondrial associated ER membrane
NRK	Normal rat kidney cells
PEF	Penta-EF hand
PTM	Post-translational modification
ROI	Region of interest
SD	Suppressor domain
SERCA	Sarco/endoplasmic reticulum Ca^{2+} ATPase
SOCE	Store operated Ca^{2+} entry
UPR	Unfolded protein response

DRUGS/AGONISTS USED	
Agonist/Drug	**Description**
Bradykinin (BDKN)	Inflammation related agonist for B1 & B2 GPCRs
EGTA	Cell permeant chelator, highly selective for Ca^{2+}
Ionomycin	Divalent Ca^{2+} ionophore
Thapsigargin (Tg)	Non-competitive SERCA inhibitor
AP21998 (D/D solubilizer)	Conditional aggregation domain inhibitor
4-PBA	Anionic carboxylic acid, binds Sec24 B-site

LIST OF FIGURES

CHAPTER 1:

SECRETORY TRAFFICKING AND PROTEIN HOMEOSTASIS

1.1 INTRODUCTION

Eukaryotic cells are subdivided into numerous functionally distinct membrane bound organelles. These organelles create enclosed aqueous spaces separate from the cytosol, allowing for specialization and optimization for key biochemical reactions. Each of these organelles contains its own specific set of proteins conferring its characteristic structural and functional properties. The human genome encodes for tens of thousands of different proteins and any given cell could have tens of millions of protein molecules present at a given time; however, without proper localization these proteins can be completely non-functional or even detrimental for overall cell physiology. Thus, each newly synthesized protein must be correctly trafficked to its specific subcellular destination.

More than one-fifth of the proteins in the mammalian proteome begin their journey in the endoplasmic reticulum and come to eventually reside in the membrane or lumen of the various endomembrane organelles, the cell surface, or secreted into the extracellular space (Kanapin et al., 2003). The coordinated trafficking of proteins through this complex array of endomembrane organelles is referred to as the biosynthetic secretory pathway. In multicellular organisms that rely on intercellular communication and cooperation, the biosynthetic secretory pathway is essential for overall physiology because the majority of hormones, peptidases, receptors/channels, extracellular matrix components, coagulation factors, and transporters are constituents of this system (Feizi et al., 2017). Given its general importance to overall cell physiology, it is unsurprising that defects in the secretory pathway can elicit a diverse spectrum of diseases (Yarwood et al., 2020).

1.1.1 The Endomembrane System

The endomembrane system is a series of membrane enclosed, topologically contiguous organelles that serve various functions in the biosynthesis, maturation, modification, and recycling of secretory and transmembrane proteins. To accomplish their specific tasks, each of these organelles retain a distinct set of resident proteins that perform the biochemical reactions required in that luminal space.

All proteins that exist in this system begin their journey by their synthesis into the Endoplasmic Reticulum (ER). The ER is the largest membrane bound organelle in most cells, comprising close to half of all cell membrane structure and representing close to 10% of the total cell volume in its lumen. It can be structurally and functionally divided into two portions, the rough ER and the smooth ER. The rough ER is covered by ribosomes, and is the site of protein biosynthesis and trafficking, while the smooth ER is the major site for lipid synthesis within the cell. The ER lumen provides a protected, oxidizing environment rich with protein chaperones to facilitate proper folding and maturation of nascent proteins. It also serves as the major intracellular calcium (Ca^{2+}) store, allowing for purposeful Ca^{2+} release as a universal signaling event. Upon completing all maturation steps, secretory proteins are trafficked from the ER to the cis-Golgi, typically via the ER-Golgi Intermediate Compartment (ERGIC). The ERGIC, also referred to as Vesicular-Tubular Clusters (VTCs), operates as an additional protein sorting station in ER-to-Golgi trafficking. Because the ER is the major quality control point for secretory proteins, the decision to exit the ER and travel to the Golgi is highly regulated and represents the rate limiting step in the overall secretory pathway. This functionally important trafficking step will be the main focus of this work.

Upon arrival in the Golgi, proteins undergo various post-translational modifications (PTMs), most notably glycosylation, by different enzymes that each localize within a narrow range of separate Golgi cisternae. The mechanism of cargo movement through the Golgi remains controversial, but the current consensus is that Golgi cisterna move 'en bloc' and resident proteins are maintained at a given location by retrograde transport. Cargo proteins within the moving cisterna thus encounter distinct sets of Golgi resident proteins as they arrive by retrograde transport (Pantazopoulou & Glick, 2019). Proteins then exit at the trans-Golgi network (TGN) towards their ultimate destination in the endolysosomal system or on the cell surface.

The endolysosomal system integrates with the plasma membrane to control protein turnover at the cell surface. This system involves the uptake of cell surface proteins or other extracellular cargo via endocytosis. Primary endocytic vesicles then fuse to form early endosomes which serve as the major sorting stations of the endocytic pathway. Cargo within

the early endosomes can be recycled back to the cell surface or diverted in a retrograde fashion back to the Golgi. Alternatively, endosomal cargo destined for destruction will remain in maturing endosomes, known as late endosomes, which fuse with the lysosome where various lysosomal enzymes degrade the luminal content.

Protein transport between each of these endomembrane organelles is mediated by vesicular trafficking. The vesicular transport hypothesis holds that vesicle budding from a donor compartment with selective protein sorting incorporates cargo while retaining resident proteins. Vesicles are then targeted to an acceptor compartment where they unload their cargo upon vesicle fusion (Bonifacino & Glick, 2004). Vesicular trafficking occurs via a series of general steps whose details become more specific depending on the transport step examined. These general steps include: (1) cargo selection and segregation from resident proteins; (2) vesicle formation, which includes encapsulation of transport cargo, membrane deformation, and membrane scission mediated by a protein 'coat'; (3) physical movement of the vesicle towards the target compartment; (4) extended membrane tethering by protein complexes in conjunction with Rab GTPases; and (5) docking and fusion of vesicular membrane with the target compartment mediated by soluble N-ethylmaleimide-sensitive-factor attachment protein receptor (SNARE) protein complexes (Yarwood et al., 2020).

1.2 PROTEIN COATS

As discussed above, the initial steps in vesicular transport including cargo accumulation, membrane deformation, and membrane scission are mediated by protein coats. In this context, a protein ‘coat’ refers to supramolecular protein complexes encapsulating the membrane of forming membrane buds and vesicles. In the last fifty years, a number of different protein coats have been characterized, each corresponding to their own distinct transport processes and mediated by the supramolecular assembly of their own specific set of cytosolic proteins (Figure 1). Coats are often organized into a membrane-proximal "adaptor" layer and a membrane-distal "scaffold" layer, though this is not always the case. Coats often recognize specific cell membranes via their particular lipid composition and small GTPases of the Sar/Arf or Rab

families are often responsible for the recruitment of a coat to a given membrane (Dell'Angelica & Bonifacino, 2019).

1.2.1 Clathrin and Adaptor Protein (AP)-Based Coats

The first description of a protein coat came from early transmission electron microscopy (EM) images of *Aedes aegypti* L. oocyte membrane invaginations (Roth & Porter, 1964). Later studies revealed that these early coats contained the clathrin protein along with a series of adaptor protein complexes that would come to be called AP-1 and AP-2 (Pearse, 1975). Conventionally thought of as the prototypical protein coat, clathrin is not itself a coat, *per se*. Rather, clathrin is a scaffolding component of a number of different coats that include adaptor protein complexes AP-1, AP-2, and AP-3. These adaptor protein complexes each have characteristic preferences for membrane lipid composition, ARF-family GTPases, and cargo proteins, thus specifying the function of clathrin recruitment at different subcellular locations (Figure 1) (Dell'Angelica & Bonifacino, 2019; Hirst & Robinson, 1998). The clathrin outer layer consists of three-legged "triskelion" structures composed of three clathrin heavy chains and three clathrin light chains. These triskelion structures then assemble into a polyhedral lattice covering the APs to form clathrin coated vesicles around 60-100 nm in diameter (Bonifacino & Lippincott-Schwartz, 2003; Fotin et al., 2004).

AP-1 is the clathrin adaptor protein complex associated with trafficking between the TGN and the early endosome (Bonifacino & Rojas, 2006). AP-1 is recruited to membranes via interactions with PI(4)P and GTP-bound Arf1 (Ren et al., 2013). AP-2 is the clathrin adaptor associated with the classic clathrin-mediated endocytosis (CME). AP-2 is recruited to the cytosolic leaflet of the plasma membrane by activated Arf5 (Moravec et al., 2012) and through its interaction with PI(4,5)P2 (Collins et al., 2002). AP-3 is the clathrin adaptor protein complex associated with buds on endosomal tubules often involved in transport to the lysosome (Peden et al., 2004). AP-3 is recruited to endosomal tubules by GTP-bound Arf1 and interactions with PI(3)P (Baust et al., 2008; Ooi et al., 1998). Interestingly, AP-3 has also been shown to function independent of clathrin (Zlatic et al., 2013), highlighting the functionally independent roles that the heterotetrameric AP complex family can exhibit. This AP family functional independence is

exemplified by the AP-4 and AP-5 complexes that operate without clathrin and mediate transport from the TGN to pre-autophagosomal structures and from the late endosome to the TGN, respectively (Figure 1) (Dell'Angelica & Bonifacino, 2019).

1.2.2 COPI

The COPI coat is conventionally understood to operate in intra-Golgi transport and retrograde transport from the Golgi to the ER (Figure 1) (Beck et al., 2009). The major function of these trafficking steps is to retain ER and Golgi resident proteins in their appropriate compartments as constitutive anterograde trafficking and Golgi cisternal maturation occur (Arakel & Schwappach, 2018). However, COPI has also been observed coating vesicles traveling in the anterograde direction from the ERGIC to the Golgi (Presley et al., 2002) and may play a role in protein sorting at the ERGIC (Klumperman et al., 1998).

The COPI coat consists of seven subunits: α-COP, β'-COP, ε-COP, β-COP, δ-COP, γ-COP and ζ-COP. These subunits assemble into a heptamer, referred to as the coatomer, and can be dissected into cage-like (B-) and adaptor-like (F-) subcomplexes (Lowe & Kreis, 1995). In contrast to the step-wise assembly of clathrin and COPII coats, COPI is recruited to the membrane en-bloc (Arakel & Schwappach, 2018). Golgi localized guanine nucleotide exchange factors (GEFs) recruit and activate the small GTPase Arf1 which inserts into the membrane and mediates coatomer recruitment (Yu et al., 2012). Three COPI heptamers assemble into a COPI triad and these triads subsequently interact via flexible trimeric or dimeric linkages to establish the overall COPI lattice structure (Dodonova et al., 2015).

COPI cargo recognition is mediated by sorting signals present on cytoplasmic domains of retrieved proteins or their adaptor complexes. Many ER resident proteins have di-lysine KKxx and KxKxx motifs that directly contact α- or β'-COP (Ma & Goldberg, 2013) while many channels and receptors are dependent on arginine (R)-based ER retrieval signals (ϕRxR; in which ϕ represents any hydrophobic amino acid) (Zerangue et al., 1999). A number of proteins can bind COPI and serve as adaptors for luminal cargos. The most well characterized adaptor is the KDEL receptor which recognizes a distal C-terminal signal, KDEL, on many luminal ER-resident chaperones (Townsley et al., 1993)

1.2.3 COPII

The COPII coat is exclusively required for anterograde transport from the ER to the Golgi (Figure 1). COPII assembles at specific sites on ER membranes termed ER Exit Sites (ERES) (Matsuoka et al., 1998). ERES are often budding zones on distally connected ER cisternae adjacent to one another and surrounding independent ERGIC that contain COPI coat (Bannykh et al., 1996). There are three required COPII assembly subunits: Sar1 GTPase, Sec23/24 heterodimer, and Sec13/31 heterotetramer (Figure 2) (Matsuoka et al., 1998).

COPII coat assembly begins with the type II transmembrane protein Sec12 which initiates and localizes vesicle budding at ERES by functioning as the GEF for Sar1 (Matsuoka et al., 1998; J. T. Weissman et al., 2001; Zanetti et al., 2012). Sar1 GTP binding and activation causes movement of its amino-terminal amphipathic helix to expose its hydrophobic amino acids (Bi et al., 2002; Y. Rao et al., 2006) allowing for its insertion into the ER membrane. Sar1 membrane insertion then provides the initial membrane curvature that assists in subsequent COPII inner coat binding (Lee et al., 2005). Activated Sar1 recruits Sec23/Sec24 heterodimer (Matsuoka et al., 1998; Yoshihisa et al., 1993) and the Sar1-Sec23/Sec24 complex forms a 15 nm long bowtie shaped structure with a membrane-proximal concave surface that is positively charged to interact with the acidic phospholipid composition of the ERES (Bi et al., 2002). This COPII 'inner coat' is required for binding of the COPII 'outer coat' made up of Sec13/Sec31 heterotetramers (Matsuoka et al., 1998). The inner and outer coats are connected via the 'active fragment' of the Sec31 PRR loop which binds across the composite surface of the Sec23-Sar1 complex (Shibata, 2019). Sec13/Sec31 heterotetramers assemble into polyhedral cages that provide the main structural component of the COPII coat, yet exhibit the flexibility to accommodate different cargo shapes and sizes (Fath et al., 2007; Lederkremer et al., 2001; Noble et al., 2013; Stagg et al., 2006).

The inner COPII coat is responsible for accumulating protein cargo via the Sec24 subunit (E. Miller et al., 2002). Of the three characterized Sec24 binding sites (A-, B-, and C-) that are responsible for binding vesicle SNAREs and other secretory protein cargos, the B-site is the most diverse and interacts with numerous different cytoplasmic acidic cargo sorting signals

(Chatterjee et al., 2021; Mancias & Goldberg, 2008; E. A. Miller et al., 2003, 2005; Mossessova et al., 2003). Secretory cargo binding is further diversified by the four mammalian Sec24 paralogs that are differentially expressed between cell types and exhibit different cargo binding specificities (Chatterjee et al., 2021). Sec16 is a 250 kDa peripheral membrane protein that is often used to define ERES, though its localization to ERES is independent of the inner and outer COPII coats (Watson et al., 2006). At ERES, Sec16 localizes to cup-like structures that are near, but spatially distinct from, the localization of the other COPII components. Sec16 has been found to bind Sec13, Sec23, and Sec24 and has therefore been proposed to function as a scaffold for COPII assembly (Gimeno et al., 1996; Hughes et al., 2009).

After COPII coat assembly, completion of ER vesicle formation is achieved by vesicle scission from the membrane and eventual vesicle uncoating. Each of these processes is dependent on Sar1 GTPase activity (Antonny et al., 2001; Bannykh et al., 1996). Though Sar1 alone has relatively low GTPase activity, Sec23 acts as the GTPase activating protein (GAP) for Sar1. This activity is further accelerated by Sec31 binding to Sar1-Sec23, thus COPII coat assembly also triggers its eventual disassembly (Antonny et al., 2001; Yoshihisa et al., 1993).

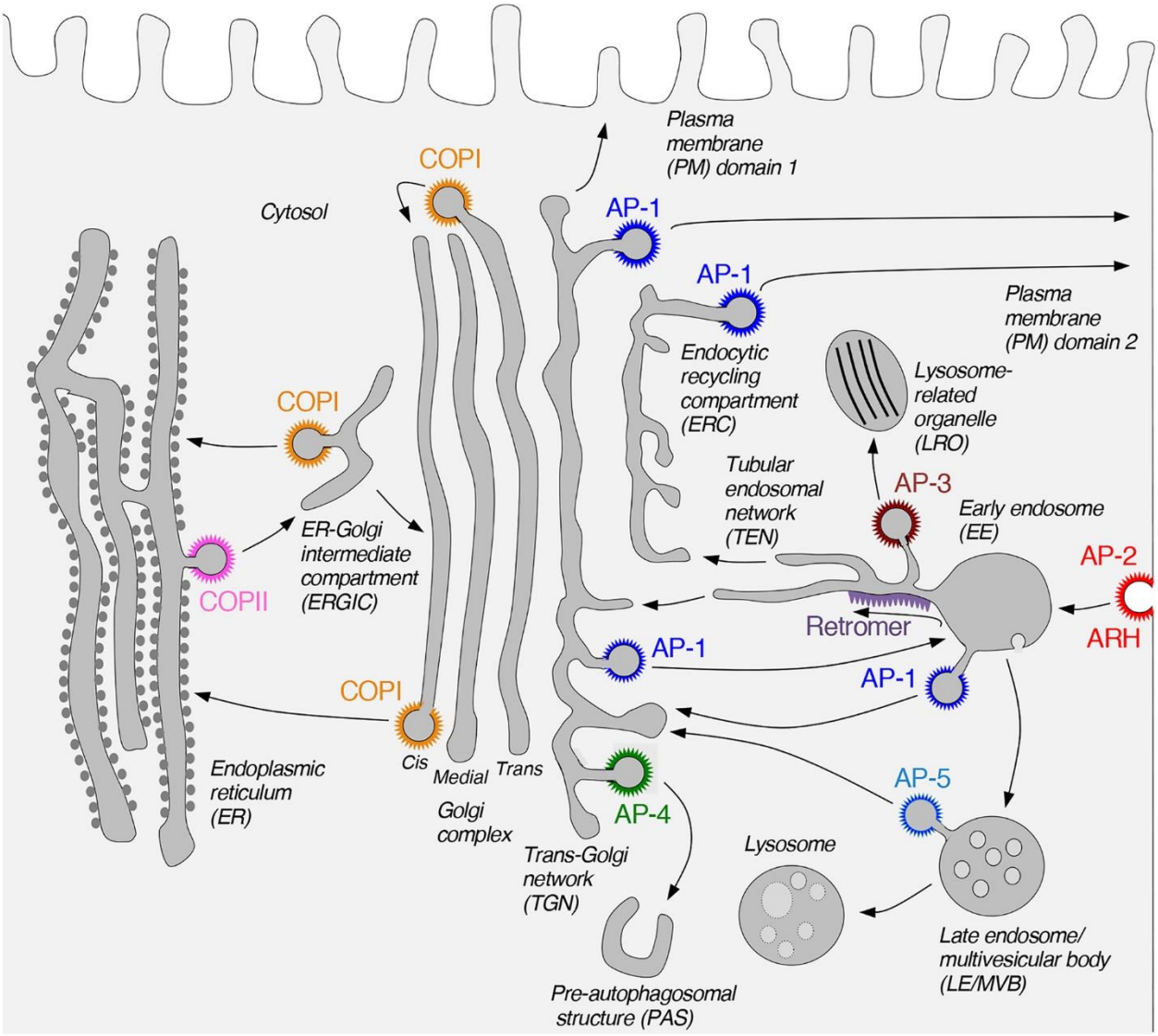

Figure 1 Protein Coats of the Endomembrane System. This diagram depicts the critical features of the secretory and endolysosomal pathways. Vesicular coat complexes and their associated trafficking steps are highlighted. Note that AP-1, AP-2, and AP-3 are Clathrin coated vesicles utilizing the indicated adaptor protein complexes.

Reproduced with permission from Figure 1, Dell'Angelica, E. C., & Bonifacino, J. S. (2019). Coatopathies: Genetic disorders of protein coats. Annual Review of Cell and Developmental Biology, 35, 131–168.

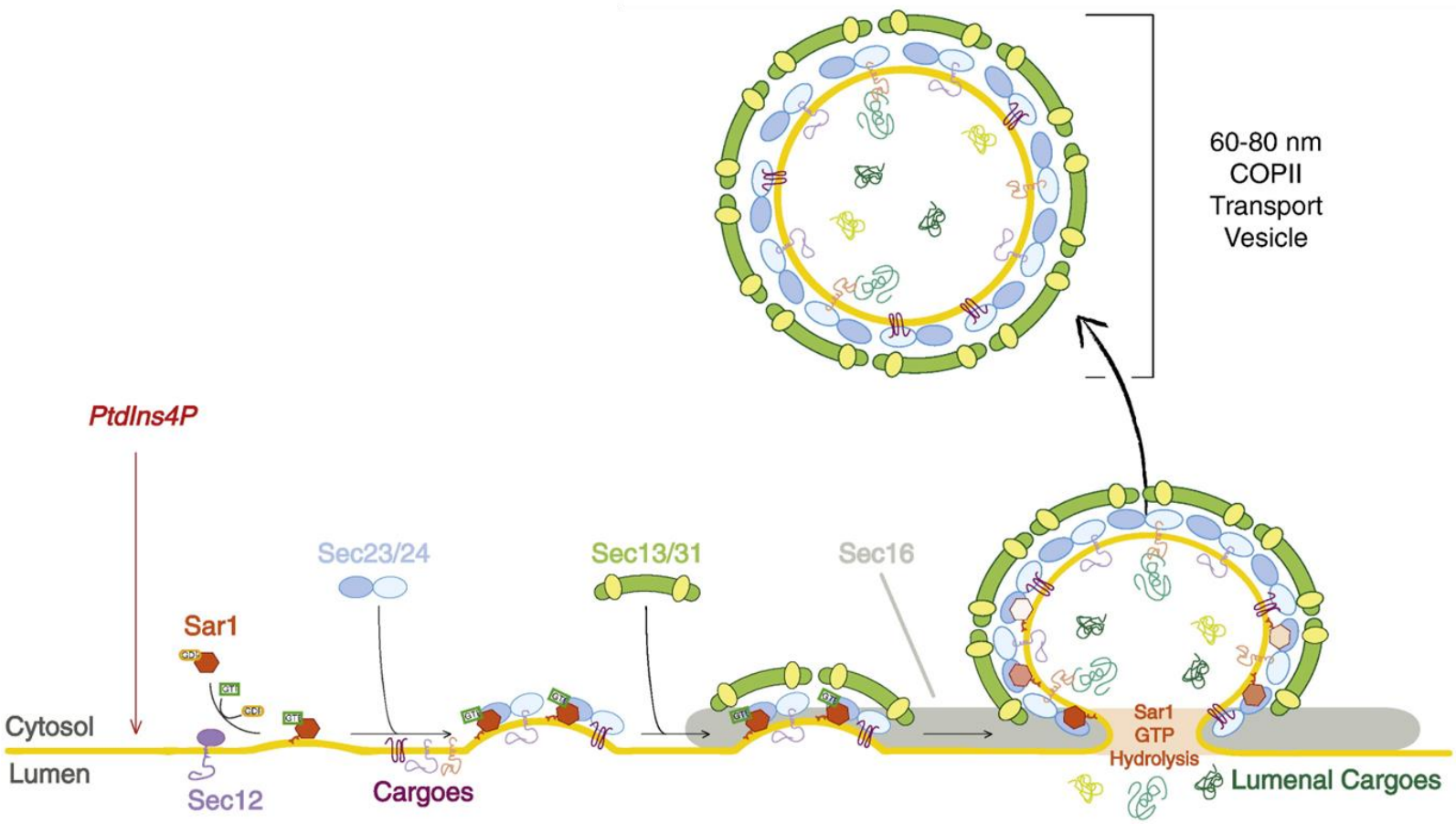

Figure 2. COPII Coat Assembly. A graphic depicting the step-wise assembly of the COPII coat as detailed in section 1.2.3.

Adapted with permission from Figure 1, D'Arcangelo, J. G., Stahmer, K. R., & Miller, E. A. (2013). Vesicle-mediated export from the ER: COPII coat function and regulation. Biochimica et Biophysica Acta - Molecular Cell Research, 1833(11), 2464–2472

1.2.4 Secretory Cargo Capture at ERES

After appropriate protein maturation is complete, secretory cargos must be loaded into nascent COPII coated vesicles. The mechanisms by which transport competent secretory cargos are selected from the milieu of proteins within the ER and accumulated from the massive ER membrane surface area to distinct ERES are still under extensive study. Additionally, little is known about how the cell adapts its ER cargo selectivity in response to environmental stimuli.

A number of strategies are utilized in overlapping fashion to establish ER export specificity (Barlowe & Helenius, 2016). Cargo capture is perhaps the most well characterized. Cargo capture entails the recognition of secretory cargos by receptors, adaptors and parts of the COPII coat. As described above, the Sec24 subunit is responsible for linking cargo proteins to the forming COPII vesicle (E. Miller et al., 2002). Sec24 cargo recruitment is mediated by direct interaction between the previously described cargo binding sites on Sec24 and specific ER export motifs on the cargo protein. The binding site variability seen across the Sec24 paralogs allows for a diversity of export motif recognition, but the cytosolic localization of Sec24 necessitates cytosolic export motifs. Therefore, ER luminal proteins are reliant on ER membrane cargo receptors and adaptors for COPII vesicle loading. ERGIC53 is an ER cargo receptor that binds all Sec24 paralogs and is required for ER export of blood clotting factors V and VIII (Moussalli et al., 1999), cathepsin C and Z (Nyfeler et al., 2006) and alpha1-antitrypsin (Nyfeler et al., 2008). GPI anchored proteins rely on p24 complexes for ER export (Bonnon et al., 2010; Fujita et al., 2011; Takida et al., 2008). This p24 reliance also makes GPI anchored proteins dependent on the Sec24c and Sec24d paralogs because p24 complexes interact with a surface groove that is occluded in Sec24a and b (Mancias & Goldberg, 2008). The cargo capture strategy helps to ensure that cargo proteins are correctly folded and oligomerized because export signals are often not available to binding by cargo receptors or adaptors until proper assembly is complete. This is particularly clear for a number of secretory cargo receptors such as ERGIC-53 that are lectins specific for extensively trimmed, high-mannose N-linked glycans on proteins that have successfully passed through the calnexin-calreticulin cycle (Appenzeller et al., 1999).

In addition to its role in the establishment of cargo specificity, cargo capture is vitally important for the accumulation of protein cargos at ERES. As discussed above, Sar1 GTPase activity controls COPII vesicle uncoating and COPII assembly accelerates Sar1 GTP hydrolysis. Thus, COPII assembly triggers its own eventual disassembly. However, cargo binding by the inner coat helps to retain COPII components on forming vesicles after Sar1 GTP hydrolysis, thus preventing premature uncoating (Forster et al., 2006; Sato & Nakano, 2005). As Sar1 undergoes multiple rounds of GTP binding and hydrolysis, it induces coat assembly and disassembly, only retaining those COPII subunits that successfully bind cargo. This selection for cargo-bound COPII subunits accumulates cargo at ERES, thus accelerating the overall rate of ER export. Interestingly, cargo accumulation at ERES can also serve as a mechanism of cargo sorting and retention (discussed below).

Bulk flow is the main strategic alternative to cargo capture. Bulk flow involves the inclusion of proteins and lipids by mass action as they diffuse into the membrane or lumen of the forming COPII vesicle. This requires no export signals or cargo receptors and this lack of active mechanism makes bulk flow transport difficult to study. The main evidence for its existence comes from the observations that many proteins lacking any direct or indirect interaction with COPII still transport very effectively (Phillipson et al., 2001). Some studies have even found bulk flow to be a faster delivery method than cargo capture (Thor et al., 2009). Theoretically, bulk flow cargo selectivity is purely based on retention mechanisms, however recent studies have also illustrated that vesicular crowding by cargo capture mechanisms can influence bulk flow secretion rates. (Gomez-Navarro, Melero, et al., 2020).

ER resident proteins and secretory proteins that are incompetent for transport must be kept from progressing through the secretory pathway. One way to do so is the aforementioned retention mechanism where proteins are actively prevented from exiting the ER by limiting their entry into ERES. While the mechanistic detail has yet to be determined, there is clear evidence for the existence of such a system. ER resident proteins such as calreticulin, BiP, PDI, ERp57, and calnexin are not detected at ERES despite their relatively uniform distribution otherwise (W. E. Balch et al., 1994; Mezzacasa & Helenius, 2002). Misfolded proteins incompetent for ER exit are also absent from ERES implying that bound chaperones may be helping to exclude them

(Mezzacasa & Helenius, 2002). A number of the ER chaperones are known to have multiple interactions with each other, both with and without client protein binding (Jansen et al., 2012). This is proposed to create large protein complexes made up of resident proteins and incompletely folded cargo, forming a relatively immobile phase in the ER and contributing to protein retention (Barlowe & Helenius, 2016). Importantly, these chaperone-chaperone and client-chaperone interactions are often dependent on ER luminal Ca^{2+} concentration (discussed below), thus providing a possible explanation for why Ca^{2+} depletion often results in the secretion of misfolded cargo and ER resident proteins (Booth & Koch, 1989).

Retention mechanisms are sure to be an imperfect solution and ER resident proteins often escape from the ER. Additionally, cargo receptors utilized during cargo capture processes must return to the ER to continue their functional role in transport. In each scenario COPI mediated retrieval helps to return proteins to the ER via retrograde transport as discussed above. Finally, if a secretory protein proves incapable of obtaining a transport competent conformation, it can be retrotranslocated to the cytosol and degraded by the proteosome in a process termed ER-Associated Degradation (ERAD) (Sun & Brodsky, 2019).

Recent high resolution dynamic imaging studies using whole-cell FIB-SEM technology in combination with multi-modality light microscopy have produced a new model for ERES structure that redefines the roles of COPI and COPII in ER-to-Golgi transport and challenges our current understanding of protein cargo loading at ERES. The conventional model, as described above, proposes that COPII coated spherical vesicles bud from ERES on the ER membrane and fuse with ERGIC where anterograde cargo subsequently interacts with COPI and traffics to the cis-Golgi via vesicular trafficking along microtubules (Appenzeller-Herzog & Hauri, 2006). The new model proposes a highly complex, branched, and adaptable ERES structure budding off, but importantly still connected to, the ER via a narrow, COPII coated neck. COPI is found at the more distal parts of the branched ERES and travels with anterograde cargo that is within tubular transport intermediates as they traverse microtubules towards the Golgi (Figure 3). The authors propose that COPII's main function in this model is to regulate cargo entry into ERES via Sar1 GTPase cycling while COPI is responsible for additional cargo sorting and ER exit in transport intermediates (Weigel et al., 2021). It remains to be seen how this new model of ERES structure

and function can accurately align with the decades' worth of mechanistic data regarding early secretory protein trafficking. Additionally, it remains possible that this describes only a subset of the functional ERES possible in a cell and that other ERES models remain viable.

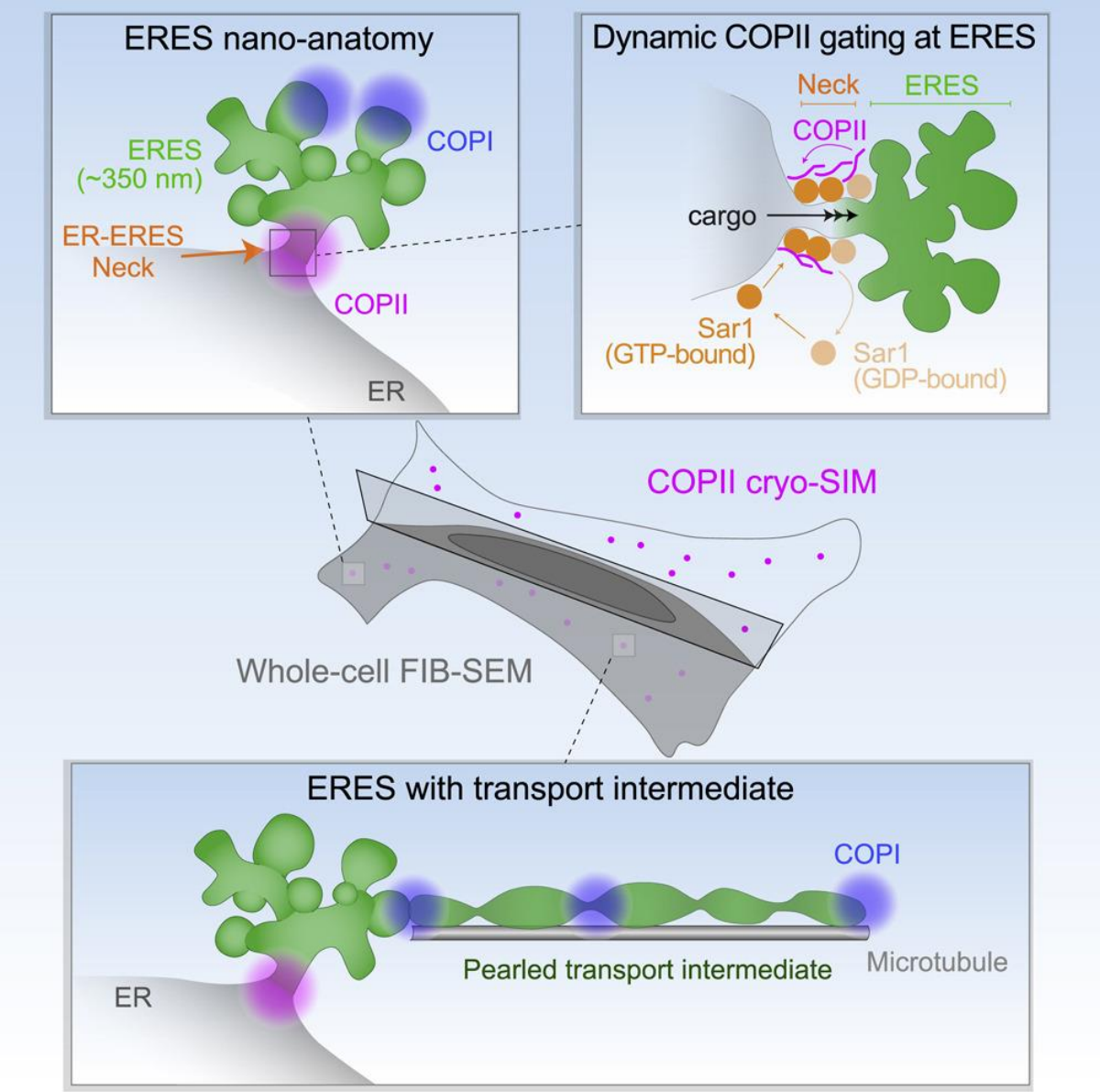

Figure 3. A New Model for ERES Structure. A New model for ERES structure proposed by Weigel et al. in which ERES are dynamic tubular networks extending out from the ER membrane. COPII is localized to the neck where it is responsible for cargo loading into the tubular network. COPI is localize to the distal tips of the tubules and is responsible for physical transport, traveling with the cargo along microtubules in transport intermediates.

Reproduced with permission from the graphical abstract, Weigel, A. V., Chang, C. L., Shtengel, G., Xu, C. S., Hoffman, D. P., Freeman, M., Iyer, N., Aaron, J., Khuon, S., Bogovic, J., Qiu, W., Hess, H. F., & Lippincott-Schwartz, J. (2021). ER-to-Golgi protein delivery through an interwoven, tubular network extending from ER. Cell, 184(9), 2412-2429

1.3 ER PROTEIN HOMEOSTASIS

As previously discussed, the ER is the site of synthesis and maturation for a myriad of proteins. This capacity exists due to a diverse compliment of chaperones and folding enzymes that reside in the ER lumen. These proteins promote folding and minimize aggregation of nascent proteins while also targeting proteins that fail to achieve their native structure for degradation.

The most abundant and well-known ER chaperone, Grp78/BiP, is a master regulator for a variety of ER functions. Like all Hsp70 chaperones, BiP contains a nucleotide-binding domain (NBD), a substrate-binding domain (SBD), and a linker that controls the allosteric interactions between the two (Pobre et al., 2019). BiP functionality is dependent on an ATP consuming cycle. In the ATP bound state, the NBP 'lid' is open, allowing for client binding at a high on-off rate. ATP hydrolysis triggered by co-chaperones (EDdjs) closes the NBD lid and retains the client protein in a high affinity bound state. ADP release and ATP rebinding promoted by nucleotide exchange factors reopens the lid, allowing for client release (Pobre et al., 2019; Wiseman et al., 2022; Zimmermann & Lang, 2020). In addition to its role as a chaperone, BiP is involved in a number of ER functions including gating the Sec61 ER translocon (Alder et al., 2005; Haigh & Johnson, 2002), maintaining unfolded protein response (UPR) transducers (discussed below) in an inactive state (Bertolotti et al., 2000), and targeting proteins that fail to mature for degradation (Skowronek et al., 1998). While there are a number of other chaperones and folding enzymes including Calnexin, Calreticulin, Grp94, and protein disulfide isomerase (PDI) family proteins, discussion of each of their mechanisms of action is beyond the scope of this work

1.3.1 ER Stress and the Unfolded Protein Response (UPR)

Failure of the homeostatic proteostasis machinery can result in the accumulation of misfolded or aggregated proteins in the ER lumen. This ER stress triggers the UPR in an attempt to alleviate the luminal protein burden by upregulating genes associated with ER protein folding and dampening global translation.

The UPR is mediated by type-I ER transmembrane proteins PKR-like endoplasmic reticulum kinase (PERK), Inositol Requiring Enzyme 1 (IRE1α), and type-II transmembrane protein Activating Factor 6 (ATF6) (M. Wang & Kaufman, 2016). The most immediate response to ER stress is the activation of PERK which phosphorylates eukaryotic translation initiation factor 2 subunit-α (eIF2α), leading to a dampening of global protein synthesis (Ron & Walter, 2007). Interestingly, while dampening general translation activity, phosphorylated eIF2α also initiates the translation of a specific subset of mRNAs including that of ATF4 (Lu et al., 2004). ATF4 acts as a stress-inducible transcription factor to activate a variety of genes associated with redox homeostasis, amino acid metabolism, protein synthesis, and autophagy (Harding et al., 2003). IRE1α oligomerizes and autophosphorylates upon induction of ER stress (Zhou et al., 2006). This activated IRE1α causes alternative splicing of the mRNA encoding the transcription factor X-box-binding protein 1 (XBP1), resulting in XBP1s protein expression. XBP1s then upregulates various genes involved in protein translocation, folding, and secretion (Hetz et al., 2020). Activated IRE1α can also cleave a set of mRNAs and microRNAs to elicit their degradation in a process termed regulated IRE1-dependent decay (RIDD) that is thought to lower mRNA abundance and thus protein folding load (Hollien & Weissman, 2006). Finally, ATF6 traffics from the ER to the Golgi upon ER stress induction. In the Golgi, ATF6 is cleaved by site-1 protease (S1P) and site-2 protease (S2P), releasing a cytosolic fragment that acts as a transcription factor to upregulate proteostasis machinery in concert with XBP1s (Haze et al., 1999). Each arm of the UPR attempts to alleviate the misfolded protein burden in the ER via distinct yet overlapping mechanisms.

When the ER stressors overwhelm the adaptive UPR's ability to cope, UPR can also induce apoptosis. This apoptotic signaling is mainly mediated by the PERK- eIF2α-ATF4-CHOP pathway. CCAAT/enhancer- binding protein (C/EBP) homologous protein (CHOP) is a protein upregulated by ATF4 that then dimerizes with ATF4 to alter the transcriptional landscape that ATF4 regulates. CHOP induces upregulation of a number of pro-apoptotic proteins while simultaneously downregulating the anti-apoptotic protein Bcl-2 (Han et al., 2013).

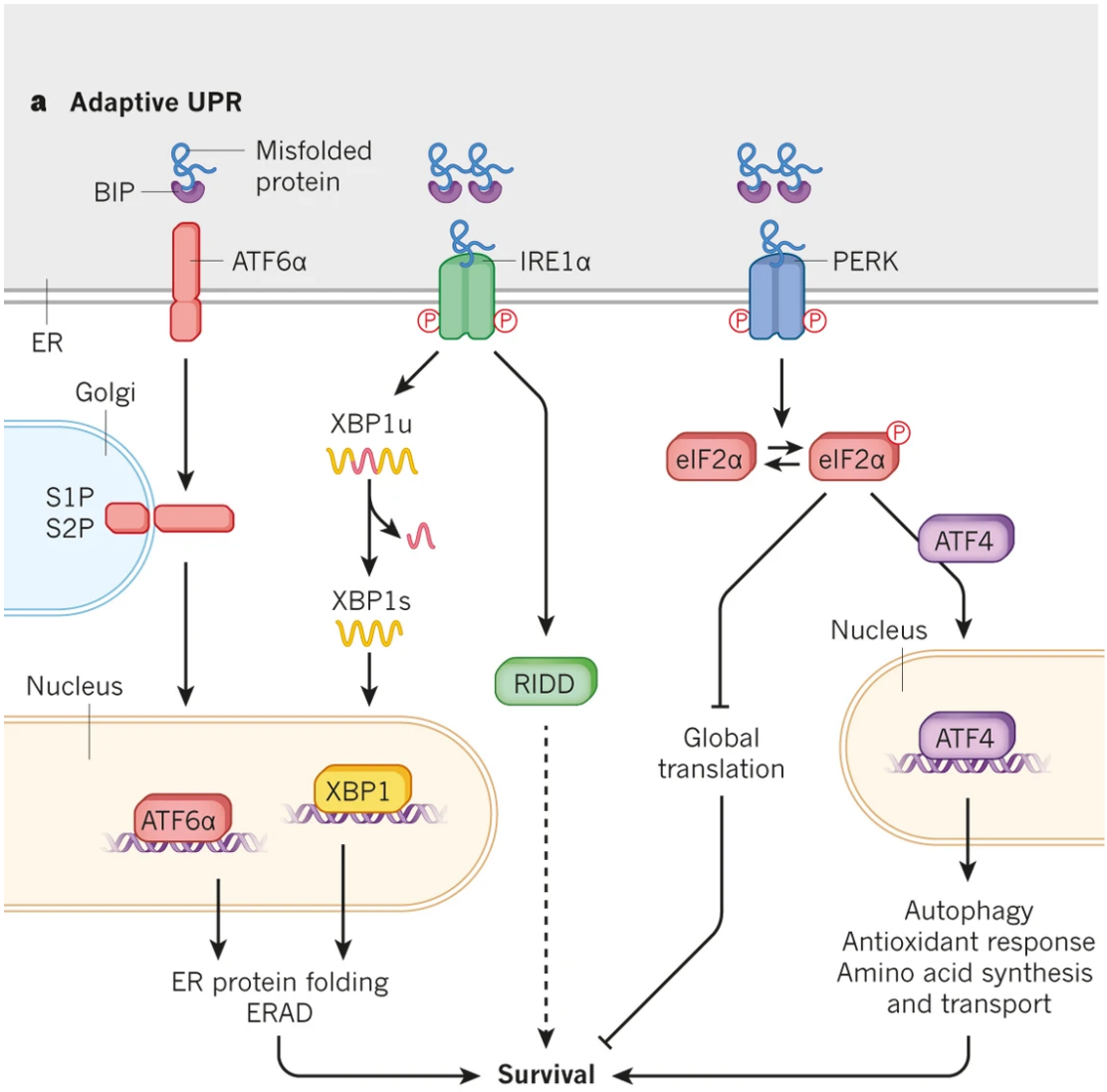

Figure 4. Signaling Pathways of the Unfolded Protein Response. This diagram depicts the major players in the signaling cascades of each arm of the adaptive UPR.

Adapted with permission from figure 2, Wang, M., & Kaufman, R. J. (2016). Protein misfolding in the endoplasmic reticulum as a conduit to human disease. Nature (Vol. 529, Issue 7586, pp. 326–335).

1.3.2 Ca^{2+} and ER Proteostasis

In addition to its role in protein biosynthesis and trafficking, the ER is the major intercellular Ca^{2+} store in the cell. The Ca^{2+} concentration in the ER lumen is orders of magnitude higher than that in the cytosol. This large Ca^{2+} store is utilized for a variety of signaling events (discussed below), but it is also proposed to be instrumental in the maintenance of ER luminal proteostasis.

It has long been known that ER luminal Ca^{2+} depletion can activate the UPR transducers (Sans et al., 2002; Welch et al., 1983; Wong et al., 1993). However, the actual proteostatic challenge, meaning actual protein misfolding, elicited by these conditions is poorly understood (Preissler et al., 2020). Some proteins maturing in the ER lumen such as the low-density lipoprotein receptor are physically stabilized by binding Ca^{2+} (Fass et al., 1997). Other proteins are obviously compromised in their maturation by ER Ca^{2+} depletion (Cooper et al., 1997; Guest et al., 1997; Lodish et al., 1992). But again, it is unclear if the Ca^{2+} was directly implicated in the proteostatic environment. Additionally, the maturation of some proteins, for example the secretory protein albumin, are completely unaffected by ER Ca^{2+} depletion (Lodish et al 1992).

A number of different ER luminal chaperones, which have a direct impact on the proteostatic environment, have Ca^{2+} binding sites including calnexin, calreticulin, Grp94, PDI, and BiP (Preissler et al., 2020). For some of these proteins it is clear that Ca^{2+} binding directly impacts chaperone function. For example, calnexin and calreticulin are completely dependent on Ca^{2+} binding to facilitate the oligosaccharide binding required for their function (Vassilakos et al., 1998). Ca^{2+} also enhances BiP affinity for ADP, thus influencing its ATP-dependent chaperone cycle. Without bound Ca^{2+}, BiP loses ADP affinity, thus losing its ability to retain bound substrate proteins including the UPR transducers (Preissler et al., 2020). These observations prompt the general assumption that there is a direct, positive correlation between ER luminal Ca^{2+} concentration and the proteostatic environment. However, it is important to note that a number of other factors influence ER proteostasis, namely ATP. The three most abundant molecular chaperones, BiP, GrP94 and GrP170 consume ATP in their chaperone cycle (Wiseman et al., 2022) and ATP is required for a number of different ER processes (Depaoli et al., 2019).

1.4 CA^{2+} SIGNALING TOOLKIT

Ca^{2+} is an extremely versatile intracellular signaling molecule that regulates a multitude of different cellular functions (Berridge et al., 2000). Ca^{2+} can act as a signal in this way because its concentration in the cytosol is kept very low (~100 nM) in contrast with the high concentrations in places like the ER lumen (~500 µM) and extracellular space (~1.5 mM) (Sargeant & Hay, 2022). As previously discussed, high ER luminal Ca^{2+} concentration is thought to play an important role in ER proteostasis. The large concentration gradient across both the ER and plasma membranes can also be utilized by the action of regulated, Ca^{2+} specific cation channels which release Ca^{2+} into the cytosol to modulate the activity of a myriad of Ca^{2+}-responsive proteins. Thus, numerous aspects of cellular physiology are dependent on proper functionality of a number of Ca^{2+} pumps and channels.

The ER's prominent role as a hub for both secretory protein trafficking and intracellular Ca^{2+} signaling makes its Ca^{2+} handling processes particularly interesting with regards to their potential roles in proteostasis. Thus, this section will focus specifically on ER Ca^{2+} pumps and channels as well as inter-organelle membrane contact sites that the ER participates in to efficiently communicate Ca^{2+} to its many sites of action.

1.4.1 Sarco/Endoplasmic Reticulum Ca^{2+} ATPase (SERCA)

To maintain the large concentration gradient across the ER membrane, Ca^{2+} must be actively pumped from the cytosol into the ER lumen. This action is accomplished by the SERCA pump which hydrolyzes ATP to pump Ca^{2+} against its concentration gradient. SERCA belongs to the family of P-type ATPases that includes plasma membrane Ca^{2+} ATPase (PMCA), Na+/K+ ATPase, and H+/K+ ATPase (Sweadner & Donnet, 2001). SERCA is coded by three genes located on three different chromosomes, each of which has alternative splice sites leading to at least 14 SERCA mRNAs and numerous isoforms expressed in a species- and tissue-specific manner (Chemaly et al., 2018). The resultant protein is a 110 kDa monomeric polypeptide that couples the movement of two Ca^{2+} ions with each hydrolyzed ATP molecule. The process of SERCA Ca^{2+} transport is initiated by Ca^{2+} binding to the high-affinity sites on the cytoplasmic face. Once

those sites are occupied, ATP hydrolysis is triggered, and the subsequent phosphorylation event causes a series of conformational changes resulting in Ca^{2+} transport across the membrane. A number of factors can influence SERCA activity including luminal and cytoplasmic Ca^{2+} concentration, ATP levels, pH, ADP, and inorganic phosphate (Periasamy & Kalyanasundaram, 2007).

1.4.2 Ryanodine Receptors (RyRs)

The Ryanodine receptors are high conductance, relatively non-specific cation channels that are ubiquitously expressed and support a wide variety of signaling events by releasing Ca^{2+} from the ER into the cytosol. The mammalian genome includes three RyR genes located on different chromosomes. The three isoforms exhibit ~70% sequence homology and each has numerous splice variants and posttranslational modifications (PTMs). Interestingly, though the protein functions as a tetramer and there is significant overlap of RyR isoform expression between cell types, RyRs only function as homotetramers (Fill & Copello, 2002). This differs from the Inositol 1,4,5-Trisphosphate Receptors (IP3Rs) which can also form heterotetramers (discussed below).

The RyRs are true Ca^{2+}-induced Ca^{2+} release (CICR) channels, meaning that Ca^{2+} binding is required for channel activation. However, channel opening is also inhibited by high cytosolic Ca^{2+} concentrations. The three RyR isoforms have different sensitivities for cytosolic Ca^{2+}, with RyR-1 being the most sensitive. RyR-1 exhibits a biphasic Ca^{2+} response curve within physiologic ranges, but RyR-2 and RyR-3 Ca^{2+} inhibition seems to only occur with Ca^{2+} concentrations above the physiologic range of most cells (Fill & Copello, 2002). RyRs are also influenced by ER luminal Ca^{2+} concentration, with high luminal Ca^{2+} increasing the responsiveness to cytosolic agonists (Györke & Györke, 1998). RyRs can also be regulated by ATP, Mg^{2+}, and numerous signaling cascades including PKA, PKC, cGMP-dependent protein kinase, and Ca^{2+}/calmodulin-dependent protein kinase II (Stutzmann & Mattson, 2011).

1.4.3 Inositol 1,4,5-Trisphosphate Receptors (IP3Rs)

The inositol 1,4,5-trisphosphate receptors are ligand-gated ER membrane Ca^{2+} channels involved in numerous cellular events ranging from embryonic development to cellular metabolism, gluconeogenesis, exocrine secretion, and neuronal function (Prole & Taylor, 2016). The IP3Rs are encoded by three genes on three different chromosomes and the protein can operate as homo- or heterotetramers (Danoff et al., 1991). Cryo-electron microscopy has established that IP3R tetramers have a mushroom-like shape with the stalk inserted into the ER membrane and the cap facing the cytosol (Fan et al., 2015). The large cytosolic domain has multiple key functional domains including an IP3-binding core (IBC), amino-terminal suppressor domain (SD) that reduces the IP3 binding affinity, and regulatory/coupling domains with various allosteric sites for phosphorylation, binding proteins, and Ca^{2+} binding (Hamada & Mikoshiba, 2020). The transmembrane domain of each of the four subunits has six transmembrane helices embedded into the membrane which form the ion conduction pore and allow for cation selectivity (Mangla et al., 2020).

IP3Rs are activated in part via binding of their ligand IP3. IP3 is a second messenger generated from G_q-coupled or tyrosine kinase-linked receptors on the plasma membrane including group I metabotropic glutamate receptors 1 and 5, 5-HT_{2A} receptors, muscarinic acetylcholine receptors m1 and m3, α1-andrenergic receptors, the $P2Y_1$ receptor, and several other types of P2Y and P2X receptors (James & Butt, 2002). Each of these receptors are coupled to and activate different isoforms of phospholipase C (PLC). Upon activation, PLC hydrolyzes phosphatidylinositol 4,5-bisphosphate (PIP_2) to form diacylglycerol (DAG) and IP3. In order to activate the IP3R channel, IP3 must bind to all four IP3R subunit IBCs (Alzayady et al., 2016). IP3R activation also requires Ca^{2+} binding and IP3 binding to each of the IBCs induces conformational changes that sensitize the Ca^{2+} binding sites. Ca^{2+} binding then fully activates the channel and allows for Ca^{2+} release from the ER lumen into the cytosol (Berridge, 2016). Like the RyRs, IP3Rs exhibit a bell-shaped Ca^{2+} activation curve such that low cytosolic Ca^{2+} (< 300 nM) increases the open probability while high Ca^{2+} inhibits channel opening (L. Bezprozvanny et al., 1992; Foskett et al., 2007). This Ca^{2+} sensitivity facilitates the generation of Ca^{2+} oscillations or waves (Stutzmann & Mattson, 2011). IP3R activity is also influenced by ATP and a myriad of protein binding partners. ATP binding augments the Ca^{2+} release upon IP3 stimulation (Maes et

al., 2000). The large number of IP3R binding proteins can be grouped into four categories based on whether they enhance activity, inhibit activity, act as Ca^{2+} effectors that respond to the Ca^{2+} released, or act in more general roles such as IP3R motility (reviewed in (Prole & Taylor, 2016)).

IP3R isoform expression differs markedly across cell types (Wojcikiewicz, 1995). The three isoforms differ in a number of different ways and given that IP3Rs can function as either homo- or heterotetramers, the functional significance of heterotetrameric forms are poorly understood. This lack of understanding is further complicated by the multiple alternative splice variants that each isoform exhibits (Danoff et al., 1991). IP3R isoforms have an overall sequence homology of 60-80% with the IBC, Ca^{2+} sensor domain, and pore domains being highly conserved and most variability existing in the regulatory domains including the SD (I. Bezprozvanny, 2005). The regulatory variability results in a significant amount of functional differences between isoforms, notably in their affinities for IP3, Ca^{2+}, and ATP (Hamada & Mikoshiba, 2020). IP3R-2 has the highest affinity for IP3, followed by R-1, while R-3 has the lowest affinity (I. Bezprozvanny, 2005; Iwai et al., 2007). Due to their differential agonist sensitivities, the three IP3R isoforms also exert differential effects on Ca^{2+} oscillations (Zhang et al., 2011). It is generally accepted that the oscillatory nature corresponds with the general IP3 affinities (R-2 > R-1 > R-3) (Morel et al., 2003); therefore, it is unsurprising that changes in subtype expression can influence a cell's oscillatory activity. Importantly, oscillatory changes would be dependent on the isoform balance that a given cell type starts with and how that balance is altered. However, multiple studies have reported a consistent anti-oscillatory function for the IP3R-3 isoform (Almirza et al., 2010; Hattori et al., 2004; Régimbald-Dumas et al., 2011; Tovey et al., 2001). Isoforms can also differ in their subcellular localization on the ER membrane. Many of the phosphorylation sites on the IP3Rs are isoform specific, therefore, kinase and phosphatase interactions can vary between isoforms and phosphorylation by a given kinase can stimulate or inhibit activity depending on the isoform. Additionally, IP3R binding partners can differ between isoforms and the stimulatory/inhibitory effect of a given binding partner can also vary (Zhang et al., 2011)

1.4.4 MERCs/MAM's

Ca^{2+} is an important cofactor for many enzymatic reactions happening within other organelles. However, global Ca^{2+} fluxes are often inefficient in communicating Ca^{2+} released from the ER to the lumen of these other membrane spaces. This necessitates the formation of signaling microdomains to increase the local Ca^{2+} concentration at uptake sites. The ER creates these signaling microdomains via membrane contact sites, the best characterized of which is the contacts with mitochondria. Ca^{2+} is required in the mitochondrial matrix to facilitate TCA cycle dehydrogenase activity, namely pyruvate dehydrogenase (PDH), isocitrate dehydrogenase (IDH), and α-ketoglutarate dehydrogenase (αKGDH) (Rizzuto et al., 2012). Voltage-dependent anion channels (VDACs) control Ca^{2+} transfer across the outer mitochondrial membrane (OMM) (Gincel et al., 2001) while the Mitochondrial Ca^{2+} Uniporter (MCU) is responsible for Ca^{2+} transfer across the inner mitochondrial membrane (IMM). A close membrane apposition is needed to create a microdomain that overcomes the low Ca^{2+} affinity of the MCU by establishing a high local concentration (10-20 μM) compared to the general cytosolic Ca^{2+} concentration which does not exceed a few μM after IP3R stimulation (La Rovere et al., 2016). These sites are referred to as Mitochondria ER Contact Sites (MERCs) or Mitochondrial Associated ER Membranes (MAMs). Though the two terms are used interchangeably, MAM is the more common nomenclature, yet some specify MAMs as the ER membrane portion of the overall MERC structure which includes the mitochondrial membrane structures. For sake of simplicity, we will use the term MAM to refer to the membrane contact site encompassing structures on both the ER and mitochondrial membranes.

Mitochondria normally move throughout the cell, traveling along microtubules at resting cytosolic Ca^{2+} concentrations. However, Ca^{2+} transients via IP3Rs or RyRs can decrease mitochondrial motility at the signaling microdomain allowing for mitochondrial accumulation at these ER membrane proximal locations (Yi et al., 2004). The molecular chaperone glucose-related protein 75 (Grp75) physically links IP3Rs on the ER membrane to VDAC on the mitochondrial membrane (Szabadkai et al., 2006). The IP3R-3 isoform has been observed to preferentially colocalize with mitochondria in some cell types and is the most implicated IP3R isoform in Ca^{2+} communication at MAMs both for basal and apoptotic function (Kuo et al., 2019; Mendes et al., 2005). Mitofusin-2 (Mfn2), a protein typically associated with mitochondrial

fusion/fission processes, has been proposed to play a structural role in MAMs, though it is unclear whether it acts as a tether (De Brito & Scorrano, 2008) or as a spacer (Filadi et al., 2015).

MAMs play physiologically important roles in both cellular homeostasis and the response to cellular stressors. TCA cycle function is necessary both for aerobic ATP production as well as general cell growth and proliferation via nucleotide production. The Ca^{2+} dependence of the TCA cycle dehydrogenases necessitates MAM functionality to maintain these indispensable processes. In non-tumorigenic cells, disruption of constitutive Ca^{2+} communication to the mitochondria via MAMs impairs aerobic ATP production, activates AMP-activated kinase (AMPK), and induces autophagy (Cárdenas et al., 2010, 2016). Alternatively, in tumor cells which proliferate uncontrollably regardless of mitochondrial energetic status, MAM disruption will still activate autophagic processes via AMPK upon MAM disruption, but the lack of sufficient nucleotide availability causes mitotic catastrophe and cell death (Cárdenas et al., 2016). MAMs are also implicated in the ER stress response as ER and mitochondrial networks are redistributed to increase MAMs in a microtubule-dependent fashion. The redistributed mitochondria exhibit increased transmembrane potential and increased ATP production, oxygen consumption, reductive power, and Ca^{2+} uptake from IP3Rs. Blocking MAM function makes cells more vulnerable to ER stress, though the exact mechanism by which the increased ATP production helps to alleviate ER stress is unclear (Bravo et al., 2011). Should a given cellular stress prove too great, MAMs also play an important role in apoptosis as apoptotic conditions induce a narrowing of the space between ER and mitochondria resulting in mitochondrial Ca^{2+} overloading and ensuing opening of the permeability transition pore (Csordás et al., 2006). Cytochrome C released from the mitochondria during apoptosis also binds to the IP3Rs to enhance Ca^{2+} release and thus potentiate the opening of the permeability transition pores (Boehning et al., 2003). MAM functionality in apoptosis is exemplified by Phosphatase and Tensin homolog (PTEN) deficient cancers. PTEN competes with F-box and leucine rich repeat protein 2 (FBXL2) for binding to IP3R-3. FBXL2 promotes IP3R-3 degradation, thus PTEN loss enhances FBXL2 binding and subsequent degradation of IP3R-3. Loss of IP3R-3 decreases the

mitochondrial Ca^{2+} signaling upon apoptotic stimuli, thus promoting tumorigenesis (Kuchay et al., 2017).

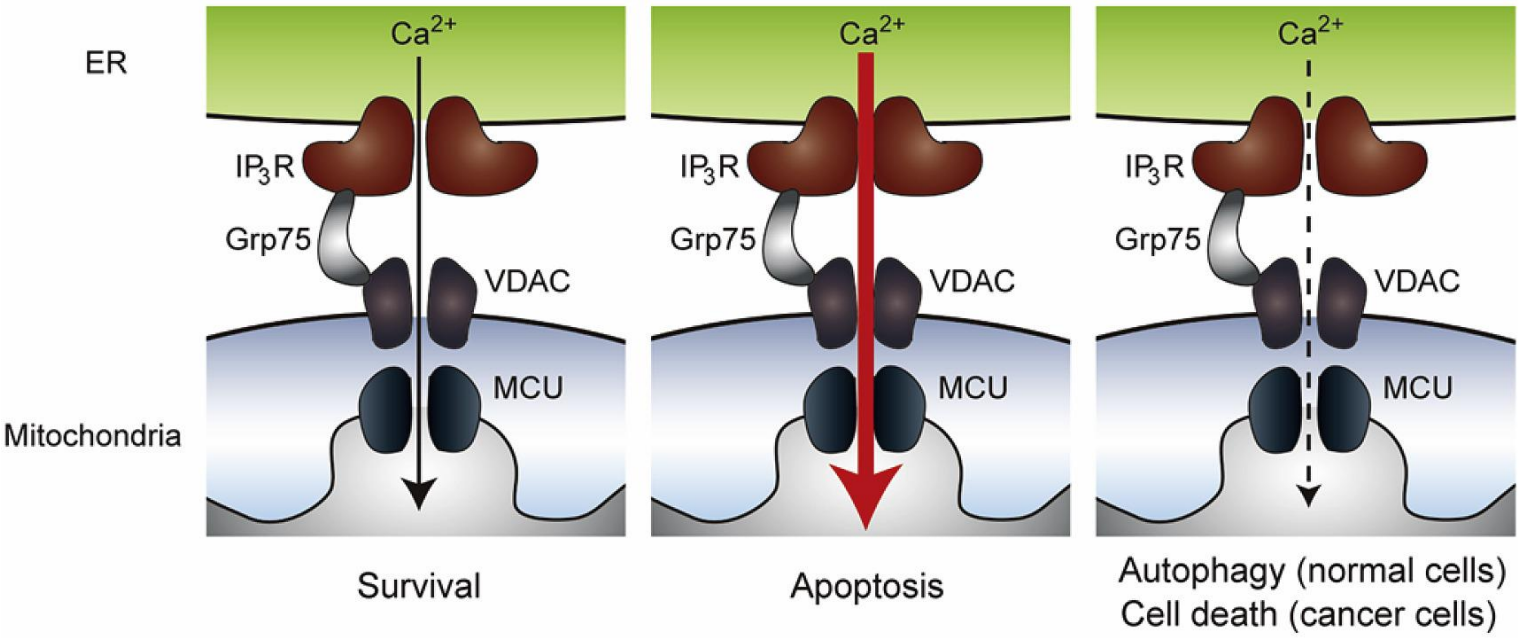

Figure 5. MAM Function in Ca^{2+} Communication to the Mitochondrial Matrix. A cartoon depiction of the major protein components of functional MAMs. Regular Ca^{2+} communication from the ER to the mitochondrial matrix is required for basal mitochondrial function. Reduction in MAM function can induce autophagy in non-tumorigenic cells and cell death in cancer cells. Excessive Ca^{2+} communication via MAMs induces opening of the mitochondrial permeability transition pore and apoptosis.

Reproduced with permission from Figure 2, Ando, H., Kawaai, K., Bonneau, B., & Mikoshiba, K. (2018). Remodeling of Ca^{2+} signaling in cancer: Regulation of inositol 1,4,5-trisphosphate receptors through oncogenes and tumor suppressors. In Advances in Biological Regulation (Vol. 68, pp. 64–76). Elsevier Ltd. https://doi.org/10.1016/j.jbior.2017.12.001

1.5 CA^{2+} REGULATION OF ER EXPORT

Ca^{2+} is well established as a required cofactor in evoked exocytosis but has also been implicated in the regulation of numerous other intracellular membrane trafficking phenomena including ER-to-Golgi (Beckers & Balch, 1989), intra-Golgi (Porat & Elazar, 2000), endosomal, and lysosomal trafficking (Cao et al., 2015). The exact mechanisms by which Ca^{2+} signaling influences each of these membrane transport events are still being elucidated. While Calmodulin has been implicated in several transport steps (Burgoyne & Clague, 2003), there are a variety of Ca^{2+}-sensitive proteins that have been established to exert influence on transport events in what is most likely an intricate and interwoven Ca^{2+} response system. A thorough review of the Ca^{2+}-sensitive proteins involved in all points of secretion was recently published (Sargeant & Hay, 2022). Here we focus on the Penta-EF Hand (PEF) proteins ALG-2 and Peflin whose influence on ER-to-Golgi trafficking is still being elucidated.

1.5.1 ALG-2

Apoptosis-linked Gene 2 (ALG-2) is a 22 kDa cytosolic protein product of the PDCD6 gene (Maki et al., 2002). There are two alternatively spliced transcripts resulting from the PDCD6 gene. One is slightly truncated, lacking the Gly121 and Phe122 found on the full-length form. Both transcripts are expressed in many tissues with the longer transcript expressed at about double the amount (Tarabykina et al., 2000). Like all PEF proteins, ALG-2 contains five Ca^{2+}-binding EF-hand domains that exert significant control of ALG-2 function based on the cytosolic Ca^{2+} environment (Lo et al., 1999; Maki et al., 2016). The first two EF-hand domains are on the amino-terminus, while the remaining three are on the carboxy-terminal domain. Though ALG-2 is capable of forming a weak homodimer even in the absence of Ca^{2+}, Ca^{2+} binding allows for enhanced ALG-2 homodimerization mediated by the EF-5 domain (Lo et al., 1999).

Functional examination has found that ALG-2 has no catalytic function, rather, it acts via its interactions with its various target proteins. More than 20 ALG-2 binding partners have been identified at a number of different subcellular locations (Maki et al., 2016). At the ER, ALG-2 interacts with Sec31A, Scotin, Trk-fused gene (TFG), and MAPK1-interacting and spindle-

stabilizing (MISS)-like (MISSL). ALG-2 can also act more distally in the endocytic system where it interacts with ALG-2 interacting protein X (ALIX), tumor susceptibility gene 101 (TSG101), vacuolar protein sorting 37C (VPS37C), IST1, various Annexin family proteins, and mucolipin-1/TRPML1. Finally ALG-2 may play some role in nuclear function through its interactions with RBM22 and Ca^{2+} homeostasis endoplasmic reticulum protein (CHERP) (Shibata, 2019). The two ALG-2 splicoforms differ slightly in their binding partners, with the shorter form lacking interaction with canonical binding partners like ALIX, TSG101, Scotin, Annexin A7, and Annexin A11 (Shibata, 2019). Some of the ALG-2 binding partners are themselves Ca^{2+} binding proteins which may add an additional layer of Ca^{2+} regulated activity modulation. This may help to explain the range of functional effects seen upon ALG-2 manipulation (discussed below) (Shibata et al., 2015).

1.5.2 Peflin

Peflin, encoded by the PEF1 gene, is another member of the PEF protein family whose PEF domain has the highest similarity with that of ALG-2 (40.9% identity). The majority of this structural similarity exists in the EF-1 and EF-3 domains (Kitaura et al., 1999). The only known function of Peflin is to heterodimerize with ALG-2. The EF-5 domain in both Peflin and ALG-2 is required for heterodimerization, but because EF-5 is also required for ALG-2 homodimerization, there is a competition between ALG-2 homodimer and ALG-2-Peflin heterodimer formation. The ALG-2-Peflin heterodimer forms in the absence of Ca^{2+} allowing for Peflin localization at ERES (Kitaura et al., 2001; Rayl et al., 2016; Sargeant et al., 2021). Higher cytosolic Ca^{2+} concentration disrupts the heterodimer and induces proteosomal degradation of both monomers, thus favoring ALG-2 homodimerization (Kitaura et al., 2001, 2002).

1.5.3 PEF Protein Function

ALG-2 has long been thought to play a role in cell death caused by ER stress (R. V. Rao et al., 2004), TNF-receptor 1 (Mahul-Mellier et al., 2008), and DNA damage (Suzuki et al., 2012), hence its name. However, its actual role in apoptosis is unclear because it is also upregulated in a variety of tumors and PCDC6-deficient mice retain susceptibility to apoptotic stimuli (Shibata, 2019). The most accepted role for ALG-2 is its modulation of membrane dynamics via its

interactions with a number of different membrane binding proteins. While ALG-2 has been implicated in processes like endosomal function and plasma membrane repair, its longest standing and most well characterized function is in ER-to-Golgi secretion. This function is mediated by ALG-2's interaction with Sec31a concomitant with intracellular Ca^{2+} oscillations (la Cour et al., 2007; Maki et al., 2016; Shibata et al., 2007, 2010; Yamasaki et al., 2006). This interaction is facilitated by EF-1 and EF-3 on ALG-2 and 839-PPPGFIMHGNVNP-851 on the human Sec31A PRR loop (Shibata et al., 2007, 2010). The Sec31a 'active fragment' which binds across the composite surface of the Sar1-Sec23 complex, is around 125 amino acids away from the ALG-2 binding site, allowing for simultaneous binding of both ALG-2 and the COPII inner coat (Shibata, 2019). Multiple studies have demonstrated that Sec31a localization to ERES is partially dependent on ALG-2 and Ca^{2+} and that ALG-2 homodimer binding enhances Sec31a affinity for, and retention to, the inner COPII coat (la Cour et al., 2013; Shibata et al., 2007, 2010; Yamasaki et al., 2006). Interestingly, vertebrates express two paralogs of Sec31, Sec31a and Sec31b (Stankewich et al., 2006). Though the two paralogs have a high degree of amino acid similarity and both have a disordered PRR loop at their carboxy-terminus, Sec31b lacks the ALG-2 binding site and is therefore theoretically insensitive to ALG-2 influence (Shibata, 2019).

As previously stated, Peflin is only known to function via its interaction with ALG-2. Our group previously found that Peflin plays a negative role in VSV-G transport by inhibiting ALG-2 homodimerization, thus dampening the stimulatory action of ALG-2 (Rayl et al., 2016; Sargeant et al., 2021). ALG-2 and Peflin have also been implicated in the ubiquitylation of Sec31a. In this model, the ubiquitin ligase CUL3 and its adaptor KLHL12 require both ALG-2 and Peflin for Sec31a recognition. Sec31a ubiquitylation by $CUL3^{KLHL12}$ is further proposed to trigger the formation of larger COPII coated vesicles to facilitate the transport of exceptionally large cargos such as collagen (McGourty et al., 2016). However, a complete understanding of this mechanism has yet to be elucidated and some of the mechanistic implications have been challenged. For example, the model argues a positive role for Peflin in collagen secretion, but our group found that Peflin knockdown increases the secretion of both transfected and endogenous collagen in multiple cell types (Sargeant et al., 2021).

ALG-2 activity seems to exert influence on COPII and should therefore affect ER-to-Golgi transport kinetics. However, functional studies have given mixed results. Yamasaki et al. found no change in VSV-G transport in HeLa cells upon ALG-2 depletion (Yamasaki et al., 2006). Other groups, utilizing a number of different cell types, have reported a negative role for ALG-2 in transport (Bentley et al., 2010; la Cour et al., 2013; Shibata et al., 2015); while still other studies by some of the same groups and utilizing some of the same cell types have implied a positive regulatory role for ALG-2 (Helm et al., 2014; Rayl et al., 2016; Shibata et al., 2007, 2010). There are a number of factors that may explain the seemingly disparate results seen in these studies. First, many of these studies manipulated ALG-2 expression levels via knockdown or recombinant ALG-2 transfection. It is possible that ALG-2 may exert differential control of transport depending on expression level. Second, ALG-2 has a number of different ER proximal binding partners that may contribute to its regulation of Sec31a function, including Peflin (discussed above). These binding partners may have different expression profiles between cell types thus imparting different ALG-2 functionality. Third, cell types can differ dramatically in their Ca^{2+} signaling dynamics. It is likely that different Ca^{2+} signaling profiles could alter the effect that ALG-2 has on transport. Some of these ideas were examined in detail in a recent study published by our group and discussed in more detail below (Sargeant et al., 2021).

1.5.4 CADEE and CAEEE

The functional discrepancies described above prompted further examination of ALG-2 influence on transport in various cellular contexts (Sargeant et al., 2021). Experiments varying the expression levels of ALG-2 and Peflin in Normal Rat Kidney (NRK) cells found that ALG-2 fluctuations had little effect on VSV-G transport. Alternatively, changes in Peflin expression had significant impacts on VSV-G transport in both positive and negative directions; depletion of peflin stimulates transport while over-expression inhibits transport, indicating that Peflin acts as a negative regulator of transport. Additionally, Peflin influence was completely dependent on the presence of ALG-2. Interestingly, experiments examining ALG-2 response to Ca^{2+} signaling found that ALG-2 is capable of increasing or decreasing transport, independent of Peflin, depending on the specific Ca^{2+} signaling characteristics. These two alternate scenarios were

termed Ca^{2+} Activated Depression of ER Export (CADEE) and Ca^{2+} Activated Enhancement of ER Export (CAEEE) (Figure 6).

CADEE was elicited in NRK cells after 60-150 minutes of histamine exposure. This resulted in decreased VSV-G transport that was dependent on ALG-2 but not Peflin. Histamine exposure of this kind caused continuous Ca^{2+} oscillations mediated by the H1 histamine receptors, but the same Ca^{2+} and transport results could be obtained using ATP as the Ca^{2+} mobilizing agonist (Figure 6C). PC12 cells responded differently to ATP stimulation, showing a single large Ca^{2+} signal followed by relative Ca^{2+} "silence". This Ca^{2+} signaling profile correlated with an increase in VSV-G transport and was thus termed CAEEE (Figure 6B). NRK cells forced into the same, single-signal Ca^{2+} pattern using the SERCA inhibitor BHQ also exhibited CAEEE, indicating that ALG-2 can differentially influence transport depending on Ca^{2+} signaling kinetics.

This work led to the proposed general mechanism in which ALG-2 acts as a flexible Ca^{2+} dependent adaptor. It is possible that the dual actions of ALG-2 rely on bridging Sec31a with other ALG-2 interacting proteins that have been identified at ERES like Annexin A11, MISSL, MAP1B, or KLHL12. ALG-2 function could also involve post-translational modifications of Sec31a such as ubiquitylation or O-GlcNAcylation.

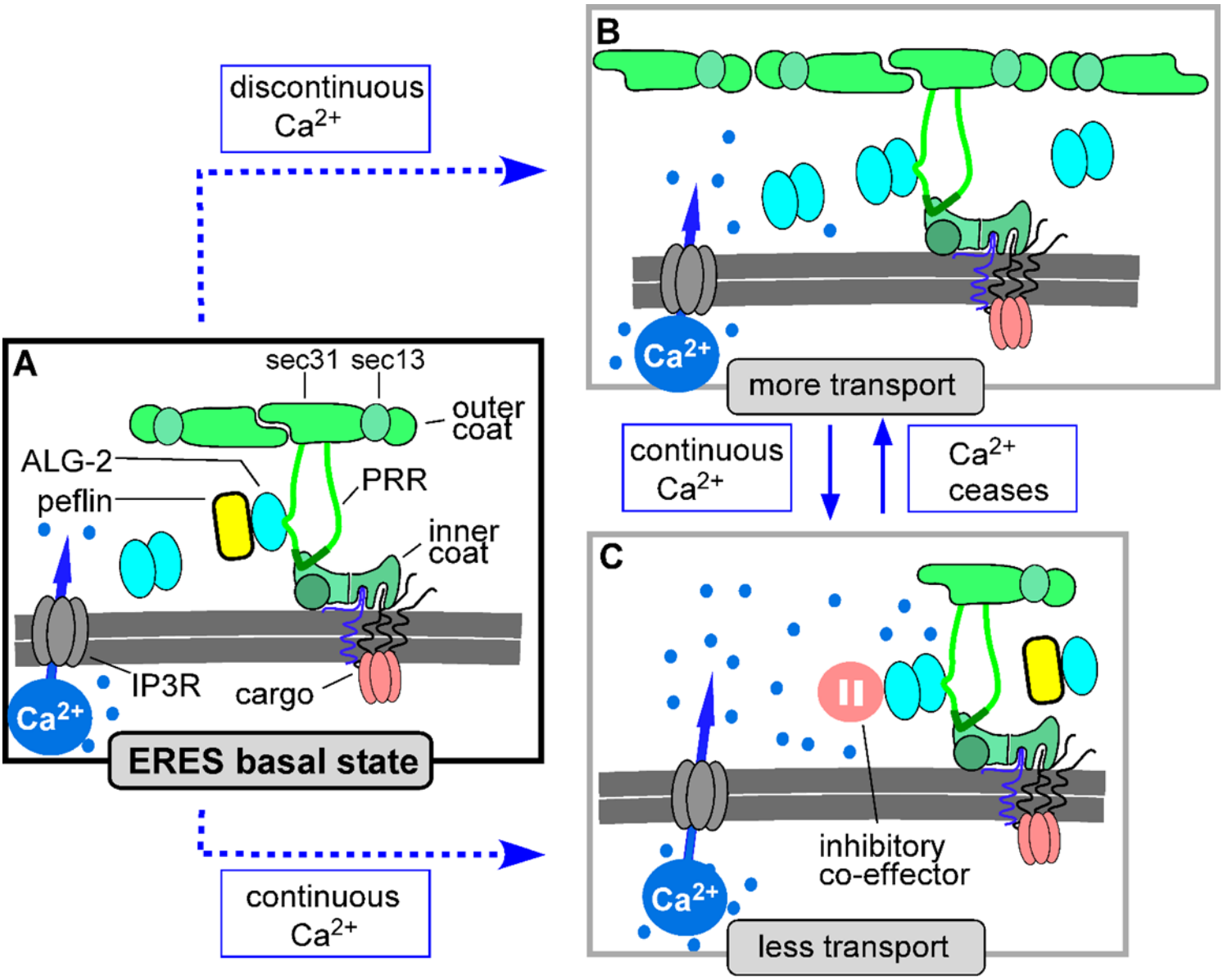

Figure 6. Model of PEF protein regulation of ER export. (A) Under basal conditions, ALG-2 homodimers and ALG-2-peflin heterodimers compete for binding to sec31A. ALG-2 homodimers stimulate transport while heterodimers inhibit transport. (B) Discontinuous agonist-driven Ca^{2+} signaling leads to more ALG-2 homodimers at ERES, greater outer coat recruitment, and greater export, termed CAEEE. (C) Continuous Ca^{2+} signals lead to an ALG-2-dependent reduction of COPII targeting and decreased export, termed CADEE.

Adapted with permission from figure 11, Sargeant, J., Seiler, D. K., Costain, T., Madreiter-Sokolowski, C. T., Gordon, D. E., Peden, A. A., Malli, R., Graier, W. F., & Hay, J. C. (2021). ALG-2 and peflin regulate COPII targeting and secretion in response to calcium signaling. Journal of Biological Chemistry, 297(6).

CHAPTER 2:

METHODS

2.1 ANTIBODIES

Mouse monoclonal anti-mannosidase II antibody was purchased from Covance Research Products (Denver, PA; product MMS-110R-200). Rabbit polyclonal anti-IP3R-1 antibody was purchased from ThermoFisher Scientific (Waltham, MA; product PA1-901). Mouse monoclonal anti-IP3R-3 antibody was purchased from BD Biosciences (San Jose, CA; item 610313). Anti-rbet1 mouse monoclonal antibody, clone 16G6, was as described (Hay et al., 1998). Rabbit polyclonal anti-peflin and chicken polyclonal anti-ALG-2 were produced previously (Sargeant et al., 2021). Rabbit polyclonal anti-sec31A, anti-sec23, anti-p24 and anti-β-Cop were produced previously against synthetic peptides (Bentley et al., 2006, 2010; Xu & Hay, 2004). Rabbit polyclonal anti-Phospho-eIF2α antibody was purchased from Cell Signaling Technology (Danvers, MA; product 9721s). Rabbit polyclonal anti Phospho-IRE1 was purchased from Abcam (Cambridge, United Kingdom; item ab48187). Rabbit polyclonal anti-ATF4 antibody was purchased from GeneTex (Irvine, Ca^{2+}; product GTX101943). Rabbit polyclonal anti-sec24c was a kind gift from Dr. William Balch (Scripps Institute). Rabbit polyclonal anti-p115 was produced in-house (T. Wang et al., 2015). Rabbit polyclonal anti-p58 was a kind gift from Dr. Jaakko Saraste (University of Bergen, Norway). I14 conformation-specific anti-VSV-G_{ts045} monoclonal antibody was kindly provided by Dr. John Ngsee (University of Ottawa). Secondary antibody conjugates with Alexa FluorTM 488 were from Invitrogen (Carlsbad, CA; product A11001). Cy3- and cy5-conjugated secondary antibodies were purchased from Jackson ImmunoResearch Laboratories (West Grove, PA).

2.2 qRT-PCR

NRK cells were transfected withIP3R-1 or IP3R-3 siRNA (see below) using Transfast (Promega Corp.; Madison WI) using manufacturer's instructions. Total RNA was isolated using the PEQLAB total RNA isolation kit (Peqlab; Erlangen, Germany) and reverse transcription was performed in a thermal cycler (Peqlab) using a cDNA synthesis kit (Applied Biosystems; Foster City, CA). mRNA levels were examined by qRT-PCR. A QuantiFast SYBR Green RT-PCR kit (Qiagen;

Hilden, Germany) was used to perform real time PCR on a LightCycler 480 (Roche Diagnostics; Vienna, Austria), and data were analyzed by the REST Software (Qiagen). Relative expression of specific genes was normalized to human GAPDH as a housekeeping gene. Primers for real time PCR were obtained from Invitrogen (Vienna, Austria).

2.3 siRNA KNOCKDOWNS AND TRANSFECTIONS

NRK cells were electroporated with 0.6 µM siRNA and grown in DMEM with 4.5 g/L glucose containing 10% fetal calf serum and 1% penicillin-streptomycin. After 2-3 days of normal growth at 37 °C, the cells were resuspended and re-electroporated, this time with a combination of the siRNA plus 7.5 µg of protein plasmid. Cells were allowed to recover and grow on coverslips at 37 or 41 °C for 24 h.

Alternatively, sub-confluent cells grown on glass coverslips in 6-well plates were directly transfected without resuspension. After ~16 h incubation in OptiMEM containing 0.3% RNAiMax (Invitrogen; Carlsbad, CA) and 0.28 µM siRNA, transfection medium was supplemented with an equal part of OptiMEM containing 5% fetal calf serum, 2 mM CaCl2, and 1% penicillin-streptomycin and incubated for another 3-5 h. Subsequently, this post-transfection medium was removed (but saved) and replaced with DMEM containing 10% fetal calf serum, 1% penicillin-streptomycin, 0.3% PolyJet (SignaGen Laboratories; Frederick, MD) , and 1 µg/ml plasmid. After ~12 h incubation, the plasmid solution was removed, cells were washed twice with PBS and returned to their siRNA-containing OptiMEM medium at 37 or 41 °C to recover while continuing the knockdown for another 24 h. There was no noticeable difference in knockdown or transfection efficiency between the two transfection protocols. Cells from all transfections were either lysed directly in SDS-PAGE sample buffer for quantitative immunoblotting, or else processed for transport, colocalization, or FRET assays as described below.

Plasmid constructs GFP-VSV-G_{ts045}, GFP-FM_4-$VSVG_{tm}$, and GFP-FM_4-hGH were described previously (Sargeant et al., 2021). RUSH-VSV-G-GFP was purchased from Addgene (Watertown,

MA; catalog # 65300). D1ER (Palmer et al., 2004), 4mtD3cpv (Palmer et al., 2006), and D3cpv (Palmer et al., 2006) were described previously.

Custom siRNAs were purchased from Ambion/Thermo Fisher (Waltham, MA) or Gene Link (Elmsford, NY) and contained no special modifications. We used two different siRNAs for IP3R-3 which appeared to perform similarly in knockdown efficiency and effects on Ca^{2+} and secretion; the large majority of experiments were performed using siRNA Itpr3-7848 (5' GCA GAC UAA GCA GGA CAA A dTdT 3'). siRNA Itpr3-0452 (5' GGA UGU GGA GAA CUA CAA A dTdT 3') was used intermittently for confirmation purposes. IP3R-1 siRNA Itpr1-9306 (5’ GGC UGA CGG AAG AUA AGA A dTdT 3’) was used for all IP3R-1 knockdowns. ALG-2 and Peflin siRNAs were described and their effects on secretion confirmed previously (Helm et al., 2014; Rayl et al., 2016). Sec31A siRNA had the following sense strand sequence: 5’ GAC CUU UGU UUA CAC GAU dTdT 3’. Sec31B siRNA had the following sense strand sequence: 5’ CCU UGA UUG CCC AGA AAC A dTdT 3’ or 5’ GGA AAU CUC CUU AAU UAU U dTdT 3’. Syntaxin-5 siRNA had the following sense strand sequence: 5’ CCA UUG UAG UUC AUU GCA dTdT 3’. Control siRNAs were custom synthesized non-targeting siRNAs from the same manufacturer. Immunoblotting of cell lysates enabled validation of knockdown efficiencies for each siRNA experiment that was functionally analyzed.

2.4 ER-TO-GOLGI TRANSPORT ASSAY

NRK cells were transfected with cargo protein plasmid and siRNA as described above and plated on poly-L-lysine coated coverslips. For VSV-G_{ts045}, cells were shifted to 41 °C for 6 to 15 h prior to transport, to accumulate the cargo in the ER. For the transport assay, cells were either fixed by dropping coverslips directly into fixative or into 6-well transport chambers with pre-equilibrated 32 °C medium for 10 min prior to transfer to fixative. Alternatively, for FM_4-containing cargo constructs and RUSH-VSV-G, transfected cells were kept at 37 °C, and coverslips were fixed either by dropping coverslips directly into fixative or into 6-well transport chambers for 10 min prior to transfer to fixative. In this case, transport chambers contained 37 °C media containing either 500 nM AP21998, also known as D/D solubilizer (TakaraBio: 635054),

for FM4-containing cargos; or 40 µM Biotin for RUSH cargos. Coverslips were fixed and labeled using anti-mannosidase II antibody as described in the immunofluorescence section below. For transport experiments using 4-phenylbutyrate (4-PBA) as shown in Figure 14 G-H, transfected cells were incubated in media with 10 mM 4-PBA for 1 h prior to transfer to transport chambers also containing 10 mM 4-PBA. 4-PBA was kindly provided by Dr. Michael Kavanaugh (University of Montana). For live-cell transport assays as shown in Figure 11 C-E, coverslips were placed in a perfusion chamber and imaged on a Nikon TE300 inverted microscope equipped with a 40x objective, Crest Optics X-Light v1 spinning disk scanner, 89 North LDI-7 laser launch, and a PCO Edge 4.2 sCMOS camera, all automated with MicroManager software. Imaging was carried out using a constant perfusion rate of 2 ml/min maintained at 37 °C with imaging at 60-second intervals. After 2 min of DMEM, the perfusion was switched to DMEM + 500 nM D/D solubilizer and imaged for another 20 min.

Morphological quantitation of ER-to-Golgi transport was accomplished as described previously (Rayl et al., 2016; Sargeant et al., 2021). Images were collected in a consistent manner with regard to cell morphology, protein expression levels and exposure. A single image plane was collected for each color channel (GFP and mannosidase II) for each field of cells randomly encountered; image deconvolution was not performed. In most cases widefield images were used (microscope is described below in immunofluorescence section), while in others (Figure 11C-E and Figure 13A-J), spinning disk confocal images were used for quantitation of transport with similar results. Images were analyzed using ImageJ open source image software with automation by a custom script (available upon request) that randomizes the images and presents them to the user in a blind fashion. The user identifies transfected cells and subcellular regions while the script extracts parameters including extracellular background, Golgi intensity and diffuse cytoplasmic ER intensity. Transport index is calculated for each individual cell as ($Golgi_{max}$ - background) / (ER_{mean} - background), and all extracted parameters are written to an appendable output file along with a cell number and image title so that the data was traceable. Using this method, the user quantitates about 60 cells per hour. Once transport indices have been obtained for all conditions in an experiment, each value is subtracted by the mean transport index value for cells that were transferred directly to fixative

without a transport incubation (typically a value between 1.0 and 1.5) to generate the net transport index. Net transport indices are then normalized to the mean siControl value for the particular experiment, prior to plotting and comparison between experiments. Each result reported here was obtained in at least three separate experiments on different days.

For 10 °C ERES loading experiments as shown in Figure 13 A-B, cells were transfected with VSV-G_{ts045} and prepared as described above, then either fixed by dropping coverslips directly into fixative or into 6-well transport chambers with pre-equilibrated 10 °C medium for 1 h prior to transfer to fixative. Quantitation of GFP spot prominence was accomplished using a custom ImageJ script (available upon request). Briefly, GFP spots are identified visually and a compound ROI is created around each spot. The compound ROI consists of a circular inner ROI fully encompassing the spot and a larger circular outer ROI encompassing the inner ROI. The script then extracts parameters including extracellular background, inner ROI intensity, and outer ROI intensity. The outer ROI intensity measurement excludes the area comprising the inner ROI, thus specifically measuring GFP intensity directly adjacent to the identified spot. Spot prominence is calculated for each individual cell as (Inner ROI_{max} – background) / (Outer ROI_{mean} – background).

2.5 ER STRESS INDUCTION

To measure UPR activation upon induction of ER stress as in Figure 21, NRK cells were transfected with siRNA as described above and plated on poly-L-lysine coated coverslips at 37 °C. After 24 h ER stress was induced by dropping coverslips into 6-well chambers with 37 °C media containing 1 µM Tg for 4h. Cells were then lysed directly in SDS-PAGE sample buffer for quantitative immunoblotting.

2.6 IMMUNOFLUORESCENCE MICROSCOPY

Coverslips were fixed with 4% paraformaldehyde containing 0.1 M sodium phosphate (pH 7.0) for 30 min at room temperature and quenched twice for 10 min with PBS containing 0.1 M glycine. Fixed cells were treated for 15 min at room temperature with permeabilization solution containing 0.4% saponin, 1% BSA, and 2% normal goat serum dissolved in PBS. The cells were then incubated with primary antibodies diluted in permeabilization solution for 1 h at room temperature. Next, coverslips were washed 3x with permeabilization solution and incubated 30 min at room temperature with different combinations of Alexa FluorTM 488-, Cy3-, and/or Cy5- conjugated anti-mouse, anti-rabbit, or anti-chicken secondary antibodies. After the secondary antibody incubation, coverslips were again washed 3x using permeabilization solution and mounted on glass slides using Slow Fade Gold antifade reagent (Invitrogen product S36936) and the edges sealed with nail polish. Slides were analyzed using a 40x or 60x objective on a Nikon E800 widefield microscope with an LED illumination unit (CoolLED pE 300white), PCO Panda sCMOS camera, Prior excitation and emission filter wheels and Z-drive, all automated using Micro-Manager software.

2.7 COLOCALIZATION ASSAYS

For immunofluorescence co-localization experiments, fixed NRK cells such as in Figure 10 were captured using a 60x/1.40 Plan Apo objective as z-stacks in eleven 200-nm increments for each color channel. Image stacks were deconvolved using Huygens Essential Widefield software (Scientific Volume Imaging, Hilversum, The Netherlands). Final images for display and quantitation represent maximum intensity projections of deconvolved stacks. ERES area was assessed by a custom ImageJ script (available upon request). Briefly, background labeling was removed by defining a dark extracellular area of each channel image as zero. For each cell an object binary image mask (excluding the nucleus) was generated for each individual channel by thresholding using the ‘Moments’ (for rbet1) or ‘Renyi Entropy’ (for VSVG, ALG-2, Peflin, and sec31a) algorithms. Next, each channel mask was compared to the other using a Boolean ‘and’ operation to create co-localization binary masks. Individual channel masks and co-localization masks were converted into ROIs and applied to each original channel image to measure total

area and fluorescence intensity within the area specified by the mask. All measurements were extracted and written to an appendable output file along with the cell number and image title so that the data was traceable. Colocalization area and fluorescence intensity measurements for each cell were then normalized to the mean siControl value for the particular experiment, prior to plotting and comparison.

2.8 3D STRUCTURED ILLUMINATION (SIM) SUPERRESOLUTION MICOSCOPY

NRK cells were transfected with D1ER and siRNA as described above and plated on glass coverslips. After two days, cells were stained for 10 min with 200 nM MitoTracker® Red CMXRos (Invitrogen) and imaged with 488 nm laser excitation (D1ER) and a 561 nm laser with a CFI SR Apochromat TIRF 100×oil (NA1.49) objective mounted on a Nikon-Structured Illumination Microscopy (N-SIM; Nikon, Tokyo, Japan) system equipped with an Andor iXon3 EMCCD camera. 3D-SIM was used in both channels with very short 30 ms exposure time per image. SIM images were reconstructed using Nis-Elements (Nikon). Images were background corrected with an ImageJ-Plugin (Mosaic Suite, background subtractor). Further, the ImageJ/Fiji tool coloc2 was used to determine colocalization coefficients.

2.9 CA^{2+} IMAGING

Subconfluent NRK cells growing on glass coverslips were transfected with genetically encoded Ca^{2+} sensors D1ER or D3cpv and siRNA as described above and imaged the next day. In some experiments (Figures 1C-F and 2) control or knockdown cells were loaded with FURA-2-AM for 30 minutes at 37°C directly prior to imaging, rather than transfection with a Ca^{2+} sensor. Coverslips were placed in a perfusion chamber and imaged on a Nikon TE300 inverted microscope equipped with a 40x objective, motorized high speed Sutter Lambda filter wheel for emissions, CoolLED pe340 excitation system, and PCO Panda sCMOS camera, automated with

Micro-Manager software. Imaging was carried out using various perfusion protocols as described below with imaging at 3 or 4-second intervals.

For examination of basal Ca^{2+} oscillations as in Figure 8, cells were labeled with FURA-2AM and imaged for 20 minutes in non-perfusing DMEM containing 10% FBS maintained at ~37°C. For examination of agonist-dependent Ca^{2+} signaling as in Figure 7C-F, cells were labeled with FURA-2AM and imaged for a total of 10 minutes with a constant perfusion rate of 2 ml/min at room temperature. After 5 minutes of DMEM, the perfusion solution was changed to DMEM + 1 µM bradykinin. Each FURA imaging interval involved collecting an image at 510 nm emission and 340 or 380 nm excitation. For CFP/YFP FRET Ca^{2+} sensors, each imaging interval involved collecting images at 480 nm and 530 nm using 430 nm excitation. For examination of ER luminal Ca^{2+} stores as in Figures12C-E and S1A, cells were transfected with D1ER and imaged for a total of 8 minutes with a constant perfusion rate of 2 ml/min at room temperature. After 5 min of $2Ca^{2+}$ buffer (2 mM CaCl2, 138 mM NaCl, 1mM MgCl2 5 mM KCl, 10 mM D-glucose, 10 mM Hepes, pH 7.4), the buffer was changed to $0Ca^{2+}$ buffer (138 mM NaCl, 1 mM MgCl2, 5mM KCl, 10 mM D-glucose, 0.1 mM EGTA, 10 mM Hepes, pH 7.4) + 3 µM Ionomycin. For examination of cytosolic Ca^{2+} release as in Figure S1C or mitochondrial Ca^{2+} uptake as in Figure 17, cells were transfected with D3cpv (figure S1C) or 4mtD3cpv (figure 17) and imaged for a total of 15 minutes with a constant perfusion rate of 2 ml/min at room temperature. After 5 minutes, the $2Ca^{2+}$ buffer was changed to $2Ca^{2+}$ buffer + 200 nM Tg (figure S1C) or 1 µM Tg (figure 17). For analysis in ImageJ, each cell, as well as an extracellular background region was enclosed in an ROI and mean intensity was collected in each color channel at each time interval. Data was imported to Kaleidagraph software, where the intensity data was converted to ratios. For FURA, R= (emission at 510 nm when excited at 340 nm - background at 510/340) / (emission at 510 nm when excited at 380 nm - background at 510/380). For FRET sensors, with excitation at 430 nm, R= (emission at 530 nm - background at 530) / (emission at 480 nm - background at 480). The FRET or FURA ratio curves were then converted to R/R_0 by dividing every R value by the average of images 2-8 for each trace and, when necessary, fit to a polynomial or exponential decay function to remove effects of progressive photo-bleaching or baseline drift.

CHAPTER 3:

STEADY-STATE REGULATION OF COPII-DEPENDENT SECRETORY CARGO SORTING BY INOSITOL TRISPHOSPHATE RECEPTORS, CA^{2+}, AND PENTA-EF HAND PROTEINS

(This chapter is under revision for publication in Journal of Biological Chemistry)

3.1 INTRODUCTION

Ca^{2+} is a vital intracellular signaling molecule integral for a diverse array of physiological processes. Regulatory roles for Ca^{2+} in intracellular trafficking steps are still being elucidated. Recent work on ER-to-Golgi transport demonstrates involvement of luminal Ca^{2+} stores at a stage following cargo biogenesis and folding/assembly, apparently through the release of Ca^{2+} into the cytoplasm where it binds and activates the vesicle budding, docking and/or fusion machinery (Bentley et al., 2010; Helm et al., 2014). Effector mechanisms by which cytosolic Ca^{2+} modulates ER-to-Golgi transport appear to include penta-EF-hand-containing (PEF) protein adaptors that have been implicated in many Ca^{2+} -dependent cellular phenomena (Maki et al., 2002). The PEF protein apoptosis-linked gene-2 (ALG-2) acts as a Ca^{2+} sensor at ER exit sites (ERES) and can stabilize the association of the COPII coat subunit Sec31A with the membrane when Ca^{2+} is present (la Cour et al., 2007; Shibata et al., 2007, 2010; Yamasaki et al., 2006). However, regulation of ER cargo export by ALG-2 and Ca^{2+} does not follow the simple pattern suggested by these early studies. For one thing, sustained agonist-driven Ca^{2+} signaling results in a sharp ALG-2- dependent reduction of COPII targeting and ER export (Sargeant et al., 2021). For another, ALG-2 in cell extracts often exists in a stable heterodimer with another PEF protein–peflin–that binds ALG-2 in a Ca^{2+} - inhibited manner (Kitaura et al., 2001, 2002). The peflin-complexed form of ALG-2 appears to bind ERES, destabilize the COPII coat and suppress ER export, but through a distinct mechanism than during sustained Ca^{2+} signals (Rayl et al., 2016; Sargeant et al., 2021). Release of ALG-2 from either of these inhibitory states appears to switch its activity, causing ALG-2 homodimers to stimulate COPII targeting and ER export; this switch can be induced by short-lived–as opposed to continuous–Ca^{2+} signals (Sargeant et al., 2021). To summarize, it appears that Ca^{2+} signals, depending upon strength and duration, can induce either stimulatory or inhibitory actions of ALG-2 at ERES, and this regulation involves peflin, sec31A, and potentially other effectors.

But what governs ALG-2 influences at steady state? ER Ca^{2+} signals at steady state may be due to spontaneous Ca^{2+} oscillations mediated by gated Ca^{2+} channels, e.g. inositol trisphosphate receptors (IP3Rs) (Zhang et al., 2011), which have been shown to dynamically

alter ALG-2 localization (la Cour et al., 2007), or else by continuous ER leak, for example mediated by presenilin-1 (Graier et al., 2019; Nelson et al., 2011) and/or the translocon (Hammadi et al., 2013; Van Coppenolle et al., 2004). A recent study in goblet cells, another polarized epithelial cell type, found that spontaneous cytosolic Ca^{2+} oscillations requiring ryanodine receptor (RyR) Ca^{2+} channels provide a steady-state signal acting as a tonic brake to mucin granule exocytosis (Cantero-Recasens et al., 2018). In this case, however, the Ca^{2+} sensor was apparently KChIP3 localized to pre-exocytic secretory granules. Much remains to be learned about steady-state ER Ca^{2+} signals and their effectors throughout the secretory pathway.

Since IP3 receptors, during agonist-driven Ca^{2+} signaling, contribute to PEF protein-mediated regulation of ER export, we wondered whether spontaneous Ca^{2+} signals regulated by IP3Rs at steady state might also contribute to setting the basal ER export rate. Here we demonstrate that normal rat kidney (NRK) epithelial cells participate in intercellular Ca^{2+} waves (ICWs) that move back and forth across the monolayer under normal growth conditions. Depletion of IP3R-3, the major IP3R isoform in NRK cells, potentiates the remaining IP3Rs, causing greater participation in Ca^{2+} oscillations and ICWs in the absence of added agonists. Furthermore, this increased activity leads to more ALG-2 and Sec31A and less peflin at ERES, and increases the basal ER export rate of the COPII cargo VSV-G_{ts045} by up to 60%. Recruitment of more Sec31A to ERES by ALG-2 was client cargo dependent, suggesting that ALG-2 may cooperate with the sorting function of COPII. Indeed, more detailed studies indicated that the increased ER secretion was driven by greater capture and concentration of COPII client cargo at ERES at the expense of bulk flow cargo.

3.2 RESULTS

3.2.1 IP3R-3 Depletion Caused Potentiation of Agonist-Dependent Ca^{2+} Signaling

To perturb the pattern of Ca^{2+} oscillations under steady-state growth conditions, we focused on depletion of the IP3R-3 isoform. Previous literature indicated that the IP3R-3 isoform is anti-oscillatory in HeLa, COS, and NRK fibroblast cell lines (Almirza et al., 2010; Hattori et al.,

2004; Zhang et al., 2011). However, some literature suggests that decreased overall IP3R channel density should decrease basal signaling (Hattori et al., 2004). Thus, empirical documentation of effects on Ca^{2+} handling in NRK epithelial cells (ATCC CRL-6509) was essential. To characterize the expression of IP3R isoforms in NRK cells, immunoblotting was performed using antibodies to all three individual IP3R isoforms - IP3R-1, IP3R-2, and IP3R-3. Both IP3R-1 and IP3R-3 were readily detectable in NRK extracts, but IP3R-2 was undetectable (data not shown). To determine the ratio of IP3R-1 and IP3R-3 in NRK cells, qRT-PCR was carried out on NRK cell total RNA using isoform-specific primers. As shown in Figure 7A, IP3R-3 was the major isoform, representing 67% of all IP3R subunits; the ratio of IP3R-3:IP3R-1 was thus 2:1 in NRK cells. Using siRNA, IP3R-3 could be depleted by 77% (Figure 7B). Though there was detectable co-depletion of IP3R-1, the ratio of R-1:R-3 isoforms was dramatically shifted toward R-1. The IP3Rs form both functional homo-tetramers and functional hetero-tetramers (Stutzmann & Mattson, 2011; Zhang et al., 2011). Hence, IP3R-3 depletion would eliminate most IP3R-3 homo-tetramers and IP3R-3-containing hetero-tetramers, leaving mostly IP3R-1 homo-tetramers, while constituting about one-third of the normal number of channels.

To indicate whether IP3R-3 depletion led to more promiscuous cytosolic Ca^{2+} signaling, we first tested whether the remaining IP3R channels displayed potentiated responses to IP3-generating agonists. As demonstrated in Figure 7C, which displays representative FURA cell traces, most NRK cells responded to 1 µM bradykinin with a single synchronous surge of Ca^{2+} followed by a fall-off in Ca^{2+} during the ensuing 2-3 minutes (colored traces). About 20% of cells did not visibly respond (black trace), and cells with multiple, distinct oscillations were infrequently seen (not shown). Figure 7D-F displays results of systematic comparisons of control and IP3R-3-depleted cells using the bradykinin protocol from part C. Notably, as shown in Figure 7D, a significantly greater percentage of IP3R-3-depleted cells responded to bradykinin, raising the participation rate from ~80 % to ~95 %. Additionally, as shown in Figure 7E, IP3R-3- depleted cells responded with significantly higher amplitude Ca^{2+} surges than control cells, represented by a ~40 % increase in peak amplitude. We also integrated the entire Ca^{2+} response, from onset of signaling until returning to baseline, among responding cells only, which demonstrated a highly significant ~20 % increase in Ca^{2+} release (Figure 7F). In summary, Figure 7 C-F indicates

that IP3R-3 depletion caused increased Ca^{2+} signals during the synchronous response to high doses of an IP3-generating agonist.

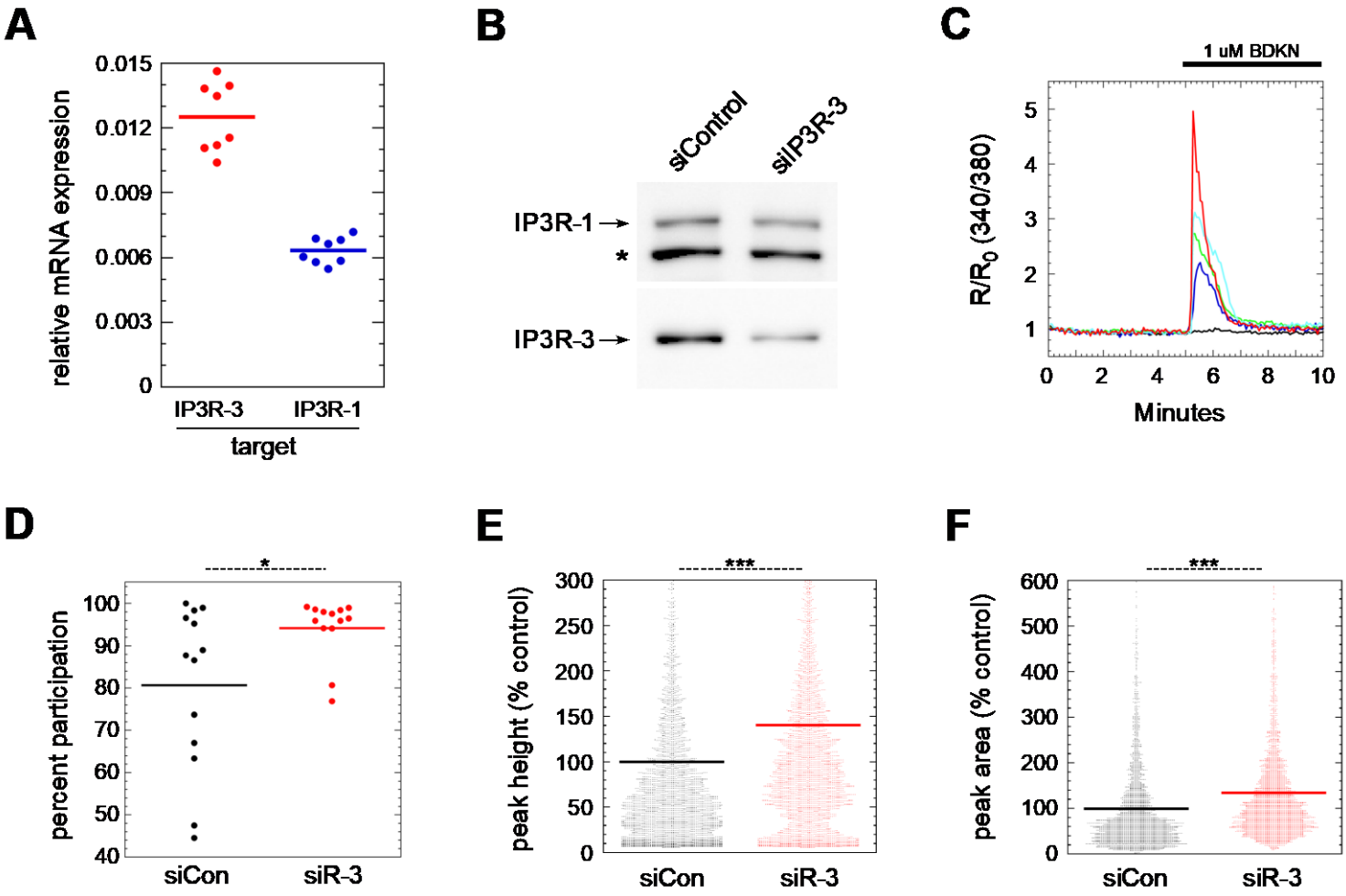

Figure 7. IP3R-3 depletion potentiates agonist-dependent Ca^{2+} signaling. (A) Expression ratio of IP3R-1 and IP3R-3 in NRK cells analyzed by qRT-PCR. The quantity of each target RNA is normalized to that determined for GAPDH in parallel reactions. **(B)** Verification by immunoblot of IP3R-3 depletion using siRNA. Asterisk marks an unknown nonspecific band recognized by the anti-IP3R-1 antibody. **(C)** FURA-2 cytosolic Ca^{2+} recording of 5 control NRK cells in one field upon stimulation with 1 µM extracellular bradykinin (BDKN). Four cells displayed cytosolic Ca^{2+} signals of varying sizes while one (black trace) remained inactive. **(D)** Quantitation of the percentage of cells per field responding to BDKN stimulation as in (C). Each field contained a total of ~300 cells. **(E,F)** Quantitation of peak height (defined as change from average baseline value) (E) and peak area (F) from traces of BDKN-challenged cells. Results in (E) contain all cells while (F) includes only the BDKN-responsive cells. Results in (D-F) consist of three replicate experiments combined. Cells were defined as BDKN-responsive in (D) and (F) if their peak height was ≥0.1. In (E,F), each dot represents one cell (N≈4000 cells per condition). p-values for two-tailed Student T-tests with unequal variance are indicated above; * = $p \le .05$; ** = $p \le .005$; *** = $p \le .0005$.

3.2.2 IP3R Depletion Caused Increased Spontaneous Ca^{2+} Oscillations and Participation in Intercellular Ca^{2+} Waves

To characterize basal Ca^{2+} signals in unstimulated NRK cells, we monitored cytoplasmic Ca^{2+} in NRK cells using the Ca^{2+}-sensitive dye FURA-2AM; cells were recorded for 20 min at 37 °C in regular growth medium containing 10% FBS in the absence of added agonists. As illustrated by representative individual cell traces in Figure 8A, some cells displayed a short burst of Ca^{2+} oscillations during the 20-minute interval. We created individual traces for all 514 cells in the image field, and determined that 52 cells or 10.1% displayed at least one burst of signaling; each burst contained 1-6 distinct oscillations in which each oscillation persisted for about 1 minute. Though it was not technically feasible to monitor for longer periods, we assume that over longer time intervals the majority of NRK cells would display similar episodes of spontaneous Ca^{2+} signaling.

Intercellular coordination of Ca^{2+} signaling was typically observed in these recordings. Coordination took the form of groups of contiguous or nearby cells that oscillated almost precisely in unison. Furthermore, in most cases successive groups of activated cells would spread laterally over time, creating waves of high Ca^{2+} that traversed the monolayer. Figure 8B shows a group of 338 cells containing the same cells plotted in Figure 8A, with their individual locations marked. Figure 8C displays the same group of cells at several distinct timepoints during the recording with the $R_{340/380}$ ratio displayed using a heatmap for contrast. In detail, cell 26 initiated a major Ca^{2+} wave at t = 04:44, when cells 118 and 126 joined and oscillated in unison a few seconds behind cell 26. Five to ten cells at a time then oscillated together in successive groups that led upward and to the right across the field, culminating in cells 238, 241, 282 and others oscillating in unison at t = 7:44 before the wave moved further rightward and out of view. This signaling propagation across a monolayer has been observed in a variety of cell types and has been termed intercellular Ca^{2+} waves (ICWs). The mechanism and functions of ICWs are not well understood; they can be driven by both cell-to-cell diffusion of Ca^{2+} and IP3 through gap junctions and also by paracrine purinergic signaling (PPS) involving vesicular and non-vesicular release of the Ca^{2+} agonist ATP (Leybaert & Sanderson, 2012). While we did not investigate the mechanisms of NRK cell ICWs further, we speculate that one relevant

consequence of ICWs is that they may help amplify and normalize cell participation in spontaneous, steady-state Ca^{2+} signaling.

We compared control and IP3R-3-depleted NRK cells for their participation in spontaneous, steady-state Ca^{2+} signaling using recordings similar to that described above. Each of the 300-500 cells in the view area of each run was analyzed using a semi-automated workflow in ImageJ and R that generated individual Ca^{2+} traces that could be rapidly scrolled through for manual scoring; each trace was scored for the number of spontaneous Ca^{2+} oscillations, from which the percentage of cells participating in oscillations was derived for each run. As shown in Figure 8D, which represents scoring of ~23,000 cells in 49 individual runs, IP3R-3-depleted cells exhibited significantly higher cell participation in spontaneous signaling, increasing about three-fold, from 5.5% to 16% cell participation during each 20-minute period. Though it was not possible to objectively score ICWs per se, a majority of recordings displayed groups of cells oscillating synchronously, indicating that intercellular coordination or spread of Ca^{2+} oscillations may be a major driver of participation in basal Ca^{2+} signaling in NRK cells. The specific recording shown in Figure 8A-C is highlighted in the composite plot (2D) with a cyan halo. While this recording displayed the linear cell-to-cell spread of signaling unusually clearly, it was not remarkably active in terms of cell participation, which ranged much higher among IP3R-3- depleted cells. We also compared the number of oscillations per cell among participating cells between control and IP3R-3-depleted cells, and found that there was a trend toward greater numbers of oscillations in IP3R-3-depleted cells (Figure 8E). In conclusion, IP3R depletion caused increased spontaneous Ca^{2+} oscillations, facilitated through ICWs.

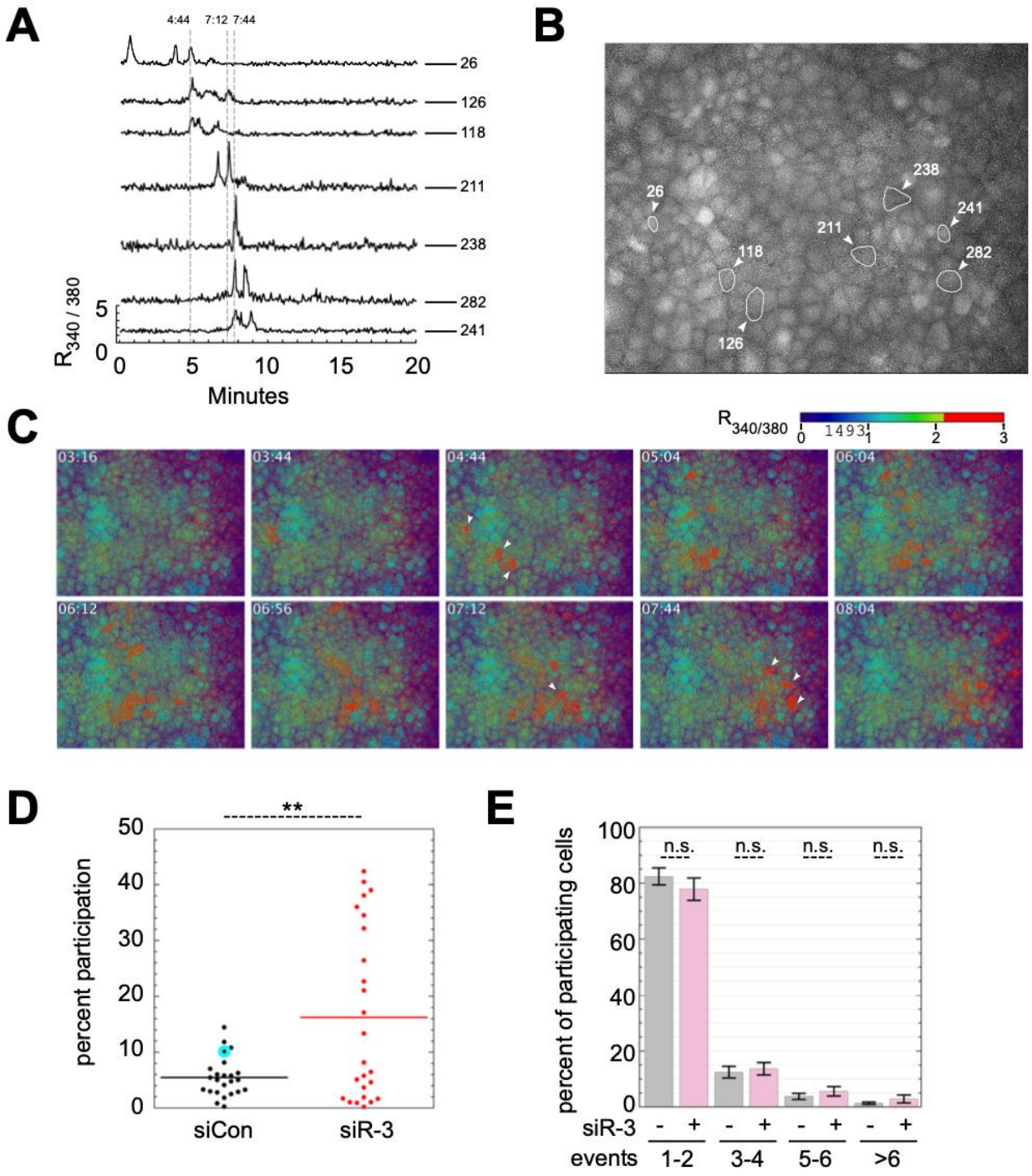

Figure 8. IP3R-3 depletion caused increased spontaneous Ca^{2+} oscillations. (A) Individual FURA-2 cytosolic Ca^{2+} traces of 7 control NRK cells in one field. **(B)** Group of 338 cells containing the same cells plotted in A, with their individual locations marked. **(C)** $R_{340/380}$ heatmap of field in (B) at distinct timepoints. White arrows indicate position and time of major cytosolic Ca^{2+} signals in cells from (A). **(D)** Quantitation of cells participating in spontaneous cytosolic Ca^{2+} signals during the 20-minute imaging period as in (A), with each dot summarizing a run of ~440 cells (49 individual runs, N=~23,000 cells). The particular run shown in (A-C) is highlighted in cyan. **(E)** Quantitation of number of oscillations per cell from (D), as percent of all cells with oscillations. p-values for two-tailed Student T-tests with unequal variance are indicated above; * = $p \leq .05$; ** = $p \leq .005$; *** = $p \leq .0005$. Error bars show SEM.

3.2.3 Effects of IP3R-3 Depletion on ER Ca^{2+} Stores

We also characterized ER luminal Ca^{2+} stores in control and IP3R-depleted cells using D1ER, a genetically encoded ER luminal FRET-based Ca^{2+} sensor (Palmer et al., 2004). As shown by representative traces in Figure S1A, upon addition of ionomycin and EGTA to live NRK cells, R/R_0, which for the first five minutes has a value near 1, quickly plunged and approached an R_{min}/R_0 value; R_{min}/R_0 ranged from ~0.75 (for control cells) to ~0.85 (for IP3R-depleted cells). The difference between the initial R/R_0 and R_{min}/R_0–or $\Delta R/R_0$–was interpreted to represent the resting ER luminal Ca^{2+} concentration of the cell. As shown in Figure S1B, which combines cells from multiple replicate experiments, $\Delta R/R_0$ was 28 % smaller in IP3R-depleted cells, indicating a lower resting ER Ca^{2+} concentration. To verify the conclusion using a different approach, we used an irreversible sarco-endoplasmic reticulum Ca^{2+} ATPase (SERCA) inhibitor, 1 µM thapsigargin (Tg), to release all ER Ca^{2+}, and then measured the magnitude of the resulting cytoplasmic Ca^{2+} surge in NRK cells transfected with the genetically encoded FRET-based cytosolic Ca^{2+} sensor D3cpv (Palmer et al., 2006). As shown in Figure S1C and D, IP3R-3-depleted NRK cells displayed smaller Ca^{2+} releases, by 33%, upon Tg addition, consistent with the conclusion from direct luminal measurements (parts A and B) that ER Ca^{2+} stores were ~30% reduced in IP3R-3- depleted cells. We also used a similar Tg addition protocol together with a genetically encoded FRET-based mitochondrial matrix Ca^{2+} sensor, 4mtD3cpv (Palmer & Tsien, 2006), and found that mitochondria took up less Ca^{2+} upon release of ER Ca^{2+} in IP3R-depleted cells (data not shown). Together these experiments indicate that, for reasons that are not obvious, depletion of IP3R-3 in NRK cells results in partial reduction of ER Ca^{2+} stores. We do not believe the increased spontaneous signaling was responsible, though we cannot eliminate that mechanism. Further speculations on the molecular cause of the Ca^{2+} store reduction are offered in the Discussion.

3.2.4 IP3R Depletion Down-Regulates PEF Protein Expression but Does Not Alter Expression of Multiple Other Trafficking Machineries

To begin the examination of IP3R-3 depletion effects on ERES and ER-to-Golgi transport, we asked whether IP3R depletion changed expression of trafficking machinery proteins. In

particular, one could imagine that altered ER Ca^{2+} handling could result in UPR activation which is known to increase expression of COPII-related components. We first examined relevant gene expression using qRT-PCR. As shown in Figure 9A, IP3R-3 knockdown did not significantly affect mRNA expression of COPII inner coat components Sec24A, B, C, or D, nor outer shell component Sec31A, nor ERES scaffolds Sec16A and B. There was perhaps a trend toward an increase of Sec24C, but it was not statistically significant and not supported by immunoblotting of cell extracts (see below). Overall, the qRT-PCR data did not support general up-regulation of ERES components as would be expected if basal UPR signaling were higher. In addition, we found that none of the UPR-related genes ATF6, CHOP, or Grp78 were affected by IP3R depletion. We found that ALG-2 and peflin were expressed at very similar levels and not affected by IP3R depletion at the transcript level. Finally, Bcl-2 transcripts were reduced by a highly significant ~30% upon IP3R-3 depletion; this demonstrates that IP3R-3 depletion influenced a gene product known to directly interact with and regulate the activity of IP3Rs (Chen et al., 2004). We complimented this analysis with immunoblotting of NRK cell extracts transfected with control or IP3R-3 siRNAs. As seen in Figure 9B, UPR mediators phospho-EIF2α, phospho-IRE-1 and ATF4 did not noticeably change upon IP3R depletion. Turning to the transport machinery, Figure 9C demonstrates no changes in coat subunits Sec31A, ß-COP, Sec24c, Sec23, the ER/Golgi tether p115, cargo receptors ERGIC-58 (labeled “p58”) and p24. These imply that IP3R depletion did not alter transport by changing expression of the required transport machinery. However, we also observed in immunoblots a small yet consistent decrease in both ALG-2 and peflin. This effect was quantified from multiple biological and technical replicates and displayed in Figure 9D, revealing on average a ~25% decrease in both proteins. Since mRNA levels were not affected (Figure 9A), it appears that this change occurs via a post-transcriptional mechanism. Note that concomitant reduction of both total cellular ALG-2 and peflin is not predicted to in and of itself significantly change ER-to-Golgi transport, since the two are still present in the same ratio. However, both proteins are high turnover proteins that are destabilized when not in the ALG-2-peflin heterodimer (Kitaura et al., 2002) which is disrupted by elevated Ca^{2+} (Kitaura et al., 2001). Hence, their reduced expression might reflect that the more dynamic cytosolic Ca^{2+}

environment in the IP3R knockdown condition creates greater flux between the ALG-2-containing complexes.

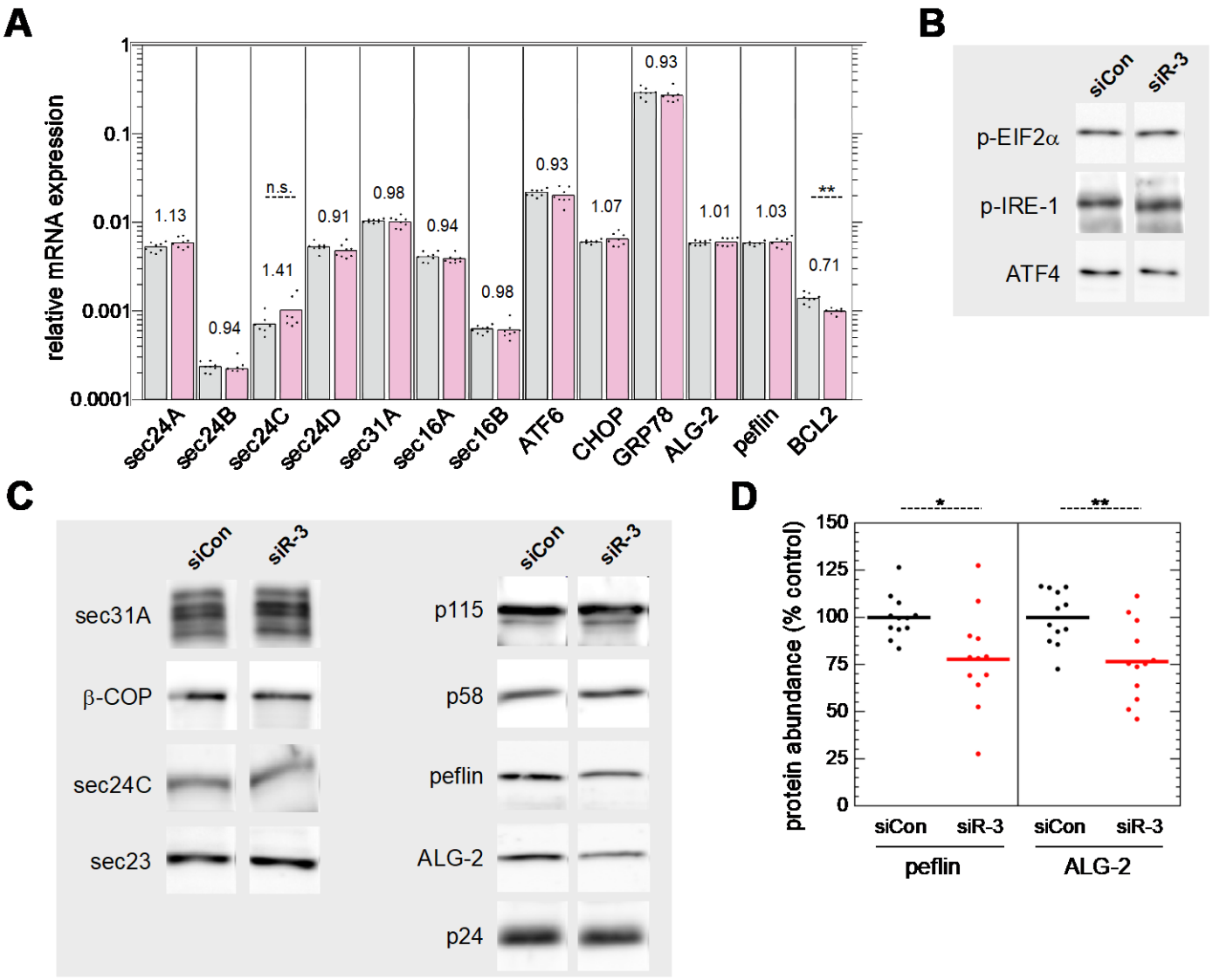

Figure 9. IP3R-3 depletion destabilizes ALG-2 and peflin but does not affect expression of other ER export machinery. (A) NRK cells were transfected with control (gray) or IP3R-3 (light red) siRNAs, grown for 48 h, lysed, and then mRNA was analyzed by qRT-PCR to detect expression of trafficking and other proteins. The quantity of each target RNA is normalized to that determined for GAPDH in parallel reactions. Value labels indicate the ratio of expression in siR-3 cells to that of control cells. **(B, C)** Immunoblots of ER stress proteins (B) and ER/Golgi trafficking machinery (C) in NRK cell extracts, 48 h after transfection with control or IP3R-3 siRNAs. No significant changes were observed, except for decreases in ALG-2 and peflin. **(D)** Quantitation of multiple technical replicates from several different experiments documented effects of IP3R-3 depletion on ALG-2 and peflin protein abundance. p-values for two-tailed Student T-tests with unequal variance are indicated above; * = $p \leq .05$; ** = $p \leq .005$; *** = $p \leq .0005$.

3.2.5 IP3R Depletion Causes Increased ALG-2 and Sec31A, but Decreased Peflin Targeting to ERES

The mild destabilization of ALG-2 complexes during IP3R-3 depletion (Figure 9D) led us to ask whether ALG-2 and peflin targeting to ERES was altered, since this could alter COPII coat targeting and thus ER export. ALG-2 binds Sec31A at ERES either as a peflin-ALG-2 heterodimer, or as the ALG-2 homodimer. While the homodimer is generally stimulatory, the ALG-2-peflin heterodimer is inhibitory (Sargeant et al., 2021). We carried out immunofluorescence of endogenous ALG-2, peflin, and Sec31A on control and IP3R-3-depleted NRK cells. For a non-COPII-related marker of ERES we used rBet1, an ER/Golgi SNARE whose distribution is mostly restricted to ERES and ERGIC elements (Hay et al., 1998). Representative images of cells are shown in Figure 10A-C. We segmented the labeling patterns into discrete objects by thresholding and then used Boolean image math to measure the areas of objects and areas of co-localization between objects representing different proteins in the same cell (Rayl et al., 2016; Sargeant et al., 2021). As shown in Figure 10D, when IP3R-3 was depleted, co-localization between peflin and rBet1 objects decreased by ~25%. The decreased co-localization was comprised of both a decrease in the percentage of total peflin objects that colocalized with rBet1, and a decrease in the percentage of total rBet1 objects that co-localized with peflin (data not shown); this reciprocity of effects, which was also true in parts E and F, establishes a true decrease in co-localization that could not result from mere changes in labeling intensity or expression. At the same time, co-localization between ALG-2 and rBet1 significantly increased by ~35% in IP3R-3-depleted cells (Figure 10E). Focusing on the outer coat, we found that the co-localization area of Sec31A and rBet1 increased by ~50% upon IP3R-3 depletion (Figure 10F). The expansion of Sec31A-rBet1 overlap most likely indicates that more outer coat was recruited to ERES, consistent with past work concluding that ALG-2 ‘stabilized’ the outercoat at ERES (Shibata et al., 2010; Yamasaki et al., 2006). Taken together the immunofluorescence changes during IP3R depletion– decreased peflin, increased ALG-2, and increased Sec31A recruitment to ERES–indicate that the increased steady-state Ca^{2+} signaling was sufficient to trigger changes to ALG-2 targeting in a pattern shown previously to increase ER-to-Golgi transport rates (Rayl et al., 2016; Sargeant et al., 2021).

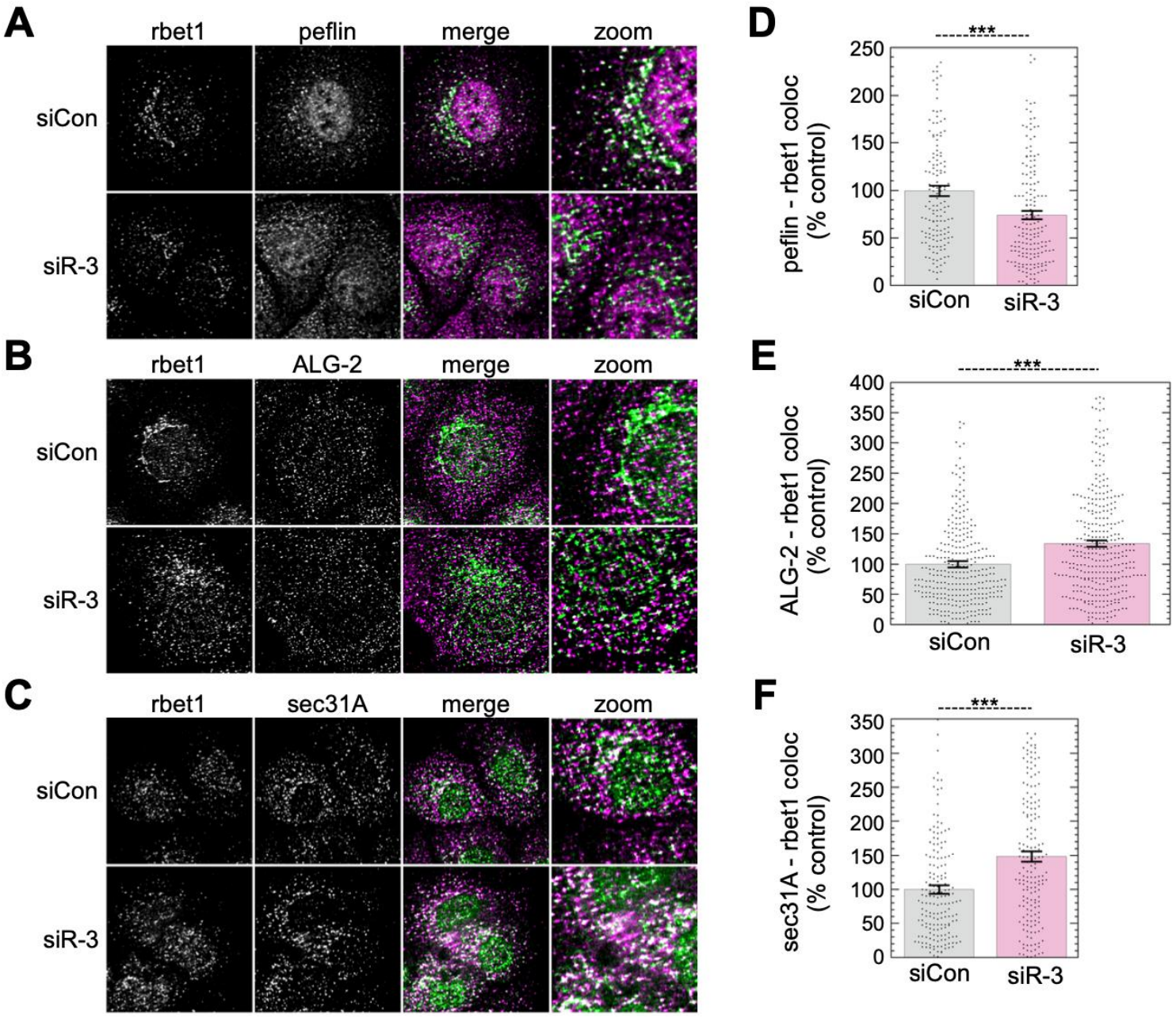

Figure 10. IP3R depletion causes a decrease in peflin and increases in ALG-2 and sec31A at ERES. (A-C) NRK cells were transfected with the indicated siRNAs. After 48 h, cells were fixed and immunolabeled for endogenous rbet1, peflin, ALG-2, or sec31A, as indicated. Representative micrographs are shown. **(D-F)** Object analysis on ~150 cells (D, F) or ≥300 cells (E) per condition to quantify overlap area between rbet1 objects and the other labeled proteins. p-values for two-tailed Student T-tests with unequal variance are indicated above; * = $p \leq .05$; ** = $p \leq .005$; *** = $p \leq .0005$. Error bars show SEM.

3.2.6 Depletion of IP3R-3 Adjusts ER-to-Golgi Transport in a Cargo-Specific Manner

To test the effects of IP3R-3 depletion on ER-to-Golgi cargo transport, we used an intact-cell transport assay (Helm et al., 2014; Rayl et al., 2016; Sargeant et al., 2021; Thayanidhi et al., 2010) employing three different synchronized release mechanisms for the transmembrane COPII client cargo VSV-G as well as a synchronized bulk-flow cargo. Cargo was released from the ER for 10 minutes, after which the cells were fixed, and a transport index was calculated consisting of the intensity of the cargo in the Golgi divided by the intensity remaining in the ER. For the GFP-tagged VSV-G constructs, we employed: 1) temperature-sensitive GFP-VSV-G_{ts045} which traffics following shift from 41 to 32 °C; 2) GFP-FM_4-$VSVG_{tm}$, which contains a luminal GFP and controlled aggregation domain connected to the wildtype VSV-G transmembrane domain and cytoplasmic C-terminus (Sargeant et al., 2021). Here, addition of the highly specific ligand D/D Solubilizer causes dissociation of large cargo assemblies allowing packaging into COPII vesicles (Rivera et al., 2000; Seiler & Hay, 2022). 3) RUSH-VSV-G-GFP (Boncompain et al., 2012; Boncompain & Perez, 2013), which traffics after added biotin outcompetes binding of the construct to an ER-localized streptavidin “hook”. For the bulk-flow cargo, we employed GFP-FM_4-hGH, an entirely luminal construct containing the controlled aggregation domain and hGH and no known functional sorting motif. Figure 11A shows example images and illustrates the morphological principle of the assay. Importantly, as demonstrated quantitatively in Figure 11B, knockdown of IP3R-3 resulted in up to a 60% acceleration of the ER-to-Golgi transport rate of all three VSV-G constructs. In parallel, IP3R-3 depletion decreased trafficking of the bulk flow construct by ~25%. The use of three distinct VSV-G constructs eliminates the possibility that structural rearrangements required for any particular synchronization method, for example folding or disaggregation kinetics, are required to generate the transport differences. The cargo specificity of the effects (GFP-FM_4-VSV-G_{tm} vs. GFP-FM_4- hGH) is identical to that caused by direct activation of ALG-2 in basal Ca^{2+} through siRNA depletion of its inhibitory subunit peflin (Sargeant et al., 2021), and thus supports that ALG-2 drives the phenomenon. While the cargo specificity could be indicative of changes in COPII cargo sorting, it could also be indicative of distinct trafficking pathways.

We also tested the effects in a live-cell assay which generated a kinetic transport timecourse for each cell. In this experiment, we employed GFP-FM_4-VSV-G_{tm}. At 37 °C 4 minutes after addition of D/D solubilizer, the cargo was restricted to the ER in both control and IP3R-3-depleted cells (Figure 11C, “4”). Cargo first became visible in the Golgi 6-7 minutes following ligand addition and accumulated more or less linearly for the subsequent 15 minutes. Upon quantitation of 40 cells per condition from sequential runs, it became clear that the IP3R-depleted population contained many more high-transporting cells, while the control cells contained many more low-transporting cells (Figure 11D). Furthermore, upon close examination of the timecourses at t=4 to t=10 m, it became clear that transport in the control cells exhibited a longer lag between ligand addition and the linear accumulation phase of cargo in the Golgi (Figure 11E). While the eventual slopes of the transport curves were also different, the pronounced difference at the onset of transport implies that the secretory machinery functioned at a higher level from the start of the reaction. Direct effects on an early step in transport such as cargo sorting or ER export are fully compatible with the ER-to-Golgi kinetics we observed.

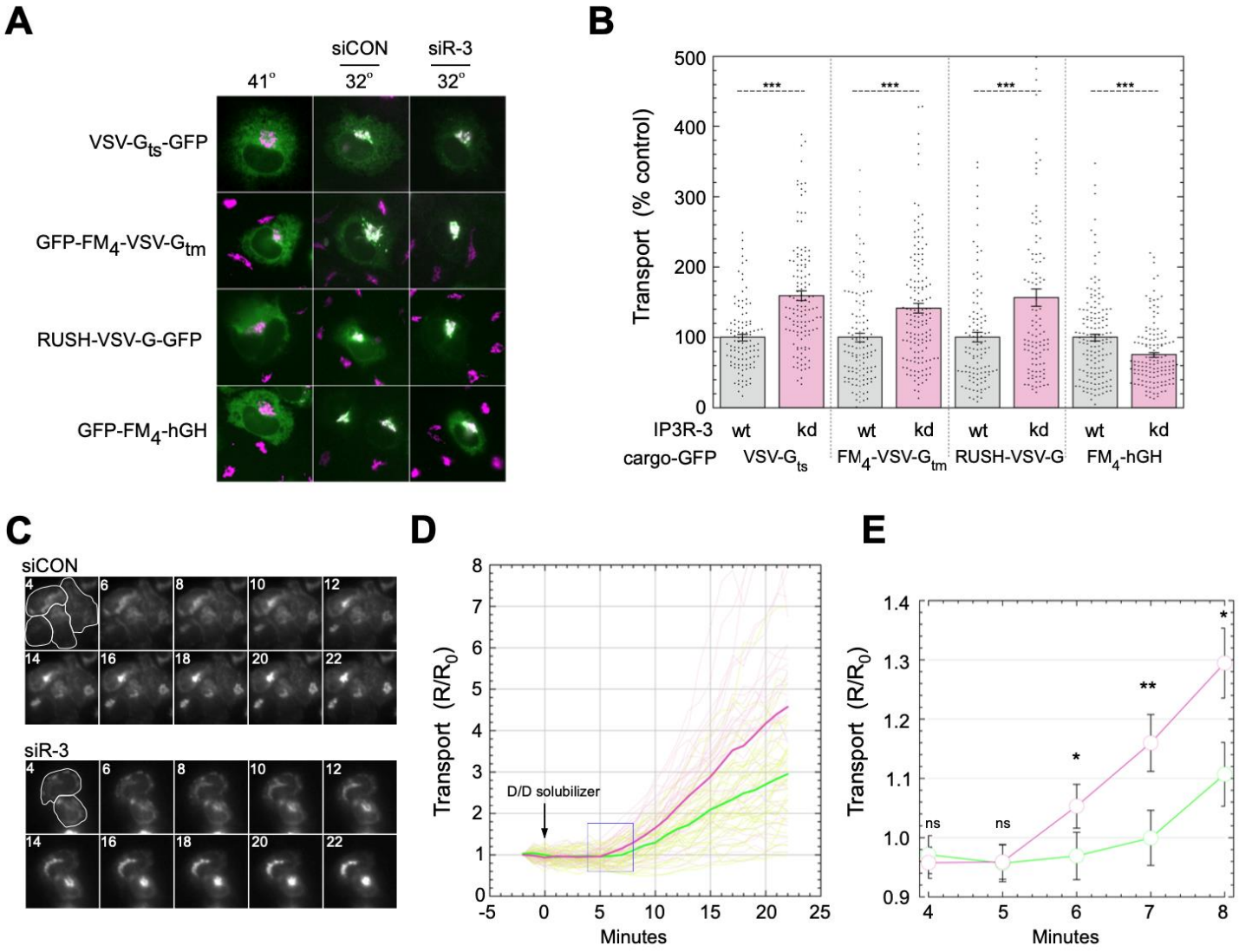

Figure 11. Expression of IP3R-3 regulates ER-to-Golgi transport in unstimulated NRK cells. (A) Representative images of NRK cells from the ER-to-Golgi transport assay quantified in B. NRK cells were transfected with VSV-G$_{ts045}$-GFP with or without siRNAs as indicated. Following growth at 41 °C for 48 h, cells were shifted to 32 °C for 10 min, to permit transport, prior to fixation. Fixed cells were immuno-labeled with mannosidase II and imaged by widefield microscopy; VSV-G-GFP and mannosidase II channels are displayed for each cell. **(B)** Each transfected cell was assigned a transport index representing trafficking of VSV-G based upon the ratio of Golgi to peripheral green fluorescence. The transport index of each individual cell is plotted. 200-300 cells were randomly quantified from each condition, and results shown are representative of at least three experiments with consistent trends. **(C-E)** A live-cell transport assay employing control and IP3R-3 siRNAs and the FM$_4$-VSV-G$_{tm}$ cargo. **(C)** Representative cells imaged in the GFP channel; cell outlines are show on the first panel and minutes post addition of D/D solubilizer are indicated on each. **(D)** R/R$_0$ traces of NRK cell transport indexes from a live-cell ER-to-Golgi transport assay. Individual cell traces are shown as faint lines while average traces are shown in bold. Control and siIP3R-3 are shown as green and red, respectively. Transport index as in (B) was calculated at each timepoint and expressed as a ratio to the initial value for each cell. N=40 cells per condition. **(E)** Closer view of average traces from (D) showing first timepoints with measurable ER-to-Golgi transport. p-values for two-tailed Student T-tests with unequal variance are indicated above; * = p ≤ .05; ** = p ≤ .005; *** = p ≤ .0005. Error bars show SEM.

3.2.7 The Increased Transport of VSV-G Requires ALG-2 and Increased Cytosolic Ca^{2+} Signals

Since ALG-2 binds Sec31A in response to Ca^{2+} signaling (la Cour et al., 2007; Shibata et al., 2007), we tested whether ALG-2 is required for the increased transport observed in IP3R-3-depleted cells. As shown in Figure 12A and quantified in Figure 12B, IP3R-3 depletion in otherwise wildtype cells increased transport by ~60% (bars 1 vs. 2), consistent with Figure 11. However, in ALG-2-depleted cells, depletion of IP3R-3 caused no further significant effect (bars 3 vs. 4, p=.257). This is the result expected if ALG-2 is required to mediate the increased transport due to IP3R depletion; ALG-2 is epistatic to IP3R-3 for transport effects. Loss of ALG-2 itself is slightly stimulatory in otherwise normal cells (bars 1 vs. 3), and slightly inhibitory in IP3R-3-depleted cells (bars 2 vs. 4). Hence it appears that the increased Ca^{2+} signaling in IP3R-depleted cells switched ALG-2 influence from that of a net inhibitor to that of a net stimulator of ER export.

Since ALG-2 is a cytosolic Ca^{2+} sensor, the data so far imply that the increased frequency of cytosolic Ca^{2+} oscillations upon IP3R-3 depletion causes ALG-2 to raise the basal secretion rate. However, the reduced luminal Ca^{2+} observed earlier (Figure S1) could present a challenge to the interpretation of effects on ER export, since it cannot be eliminated that a reduced luminal Ca^{2+} store per se could somehow regulate the transport machinery by an unknown mechanism. If this were the case, comparably reduced luminal Ca^{2+} stores would still stimulate transport, even without depletion of IP3Rs and increased Ca^{2+} oscillations. We experimentally created such a condition by treating cells with very low levels of thapsigargin–two orders of magnitude below the concentrations typically used to induce UPR. As shown in Figure 12C and D, 6 nM Tg for 24 hours resulted in partial depletion of luminal Ca^{2+} similar to that caused by IP3R-3 siRNA, while at 10 nM, the Tg caused greater depletion. We used 24 hours to simulate any potential long-term effects on secretion as well as to get well beyond any stimulatory effects caused by the initial wave of released ER Ca^{2+}. We then tested the effects of these partial ER Ca^{2+} depletions on ER-to-Golgi transport. As shown in Figure 12E, there were no significant effects on ER-to-Golgi transport at 6 nM Tg, but ~20% inhibition of transport became apparent at 10 nM Tg. Inhibition of ER-to-Golgi transport under conditions of strong ER depletion is

expected from our previous results (Bentley et al., 2010; Helm et al., 2014). The lack of transport effects at 6 nM demonstrates that partial luminal Ca^{2+} depletion for ~24 hours does not cause the increased transport observed in IP3R-depleted cells. In conclusion, the data favor the interpretation that increased spontaneous cytosolic Ca^{2+} oscillations, and not the lowered Ca^{2+} store, primarily drives the ALG-2-dependent ERES changes that result in increased transport when IP3R-3 is depleted.

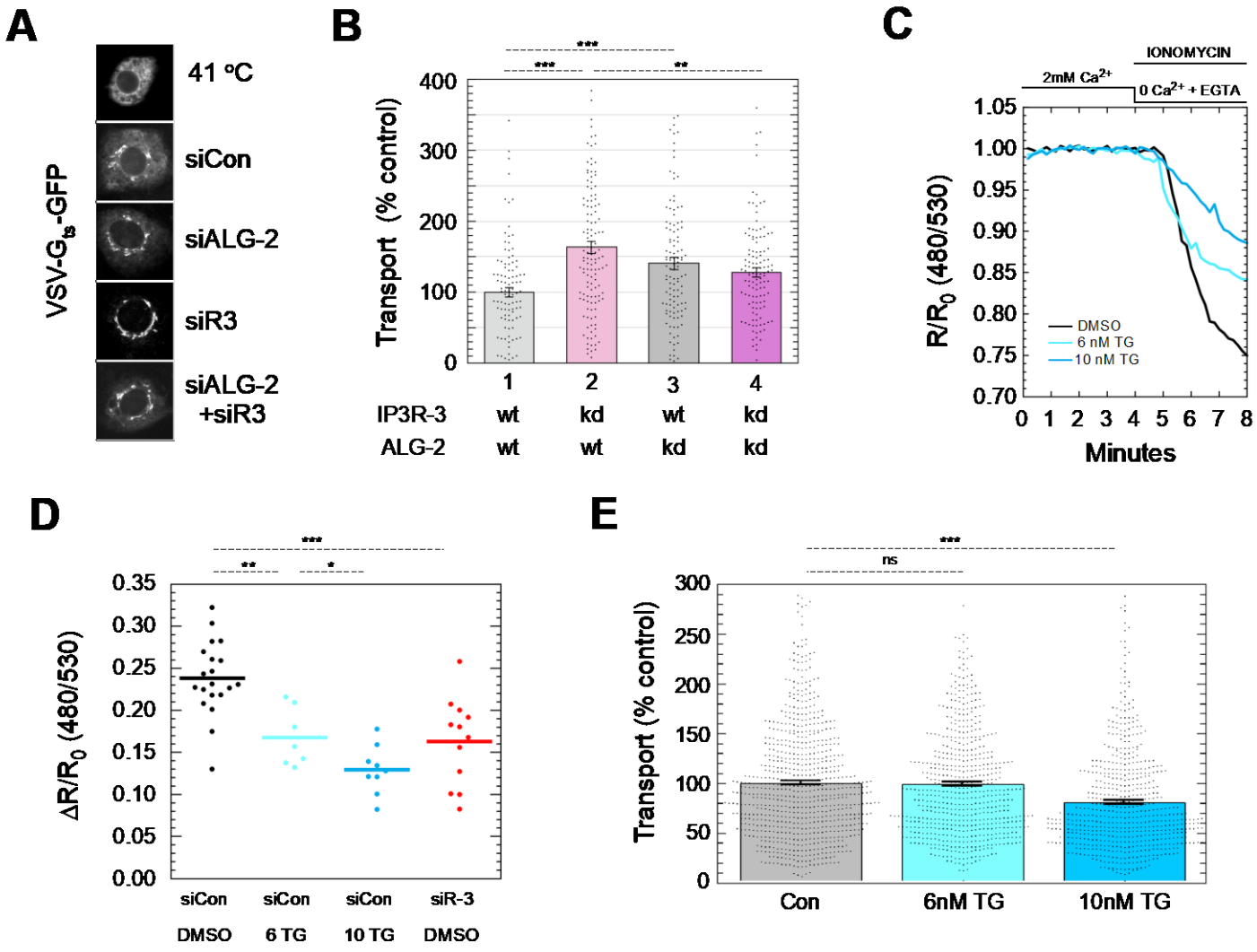

Figure 12. The increased transport of VSV-G requires ALG-2 and is not caused by decreased luminal Ca^{2+} stores. (A) Representative GFP images from a 10-min transport assay in NRK cells using VSV-G_{ts}-GFP cargo and siRNA. **(B)** Quantitation of ER-to-Golgi transport as in Figure 11B. **(C)** Example luminal Ca^{2+} depletion traces from representative live cells using the ER FRET-based Ca^{2+} sensor D1ER. Ca^{2+}, ionomycin, and EGTA are added and withdrawn using continuous perfusion as indicated above. The emission ratio for CFP and YFP was determined using 430 nM illumination at each timepoint and expressed as a ratio to initial value. Cells were treated with the indicated TG concentration for 24 h prior to assay. **(D)** Drop in FRET ratio between 0 and 8 min was determined as in part C for several cells per run in multiple runs in cells treated with TG as in (C) or with IP3R-3 siRNA. **(E)** NRK cells were treated with the indicated concentrations of TG as in parts (C) and (D) and subjected to a standard 10-min ER-to-Golgi transport assay using VSV-G_{ts}-GFP cargo. p-values for two-tailed Student T-tests with unequal variance are indicated above plots; * = p ≤ .05; ** = p ≤ .005; *** = p ≤ .0005. Error bars show SEM.

3.2.8 ALG-2 Activation Produces Higher Concentrations of VSV-G at ERES

If ALG-2 increased sorting stringency for client cargo, one would expect client cargo to be more concentrated in ERES prior to export. Early in a transport reaction, it is difficult to quantify cargo specifically at ERES due to the very high level of cargo throughout the entire ER. In one alternative approach, we allowed cargo to accumulate significantly at ERES during a temperature block. At 10 °C, VSV-G_{ts045} can fold and be loaded into ERES in a coat-dependent manner, but vesicle budding and further steps in transport cannot occur (Mezzacasa & Helenius, 2002). We activated ALG-2 Ca^{2+} -dependently by IP3R-3 depletion or Ca^{2+} -independently by depleting its inhibitory subunit peflin (Rayl et al., 2016; Sargeant et al., 2021), and then allowed VSV-G_{ts}-GFP to accumulate for 1 hr at 10 °C. As shown in Figure 13A, this resulted in prominent accumulations of cargo in spots that mostly co-localized with Sec31A. Cargo was visualized using GFP fluorescence as well as immunofluorescence using the I14 conformation-sensitive monoclonal antibody specific for conformationally mature VSV-G trimers (Lefrancois & Lyles, 1982), which agreed well with GFP fluorescence. It appeared that cargo spots were brighter in IP3R-3-depleted and Peflin-depleted cells than in control cells, which was confirmed by quantitation of spot prominence. As shown in Figure 13B, spot prominence of GFP fluorescence was significantly increased by 100% in IP3R-3-depleted cells and 125% in Peflin-depleted cells. Spot prominence was defined as the maximum intensity of each spot divided by the mean intensity of a doughnut-shaped ROI immediately surrounding but excluding the spot. Total GFP fluorescence in the same set of cells was not significantly different (Figure 13C). Parallel standard ER-to-Golgi transport assays at the permissive temperature demonstrated qualitatively similar effects (Figure 13D), suggesting that concentration of cargo at ERES may account for the effect on overall transport. In sum, this experiment demonstrates that at 10 °C, activated ALG-2 drives higher concentrations of a client cargo at ERES.

In a distinct approach that did not rely on a transport block, we returned to the conformation-specific anti-VSV-G monoclonal antibody, I14. Using immunoprecipitation with I14, we previously demonstrated that VSV-G_{ts045} in NRK cells completely folds and assembles into trimers within 3 minutes upon shift to the permissive temperature (Helm et al., 2014), while others have used more detailed velocity sedimentation approaches to reach similar

kinetic conclusions (Doms et al., 1987). Here, we characterized I14 immunofluorescence properties during ER-to-Golgi transport. Using our standard ER-to-Golgi transport assay with VSV-G_{ts045}-GFP at t=10 minutes, we found that GFP and trimer fluorescence did not match, unlike above during accumulation of trimer at 10 °C. Instead, during transport it appeared that trimer labeling lacked most of the general ER component and greatly emphasized cargo accumulations at ERES (Figure 13E, magenta arrows). When the transport assay was quantified separately in both channels (GFP and trimer), we found that both channels reported increased transport in cells depleted of IP3R-3 and in cells depleted of the ALG-2 inhibitory subunit peflin (Figure 13F, left plot). However, the trimer channel reported transport indices that were consistently about two-fold higher. Individual components comprising the transport index–Golgi and ER fluorescence–revealed that the higher transport indices reported by the trimer were indeed driven primarily by decreased detection of VSV-G in the general ER (Figure 13F, right plot). Since VSV-G_{ts045} completes folding within ~3 minutes, it would be expected that I14 should detect the yet-to-be transported, trimerized VSV-G remaining in the ER, as observed during the 10 °C experiment (Figure 13A). The fact that it does not implies that perhaps I14 preferentially recognizes densely concentrated VSV-G trimers such as those present on the virion surface used as immunogen (Lefrancois & Lyles, 1982). When trimers build up in the ER to high concentrations, such as at 10 °C, they are labeled by I14, however ongoing export at the permissive temperature must keep trimer concentrations in the ER below the threshold for I14 detection via immunofluorescence.

Since I14 can be used to visualize and quantify VSV-G at ERES that are otherwise difficult to detect due to excess unpackaged VSV-G, we used this technique to characterize the kinetics of VSV-G_{ts045} initial appearance at ERES after shift to the permissive temperature. Figure 13G displays the kinetic curve of the appearance of VSV-G spots in the I14 channel normalized to total VSV-G from the GFP channel. VSV-G appears at spots within seconds of temperature shift, and reaches a near-maximal steady-state value within ~1 minute. To identify the I14-labeled early transport intermediates in detail, we compared the I14 spots to endogenous Sec31A. As shown in Figure 13H, the I14 spots at 60 seconds following temperature shift frequently colocalize with Sec31A, though not every I14 spot was positive for this marker. Finally, to

quantify the relative density of trimers at ERES for cells with activated ALG-2, we performed 60-second incubations at the permissive temperature followed by fixation and immunostaining. As shown in Figure 13I, depletion of IP3R-3 or peflin to activate ALG-2 caused significantly greater intensity of spotty labeling in the trimer channel in cells with similar VSV-G expression indicated by the GFP channel. When this effect was quantified, we found that depletion of IP3R-3 caused an increase of 50% relative to control in cargo intensity at ERES, while depletion of peflin produced an 80% increase (Figure 13J). Figure S2A demonstrates that there were no significant differences in cargo expression levels between the same cells quantified in Figure 13J, and Figure S2B shows a standard 10-min transport assay on parallel coverslips of cells on the same day as the assay in 13J. Altogether this experiment indicates that during transport, ALG-2 activation drives significantly greater concentration of cargo at ERES, an effect that could explain the higher transport rate.

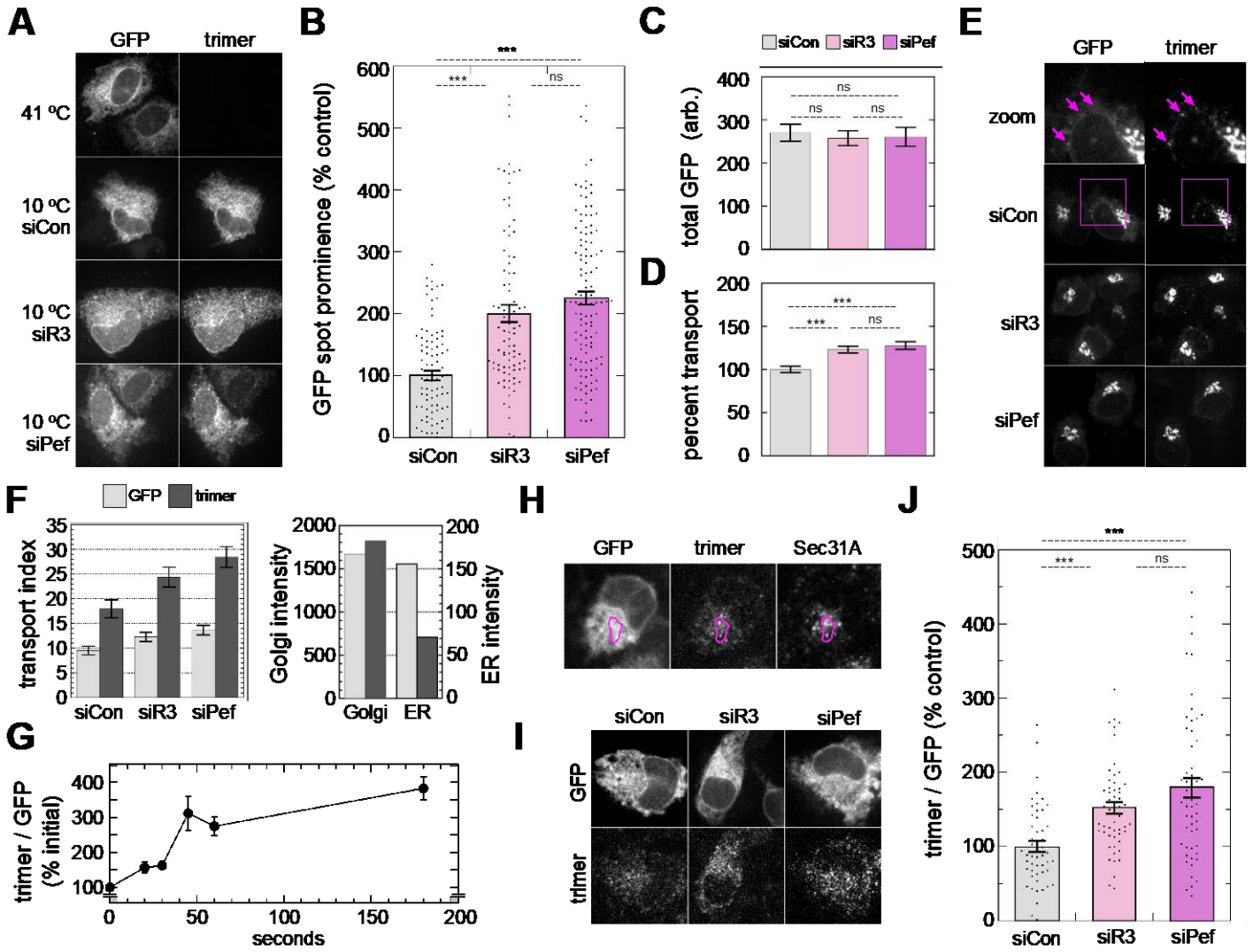

Figure 13. ALG-2 activation drives higher concentrations of VSV-G at ERES. (A) NRK cells transfected with the indicated siRNAs and VSV-G_{ts}-GFP cargo were either kept at 41 ºC or incubated at 10 ºC for 1 hr prior to fixation and immunostaining with the I14 VSV-G conformation-specific antibody. Shown are the GFP channel (left) and trimer-specific channel (right) of the same cells. **(B)** Quantitation of GFP spot prominence in cells from (A). Spot prominence is defined as the maximum intensity of each spot divided by the mean intensity of the area immediately surrounding the spot (see methods). **(C)** Quantitation of GFP intensity of the entire cytoplasmic area (nucleus excluded) of the same cells quantified in (B). **(D)** Standard 10-min transport assay on parallel coverslips from the same experiment as (B). **(E)** 10-min ER-to-Golgi transport assay using the indicated siRNAs and VSV-G_{ts}-GFP cargo. Images show GFP channel (left) and trimer-specific channel (right) of the same cells. Arrows indicate puncta prominent in the trimer channel that are weaker or absent in the GFP channel. **(F)** *Left,* quantitation of the transport assay from (E) with raw transport index values shown from the GFP and trimer channels. *Right*, individual components of the transport assay; Golgi intensity is plotted on the left y-axis while ER intensity is plotted in the right y-axis. Plotted values represent the average of all the siRNA conditions shown on the left plot. **(G)** Timecourse of appearance of trimer immunostaining upon switch from 41 ºC to 32 ºC. Trimer intensity of the entire cytoplasmic area was normalized the GFP intensity of the same area to counteract differences in transfection efficiency. **(H)** Colocalization at 60-sec of GFP, trimer, and Sec31A. ROI highlights area containing examples of precise (bottom) as well as imperfect (top) co-localization of trimer and Sec31A fluorescence. **(I)** 60-sec following shift to 32 ºC, cells that had been transfected with the indicated siRNAs and VSV-G_{ts}-GFP were fixed and immunolabeled with trimer-specific antibody. Representative cells are shown in the GFP (top) and trimer (bottom) channels. **(J)** Quantitation of cells from (I) using the same method as in (G). p-values for two-tailed Student T-tests with unequal variance are indicated above plots; * = p ≤ .05; ** = p ≤ .005; *** = p ≤ .0005. Error bars in all panels show SEM.

3.2.9 ALG-2 Activation Increases COPII Sorting Stringency Through Interactions with Sec31A

To understand the relationship between ALG-2, Sec31A, and cargo sorting, we employed a double-knockdown approach using IP3R-3 and Sec31A siRNAs and added multiple cargoes to the experiment. As shown in Figures 14A and B, for VSV-G_{ts045}-GFP, depletion of IP3R-3 in otherwise normal cells caused increased ER-to-Golgi transport, as previously documented. In Sec31A-depleted cells, however, IP3R-3 depletion caused no significant change in transport. To the contrary, for the bulk-flow cargo GFP-FM_4-hGH, depletion of IP3R-3 in otherwise normal cells caused a decrease in cargo trafficking, but in Sec31A-depleted cells, IP3R-3 depletion caused no significant change in transport. Thus, neither COPII client nor bulk-flow cargo are affected by IP3R-3 depletion when ER export is operating without Sec31A. Together with Figure 12A&B, this experiment demonstrates that the effects of basal Ca^{2+} signaling on transport require both Sec31A and ALG-2. In the same cells that were assayed for VSV-G or hGH transport, we concomitantly assayed the intensity of Sec31A immunofluorescence. When Sec31A is recruited from the cytosol to ERES, the mean cytoplasmic Sec31A intensity increases due to greater concentration of the antigen at ERES. As shown in Figure 14C, Sec31A recruitment in cells expressing VSV-G increased significantly upon IP3R-3 depletion (bars 1 vs. 2). However, in cells expressing hGH, we detected no change in Sec31A (bars 5 v. 6). Importantly, this indicates that the presence of client cargo affects whether ALG-2 activation impacts Sec31A recruitment/retention at ERES. ALG-2 activation does not result in extra Sec31A recruitment unless an abundant client cargo is present, indicating that ALG-2 may enhance the mechanism by which the inner and outer coat sense and together retain cargo. We speculate that in the case of over-expression of the client or bulk-flow cargo constructs, the effects of endogenous cargos on Sec31A targeting were minimized.

It was somewhat unexpected that depletion of Sec31A, though very inhibitory to VSV-G transport, did not block it more completely. It has been found in yeast that expression of proteins that render the membrane more deformable can suppress the requirement for the COPII outer shell (Čopič et al., 2012). We also showed in NRK cells that ≥95% depletion of Sec31A with siRNA results in a 40% increase in expression of sec23 (Helm et al., 2014), an

essential member of the COPII inner coat. On the other hand, Sec31B could account for at least some of the residual transport. Indeed, we found that Sec31B was expressed in NRK cells and that its depletion caused a 15% inhibition of transport (Figure 14D). When combined with Sec31A depletion–which in this experiment caused 25% inhibition–Sec31B depletion caused an additional 15% inhibition, indicating that Sec31B contributes to transport in the absence of Sec31A. Immunoblots and additional siRNAs are shown in Figure S2 C-E. Knockdown of either Sec31 isoform caused over-expression of the other isoform, and KD of Sec31B strongly affected the mix of splicing isoforms of Sec31A. The lack of effects on transport by IP3R-3 depletion when Sec31A is also depleted (Figure 14B, bars 3 vs. 4 and 7 vs. 8) indicates that ALG-2 activation may not impact Sec31B. As shown in Figure 14E, Sec31B indeed lacks conservation to rat Sec31A residues 870-882, which are nearly identical to human residues 839-851, the necessary and sufficient ALG-2 binding site (Shibata et al., 2010). Hence, a lack of effects of ALG-2 activation on Sec31B-supported transport is in fact predicted. Another conclusion from the experiment in Figure 14A and B is that both VSV-G and hGH rely upon Sec31A to the same degree for ER-to-Golgi transport, despite their undergoing opposite changes in transport upon IP3R-3 depletion (Figure 14B, bars 1 vs. 3 and 5 vs. 7). This demonstrates that the bulk flow cargo follows the same Sec31A-dependent pathway for transport that client cargo does. However, upon ALG-2 activation, COPII "chooses" VSV-G to the detriment of hGH. There is growing evidence that sorting involves the physical exclusion of non-client-cargo due to molecular crowding (Gomez-Navarro, Melero, et al., 2020; Ma et al., 2017). The higher Ca^{2+} environment does not merely enhance Sec31A function generally, leading to more vesicle transport of all cargoes, but rather increases the sorting stringency of COPII for client cargoes.

To more directly address the role of ALG-2 in COPII cargo sorting, we employed the drug 4- phenylbutyrate (4-PBA), which has been shown to specifically occupy the cargo-binding B-site on Sec24, occluding client cargo to cause client cargo-selective inhibition of budding (Ma et al., 2017). We reasoned that if ALG-2 activation were primarily affecting cargo sorting, then 4-PBA should neutralize any ALG-2 effects on ER-to-Golgi transport. We performed our standard transport assay and used peflin depletion to activate ALG-2. As shown in Figure 14F and G, peflin depletion produced the expected results on transport in the absence of 4-PBA; it

stimulated VSV-G-GFP transport by 50% (part G, bars 1 vs. 2) and inhibited GFP-FM_4-hGH transport by 20% (bars 5 vs. 6). Interestingly, the addition of 4-PBA to otherwise wildtype cells caused reciprocal results, with 4-PBA inhibiting VSV-G transport by 70% (bars 1 vs. 3) and stimulating hGH transport by 30% (bars 5 vs. 7). Stimulation of bulk-flow ER-to-Golgi transport by 4-PBA is predicted based upon its ability to cause secretion of ER resident proteins (Ma et al., 2017) and its ability to rescue plasma membrane localization of ER-retained quality control substrates (William E. Balch et al., 2008). However, to our knowledge, it has not been directly observed before in kinetic measurements of ER-to-Golgi transport. A recent study with several cargos demonstrated that 4-PBA selectively inhibited secretion to the medium of client cargos without effects on bulk-flow cargos (Gomez-Navarro et al., 2022). Whether the stimulation of bulk flow is observed in any given experimental system may depend upon the particular cell type's secretory capacity, intensity of competition between endogenous client and bulk flow cargoes, as well as the expression level and secretory efficiency of the model bulk flow cargo.

Finally, in Figure 14G bars 3 vs. 4 and 7 vs. 8, we found that peflin depletion had no significant effect on transport of either cargo in the presence of 4-PBA. Thus, when cargo sorting at the B site on Sec24 is blocked, ALG-2 activation cannot alter secretion of any cargo. This eliminates many other potential roles for ALG-2 in transport. For example, though ALG-2 works through the outer shell component Sec31A, it must not significantly affect the rate of vesicle budding, per se, since this would still affect transport in the presence of 4-PBA. To illustrate the specificity of this result, we subjected our bulk-flow cargo to inhibition by depletion of syntaxin 5, an ER/Golgi SNARE required for homotypic fusion of COPII vesicles (Bentley et al., 2006). As shown in Figure 14H bars 1 vs. 2, syntaxin 5 depletion significantly inhibited ER-to-Golgi transport, as expected. Furthermore, as predicted, it also significantly inhibited transport in the presence of 4- PBA (bars 3 vs, 4), demonstrating that the experimental paradigm can distinguish distinct roles for ERES components. In conclusion, ALG-2 activation, caused by changes in basal Ca^{2+} oscillations or other perturbations, primarily acts to increase the stringency of client cargo sorting by the COPII coat.

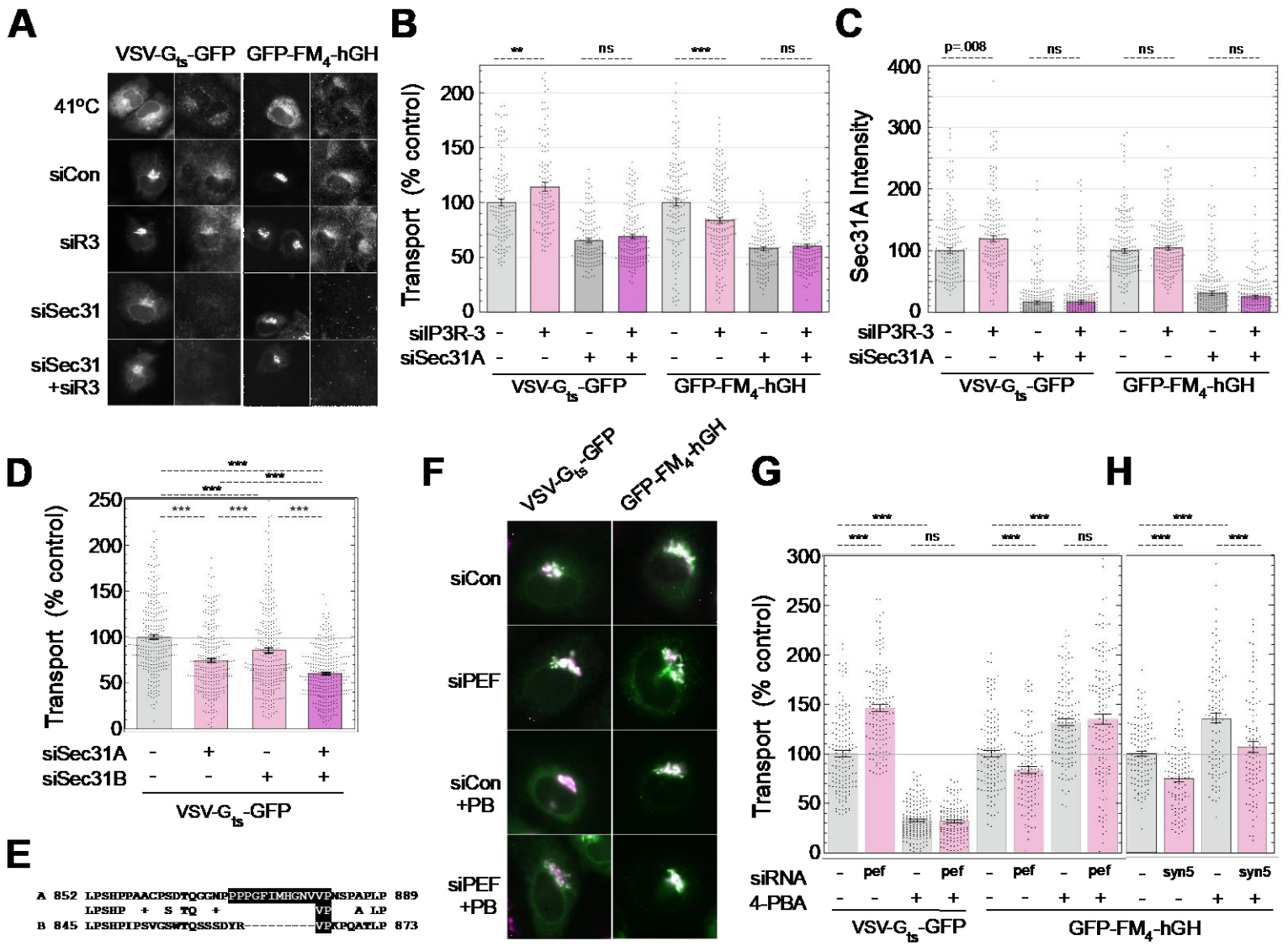

Figure 14. ALG-2 activation increases the stringency of COPII client cargo sorting through its interactions with Sec31A. (A) NRK cells were transfected with the indicated siRNAs and either VSV-G$_{ts}$-GFP or GFP-FM$_4$-hGH cargos, and subjected to a 10-min ER-to-Golgi transport assay, and immunolabeled for Sec31A. Shown are the GFP channel (left panel of each pair) and the Sec31A channel (right). **(B)** Quantitation of ER-to-Golgi transport as in Figure 11B. **(C)** Quantitation of whole-cell Sec31A intensity from the same cells quantified for transport in (B). **(D)** *Left,* quantified 10-min ER-to-Golgi transport assay on cells transfected with the indicated siRNAs and VSV-G$_{ts}$-GFP cargo. **(E)** Alignment of rat Sec31A and Sec31B surrounding the necessary and sufficient ALG-2 binding site for Sec31A (black shaded residues). **(F)** NRK cells were transfected with control or peflin siRNAs as indicated and VSV-G$_{ts}$-GFP or GFP-FM$_4$-hGH cargos. 10-min transport assays were conducted in the presence or absence of 10 mM 4-PBA as indicated. Shown are merged images of the GFP and mannosidase II as in Figure 11A. **(G)** Quantitation of the transport assay shown in (F). **(H)** A follow-up control transport assay in which syntaxin 5 siRNA was substituted for peflin siRNA to illustrate specificity of 4-PBA for the sorting step in transport. p-values for two-tailed Student T-tests with unequal variance are indicated above plots; * = p ≤ .05; ** = p ≤ .005; *** = p ≤ .0005. Error bars show SEM.

3.3 DISCUSSION

3.3.1 Mechanism of Effects on ER-to-Golgi Transport

This work elucidates a role for background Ca^{2+} signals in setting the rate and specificity of ER export by modulating the activities and/or targeting of the PEF proteins ALG-2 and peflin at ERES. Specifically, this work discovered that ALG-2 activation drives higher concentrations of client cargo at ERES (Figure 13) and increases the stringency of COPII cargo sorting (Figure 14). These conclusions are based solely on functional transport measurements in intact cells, and will hopefully stimulate structural investigations to understand precisely how ALG-2 influences COPII cargo sorting. As noted earlier, the ALG-2 binding site on Sec31A (human Sec31A residues 839-851; (Shibata et al., 2007)) is just N-terminal to the "active peptide" region (residues 981-1015) containing Trp-995 and Asn-996 that insert into the Sar1 active site to potentiate the Sec23 GAP activity that contributes to sorting (Bi et al., 2007; Shaywitz et al., 1997). We here note two distinct and non-exclusive mechanisms by which ALG-2 could regulate sorting. 1) ALG-2, in binding the PRR region, changes its conformation to render higher affinity interactions with the inner coat. Experimental support for this includes a previous study that found ALG-2 dramatically increased physical interactions between the outer and inner coat without directly bridging them (la Cour et al., 2013). Since that study involved purified COPII components and ALG-2, there were no other ERES sites to which ALG-2 could have been anchored or targeted. 2) ALG-2 could help deliver, restrain or "place" the active peptide in the vicinity of Sar1, thus increasing its local concentration to favor more frequent interactions with the inner coat pre-budding complex causing more frequent Sar1 GTPase cycles. In this model ALG-2 acts as an adaptor between the PRR region and another ERES component. Experimental support for this includes frequent observations that ALG-2 stabilizes Sec31A on the membrane (la Cour et al., 2013; Sargeant et al., 2021; Shibata et al., 2010; Yamasaki et al., 2006) and the observations that ALG-2 can target an inhibitor peptide, comprised of an isolated ALG-2 binding region to an apparently saturable site at ERES to block ER export (Helm et al., 2014). A variant of the adaptor mechanism that apparently satisfies all of the experimental observations noted would be that ALG-2 homodimers crosslink the Sec31A PRR to other Sec31A PRR molecules, possibly

nucleating a denser outer coat or alternatively making PRRs more potent or responsive to cargo by clustering them.

The precise mechanism of activation of ALG-2 by Ca^{2+} is still under investigation, though in vitro studies suggest that increased Ca^{2+} signals cause formation of ALG-2 homodimers at the expense of the ALG-2/peflin heterodimer (Kitaura et al., 2001) and favor homodimer binding to Sec31A over heterodimer; this explanation fits the prevailing concept that high Ca^{2+} favors binding of the ALG-2 homodimer to its various effectors (Maki et al., 2016). However, we also uncovered that decreases in peflin and ALG-2 protein abundance occur when IP3Rs are depleted (Figure 9). This suggests that Ca^{2+} may in addition regulate the species at ERES through altered stability or turnover of distinct PEF protein complexes. This hypothesis is supported by previous in vitro observations that heterodimer formation stabilizes both proteins against rapid proteasomal degradation (Kitaura et al., 2002), but that high Ca^{2+} causes dissociation of the heterodimer (Kitaura et al., 2001). A Ca^{2+} -dependent turnover mechanism of removing inhibitory heterodimers would also be consistent with the relatively slow onset of secretion changes following agonist-induced Ca^{2+} signaling, first detectable after 30 minutes and increasing over several hours (Sargeant et al., 2021). ALG-2 and peflin have also been implicated in Ca^{2+} -dependent ubiquitylation reactions at the ERES. Specifically, they were found to associate with $CUL3^{KLHL12}$ to ubiquitylate Sec31A to produce enlarged COPII structures in cells (Jin et al., 2012; McGourty et al., 2016). Both ALG-2 and peflin were required for the ubiquitylation which was proposed to be required for collagen secretion. However, neither ALG-2 nor peflin are required for secretory trafficking and peflin depletion increases collagen ER-to-Golgi transport in NRK cells (Sargeant et al., 2021). Furthermore, inhibition of CUL3 ubiquitylation activity with neddylation inhibitors did not affect collagen secretion, but instead $CUL3^{KLHL12}$ appeared to regulate ER-lysosome trafficking for degradation (Moretti et al., 2023). This also fits with recent observations that COPII and KLHL12 co-localized with procollagen at sites of non-canonical ER-phagy (Omari et al., 2018). Thus, $CUL3^{KLHL12}$ ubiquitylation of Sec31A does not appear to be acutely involved in production of COPII vesicles. However, this does not rule out a role for ubiquitylation in regulation of cargo export from the ER, potentially involving ALG-2 and/or peflin as adaptors. Sec23 de-ubiquitylation has a rate-limiting impact on secretion

in yeast though a ubiquitylation mechanism was not identified (Gomez-Navarro, Boulanger, et al., 2020).

3.3.2 IP3Rs and Steady-State Ca^{2+} Signals Regulate Protein Secretion From the ER

Here we demonstrated that unexpectedly, IP3R-dependent Ca^{2+} signals are a rate-limiting factor setting the basal secretion rate in resting epithelial cells under normal growth conditions. This adds to the previously reported role of IP3Rs in secretion, in which agonist-dependent activation of IP3Rs can either increase or decrease the secretion rate depending upon the intensity and duration of signaling (Sargeant et al., 2021). The new data demonstrates that periodic, spontaneous Ca^{2+} oscillations, facilitated in part by intercellular Ca^{2+} waves (ICWs), provide a stimulus that determines how much ALG-2 and peflin are bound at ERES, which alters COPII targeting, sorting stringency, and ER export.

One consequence of this work is that physiological factors known to affect Ca^{2+} oscillations or ICWs, such as Bcl-2 family protein expression (Eckenrode et al., 2010), presenilin-1 mutation (Müller et al., 2011), or gap junctions, hemichannel function, and purinergic receptor expression (Leybaert & Sanderson, 2012), may also regulate the secretion rate through this mechanism. Furthermore, we demonstrated that this phenomenon is sensitive to expression levels and/or the mix of isoforms of IP3Rs present, with lower expression levels of IP3R-3 isoform favoring more spontaneous signaling and higher secretion rates. Other Ca^{2+} channels known to regulate IP3Rs could also regulate secretion by modulating IP3R-driven oscillations. Other factors that affect IP3R expression and turnover include micro-RNAs (Ananthanarayanan et al., 2015; Takada et al., 2017), phosphatase and tensin homolog (PTEN) (Kuchay et al., 2017), BRCA1 associated protein (BAP1) (Bononi et al., 2017), nuclear factor erythroid 2–related factor 2 (NRF2) (Weerachayaphorn et al., 2015), and NF-κB (Franca et al., 2019). These factors could potentially regulate the secretory export rate through the mechanism presented here.

Physiological phenomena known to be driven by spontaneous Ca^{2+} signaling could have changes in ER export as part of their mechanism. These phenomena could include glial control of neurovascular diameter (Kuga et al., 2011; Kurth-Nelson et al., 2009), nephron formation

during kidney development (Fontana et al., 2019), and numerous aspects of neural proliferation, migration, and differentiation during neocortical development (Kuga et al., 2011; T. A. Weissman et al., 2004). While these phenomena involve spontaneous signaling, in most cases it is not known whether ICWs per se play a functional role. Retinal epithelial pigment cells are one cell type where ICWs have been established to regulate cell fate, influencing retinal development (Leybaert & Sanderson, 2012). Regulation of secretory output could be a significant effector mechanism by which ICWs alter cell fates in retinal or other cell types with ICWs. The biosynthetic secretory pathway is a rate-limiting determinant of plasma membrane and organelle biogenesis, plasma membrane composition, secretion of signaling molecules, and cell growth. Additionally, diseases associated with changes in IP3R expression, for example spinocerebellar ataxia (Takada et al., 2017), atherosclerosis (Dong et al., 2020), various liver disorders (Berridge, 2016), and multiple cancer types including uveal melanoma, mesothelioma (Mangla et al., 2020), colorectal carcinoma (Shibao et al., 2010), and breast cancer (Mound et al., 2017; Szatkowski et al., 2010), could also have a secretory component to their pathophysiology. The Ca^{2+} channel polycystin-2 (also called TRPP2) interacts with and regulates the IP3Rs (Kuo et al., 2014; Padhy et al., 2022; Sammels et al., 2010), and its dysfunction and disease pathology has been associated with excess constitutive secretion, in this case of extracellular matrix proteins (Le Corre et al., 2014). However, it should be noted that we have not tested whether other cell types besides NRK exhibit the strong link between spontaneous Ca^{2+} signaling and the secretion rate. Also note that “spontaneous” and “steady-state” are operational terms. We refer to spontaneous Ca^{2+} signaling as that which occurs in unperturbed cells growing in DMEM containing 10% FBS. The initiation of the signals could involve trace agonists, for example serotonin present in typical lots of FBS (Hamamori et al., 1988).

3.3.3 Roles of IP3Rs In Regulating the Luminal Ca^{2+} Store

The fact that IP3R depletion caused a mild reduction of luminal Ca^{2+} is challenging to interpret, since store-operated Ca^{2+} entry (SOCE) should be more than fast enough to compensate for the periodic Ca^{2+} oscillations we observed in resting NRK cells. One interpretation would be that IP3Rs play a specific role in SOCE in NRK cells. Indeed, a direct role

of IP3Rs in SOCE in Drosophila has been demonstrated (Chakraborty et al., 2016); however, their direct role in SOCE in mammalian cells, though widely discussed, is not well-supported (Thillaiappan et al., 2019). Though we did not pursue the mechanism of the effects on Ca^{2+} stores, control experiments in Figure 12 allowed us to determine that the changes in luminal Ca^{2+} caused by IP3R siRNAs did not drive the effects we observed on ER-to-Golgi transport.

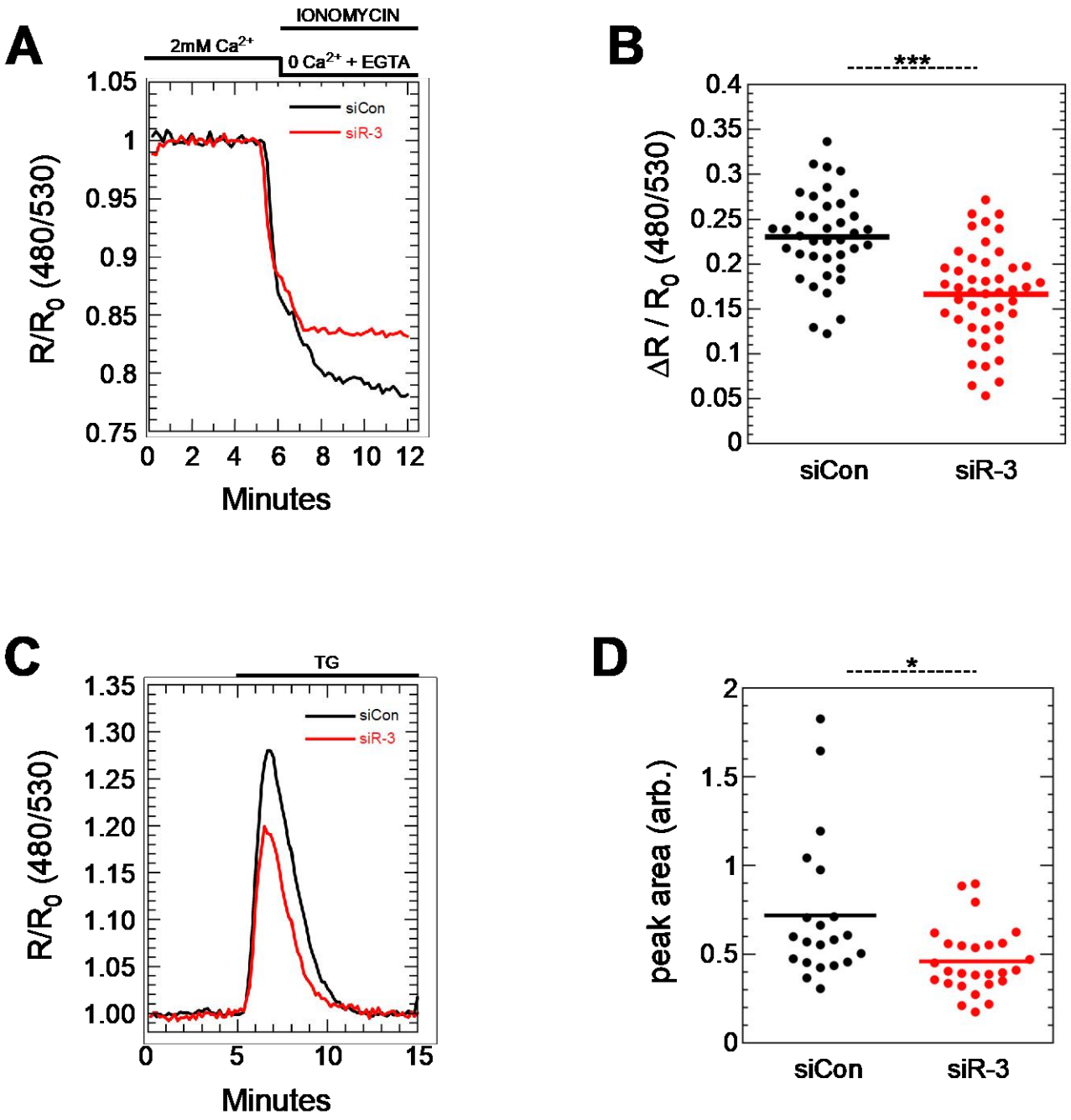

Figure S1. IP3R-3 depletion causes reduced ER luminal Ca^{2+} stores. (A) Representative traces of ER luminal Ca^{2+}, using the sensor D1ER, upon depletion with ionomycin and low Ca^{2+} medium. **(B)** Quantitation of the luminal Ca^{2+} drops in cells from three experiments of Ca^{2+} depletion traces as in (A). **(C)** Representative traces of cytosolic Ca^{2+}, using the sensor D3cpv, upon release of luminal Ca^{2+} stores by addition of thapsigargin to the extracellular medium. **(D)** Quantitation of cells from two experiments of the peak areas in traces as in (C). In (B) and (D), each dot represents one cell.

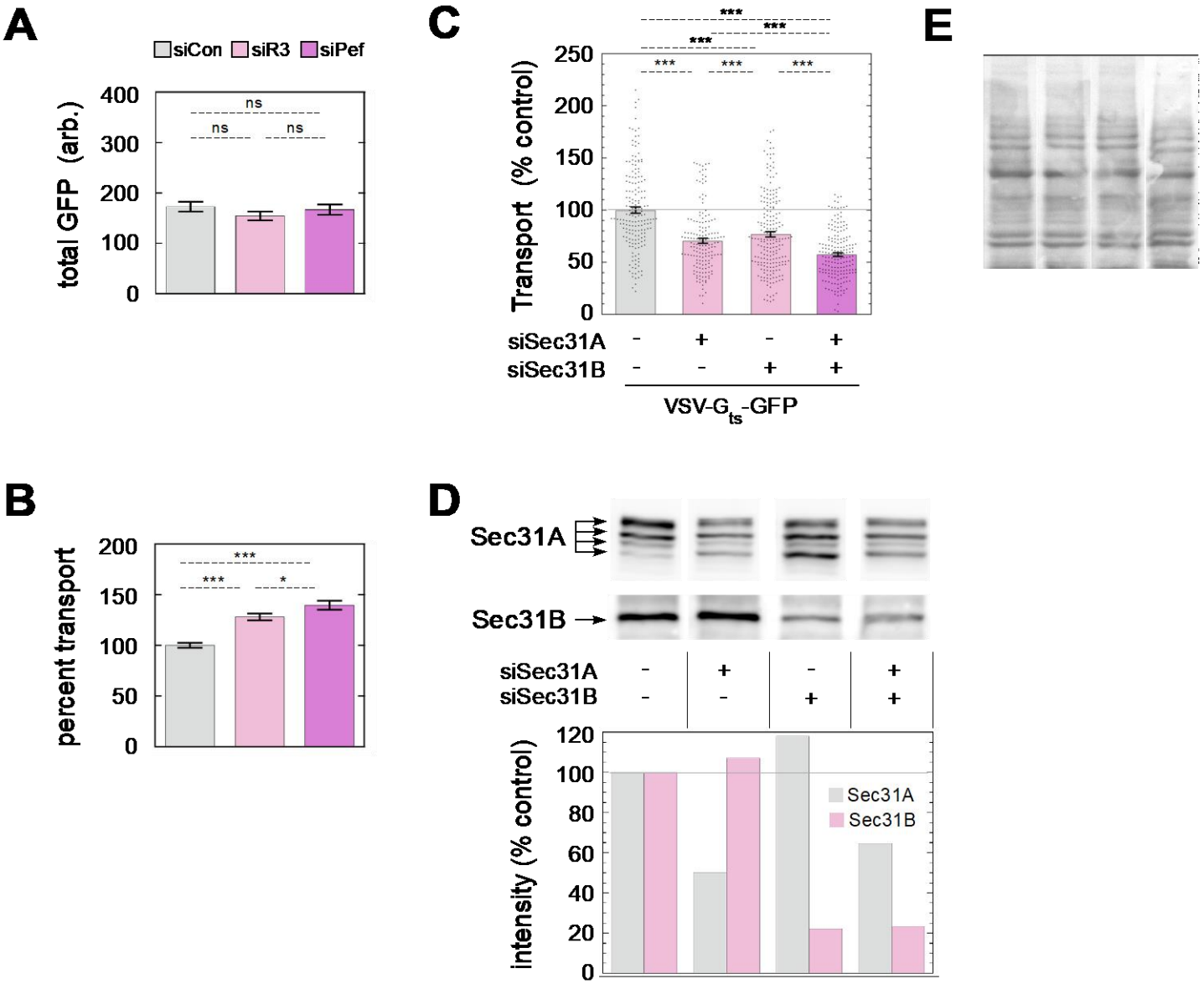

Figure S2. Additional controls for experiment in Figures 13J and 14D. (A) Quantitation of GFP intensity of the entire cytoplasmic area (nucleus excluded) of the same cells quantified in Figure 13J. **(B)** Standard 10-min transport assay on parallel coverslips from the same experiment as Figure 13J. **(C)** Repeat of transport assay from Figure 14D but using an entirely distinct Sec31B siRNA sequence. **(D)** Immunoblotting of cells from the experiment in Figure 14D (top) and quantitation of the blots (bottom). For Sec31A quantitation, all four indicated isoforms were included. The RefSeq database lists 17 predicted rat splicing isoforms of Sec31A, only the largest of which has been empirically documented. **(E)** Ponceau staining of the blot from (D) prior to immunoblotting. p-values for two-tailed Student T-tests with unequal variance are indicated above plots; * = $p \leq .05$; ** = $p \leq .005$; *** = $p \leq .0005$. Error bars show SEM.

CHAPTER 4:

ISOFORM SPECIFIC REGULATION OF ER PROTEOSTASIS BY IP3R-1

4.1 INTRODUCTION

As discussed in Chapter 1, Ca^{2+} is proposed to play an important role in the ER proteostatic environment. A number of ER protein chaperones require Ca^{2+} as a cofactor for their function, a fact that has led to the general assumption that the quality of the ER luminal folding environment tracks strictly with luminal Ca^{2+} concentration. However, many ER chaperones also require ATP in their functional cycle, highlighting the potential importance of ER ATP in the maintenance of luminal proteostasis. The interplay between Ca^{2+} and ATP dependence for chaperone functionality is best illustrated by BiP.

BiP alone has relatively poor Ca^{2+} binding capabilities, with a K_D of ~700 µM (Lamb et al., 2006). Considering that ER Ca^{2+} concentration usually rests at ~500 µM (Sargeant & Hay, 2022), ER luminal Ca^{2+} concentration can be a limiting factor in BiP Ca^{2+} binding. However, BiP K_D values for Ca^{2+} binding are ~40-fold and ~880-fold lower with saturating levels of ATP and ADP respectively. Ca^{2+} binding also influences BiP binding to ATP and ADP, lowering the K_D ~11-fold and ~930-fold respectively (Lamb et al., 2006). This demonstrates the dynamic interplay between Ca^{2+} and ATP/ADP binding to BiP. ATP/ADP are required for the functional BiP cycle described in Chapter 1. BiP requires Ca^{2+} to bind ATP/ADP, but it also requires ATP/ADP in order to bind Ca^{2+} in the first place.

The mechanisms of ER Ca^{2+} homeostasis were discussed in Chapter 1, but the ATP role in protein homeostasis raises the important question: how does the ER get ATP? There are no known ATP generating systems within the ER lumen, therefore, ATP must be supplied from external sources. Yet decades of previous work had failed to identify an ER membrane ATP transporter. Then in 2018, Klein et al. discovered that the previously noted nucleotide-sugar transporting protein, SLC35B1, is actually highly specific for ATP/ADP and works as an antiporter, bringing ATP into the ER lumen while forcing ADP out. This newly discovered function led SLC35B1 to be renamed ATP/ADP exchanger in ER membrane (AXER). They found that AXER depletion decreases ER ATP levels and BiP activity. Interestingly, AXER can be immunoprecipitated with MAM components including IP3Rs, implying that it may play a functional role at that microdomain (Klein et al., 2018). Subsequent examination by Yong et al.

found that the ATP being transferred by AXER comes from the mitochondria, as opposed to from glycolysis, further implicating AXER as a MAM component (Yong et al., 2019). These studies thus proposed that MAMs function as a two-way communication between the ER and mitochondria in which ER Ca^{2+} is transferred to the mitochondria to facilitate ATP synthesis and mitochondrial ATP is transferred to the ER lumen where it is utilized in protein folding. In support of that hypothesis, Yong et al. also found that cells experiencing ER stress communicate more Ca^{2+} to mitochondria, theoretically in an attempt to alleviate the proteostatic burden (Yong et al., 2019).

Since IP3Rs represent the main Ca^{2+} communication mechanism in MAM functionality, we wondered if manipulation of IP3R expression might influence ER stress. Additionally, since IP3R isoforms seem to have differential influence on MAM functionality (Kuo et al., 2019; Mendes et al., 2005), we wondered if the isoforms differentially affect ER stress. Notably, we discussed in Chapter 1 how knockdown of IP3R-3 had no noticeable effect on ER stress in NRK cells, even though it elicited a decrease in ER luminal Ca^{2+}. We therefore decided to examine the effect of knocking down the other NRK IP3R isoform, IP3R-1, while comparing the effects to IP3R-3 depletion. Here we present a series of preliminary experiments that suggest an isoform specific role for IP3Rs in the maintenance of ER protein homeostasis in NRK cells. We show that, though depletion of either isoform results in ER-to-Golgi transport changes, a slight ER luminal Ca^{2+} depletion, and an increase in ER-mitochondria membrane contacts, IP3R-1 depletion displays an isoform specific suppression of UPR activation. We propose a model in which IP3R-1 depletion shifts the Ca^{2+} signaling characteristics towards that of the remaining IP3R-3, more effectively communicating Ca^{2+} to the mitochondria via MAMs to stimulate ATP transfer to the ER lumen and protecting against proteostatic stressors. As noted above, these results are preliminary, and we therefore recognize the need for significant additional study to fully characterize the phenotype presented here. Caveats, knowledge gaps, and alternative interpretations will be discussed. Future directions will be discussed in Chapter 5.

4.2 RESULTS

4.2.1 Depletion of Either IP3R Isoform Affects ER-to-Golgi Transport and ER Luminal Ca^{2+} Concentration

We established in Chapter 3 that IP3R-3 depletion causes a variety of downstream effects, eventually resulting in an increase in ER-to-Golgi transport of COPII client cargo. It was unclear whether the increased transport was due to a generalized decrease in IP3R density, or was an isoform-specific phenomena. We posited that, because IP3R-3 is the anti-oscillatory IP3R isoform, and we observed increased cytosolic Ca^{2+} signaling upon R-3 depletion, the effects may be due to signaling from the remaining IP3R-1 which is a more active isoform. This argues that the observed effects of IP3R-3 depletion may be isoform specific effects.

This led us to ask if IP3R-1 depletion would have any similar effects. Using siRNA, IP3R-1 could be depleted by close to 95% (Figure 15A). To test the effect of IP3R-1 depletion on ER-to-Golgi transport we used the same intact-cell transport assay utilized in Chapter 1, using the temperature-sensitive GFP-VSV-G_{ts045} cargo. As demonstrated in Figure 15B, IP3R-1 knockdown resulted in up to a 25% acceleration of VSV-G transport compared to the 60% acceleration seen in IP3R-3 depletion. As discussed previously, NRK cells express about twice as much IP3R-3 as they do IP3R-1. The difference in magnitude of ER-to-Golgi transport acceleration between R-3 and R-1 depletion may therefore be due to the different starting expression levels. Alternatively, depletion of each isoform may accelerate transport via independent mechanisms.

To examine other possible similarities between IP3R-1 and R-3 depletion we measured ER luminal Ca^{2+} stores using the cameleon Ca^{2+} sensor D1ER. As shown by representative traces and $\Delta R/R_0$ quantitation in Figure 16, $\Delta R/R_0$ was ~28% smaller in both IP3R-1 and IP3R-3 depletion, indicating a lower resting ER Ca^{2+} concentration. This conclusion was verified by measuring the amount of Ca^{2+} taken up by the mitochondria upon addition of 1 µM Tg with a genetically encoded FRET-based mitochondrial matrix Ca^{2+} sensor, 4mtD3cpv (Palmer & Tsien, 2006). Both knockdowns showed lower mitochondrial Ca^{2+} uptake reflective of a decreased ER luminal Ca^{2+} environment (Figure 17).

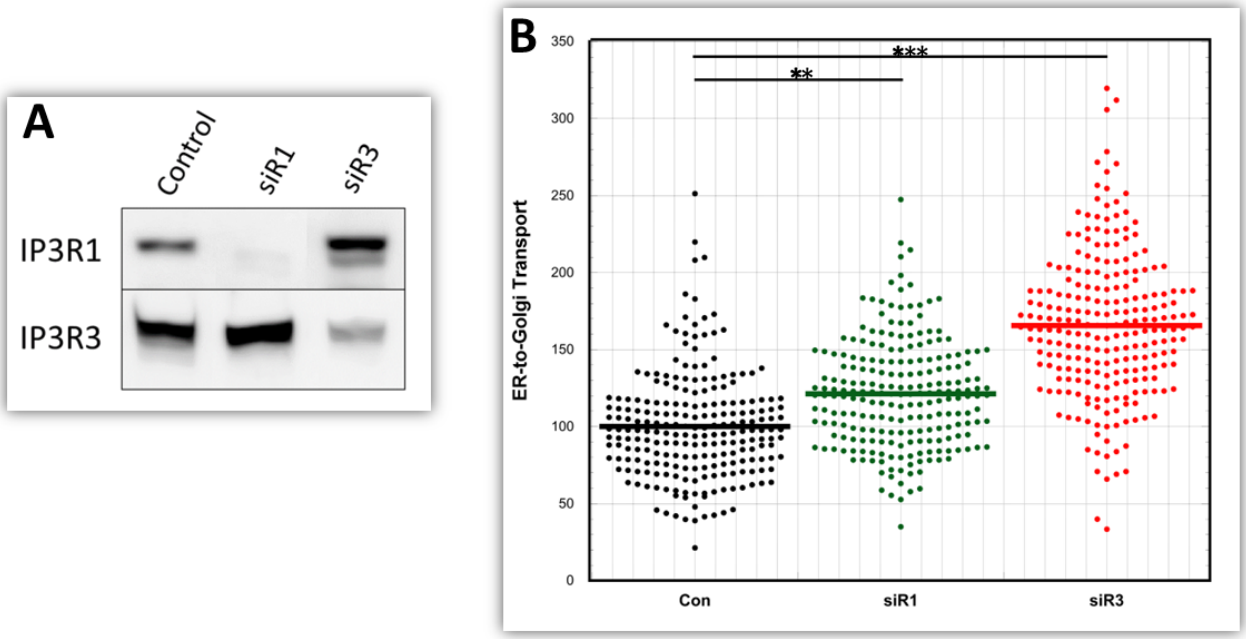

Figure 15. Depletion of either IP3R isoform accelerates ER-to-Golgi trafficking, but to different extents. (A) Verification of isoform specific siRNA depletion of both IP3R isoforms expressed in NRK cells. (B) NRK cells were transfected with VSV-G_{ts045}-GFP with indicated isoform specific IP3R siRNAs. Following growth at 41°C for 48 hr, cells were shifted to 32°C for 10 min, to permit transport, prior to fixation. Each transfected cell was assigned a transport index representing trafficking of VSV-G based upon the ratio of Golgi to peripheral green fluorescence. Results shown here are representative of at least three experiments with consistent trends.

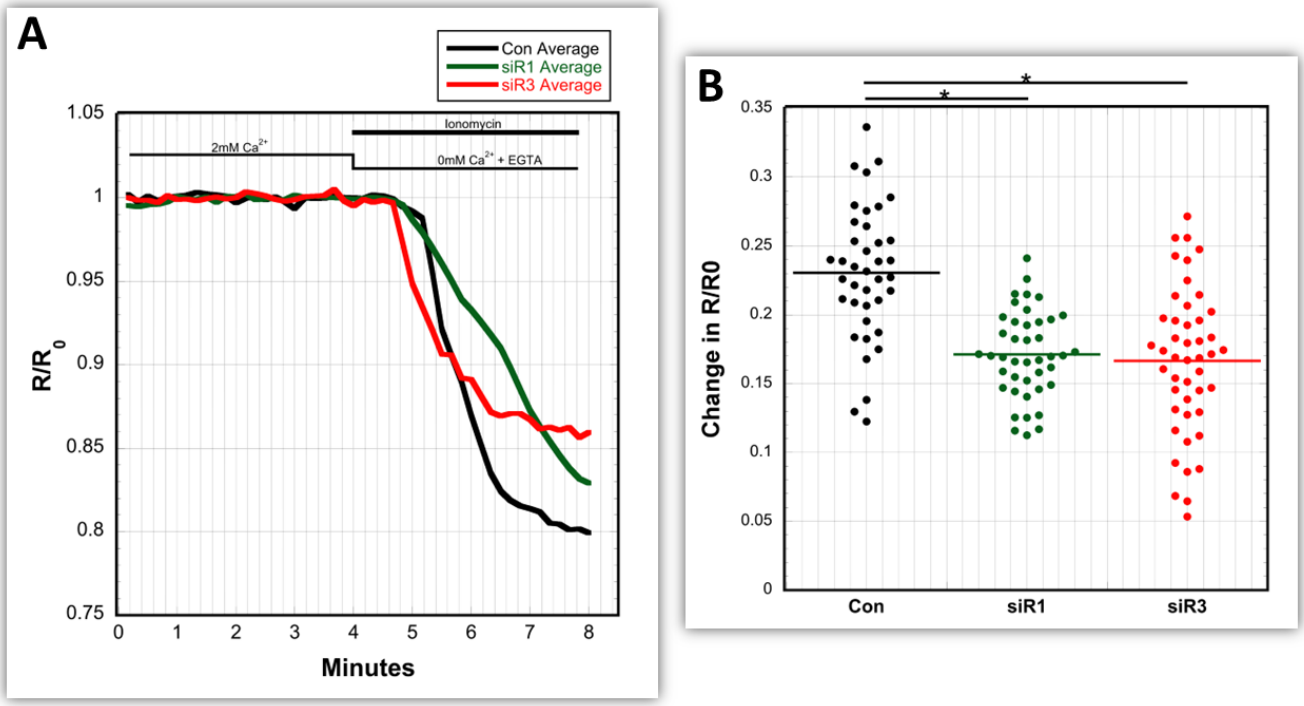

Figure 16. Depletion of either IP3R isoform causes ER luminal Ca^{2+} depletion. (A) Example luminal Ca^{2+} depletion traces from representative live cells using the ER FRET-based Ca^{2+} sensor D1ER. Ca^{2+}, ionomycin, and EGTA are added and withdrawn using continuous perfusion as indicated above. The emission ratio for (YFP/CFP) was determined using 430 nM illumination at each timepoint and expressed as a ratio to initial value. (B) Drop in FRET ratio between 0 and 8 min was determined as in part A for several cells per run in multiple runs in cells treated with isoform specific siRNAs.

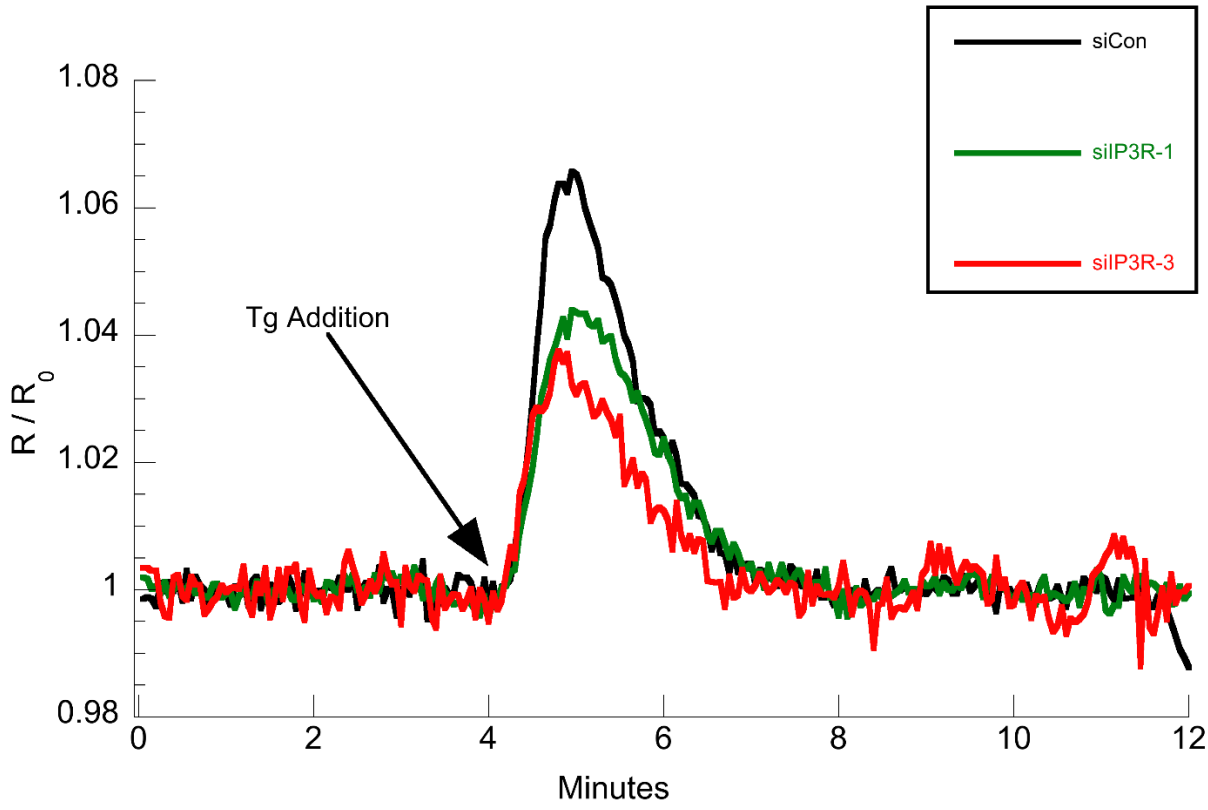

Figure 17. ER luminal Ca^{2+} depletion causes reduced mitochondrial Ca^{2+} uptake upon acute Tg exposure. Representative traces of mitochondrial matrix Ca^{2+}, using the sensor 4mtD3cpv, upon release of luminal Ca^{2+} stores by addition of thapsigargin to the extracellular medium.

4.2.2 IP3R Depletion Increases ER-Mitochondria Membrane Apposition

In order to examine potential changes in MAM formation or functionality we performed high resolution 3D structured illumination (SIM) superresolution microscopy using D1ER and MitoTrackerRed® to visualize ER and mitochondria respectively. Colocalization analysis revealed an increase in the number of contact sites between ER and mitochondrial membranes in both IP3R-1 and IP3R-3 depleted cells (Figure 18). Though the MAM biogenesis pathway is not well understood, we speculate that the reduced luminal Ca^{2+} stores in both knockdown conditions may have stimulated “excessive” MAM formation.

One way to test the functionality of these ER-mitochondrial contact sites is to measure the Ca^{2+} communicated to the mitochondria upon IP3R stimulation. Alternatively, basal MAM functionality might reasonably be assessed by measuring Ca^{2+} concentration in the mitochondrial matrix. The idea being that ER luminal Ca^{2+} is slightly depleted because it is being communicated to the mitochondria at higher rates under basal conditions. Experiments to this end were attempted using 4mtD3cpv and the same ionomycin depletion protocol used in figure 16A. However, multiple replicates produced mixed results. Potential factors for these inconsistencies include 1) ER luminal Ca^{2+} being taken up by the mitochondria prior to ionomycin fully draining mitochondrial Ca^{2+}, thus reintroducing the luminal Ca^{2+} variability; and 2) potentially ineffective dosage of ionomycin for the dual membrane of the mitochondria.

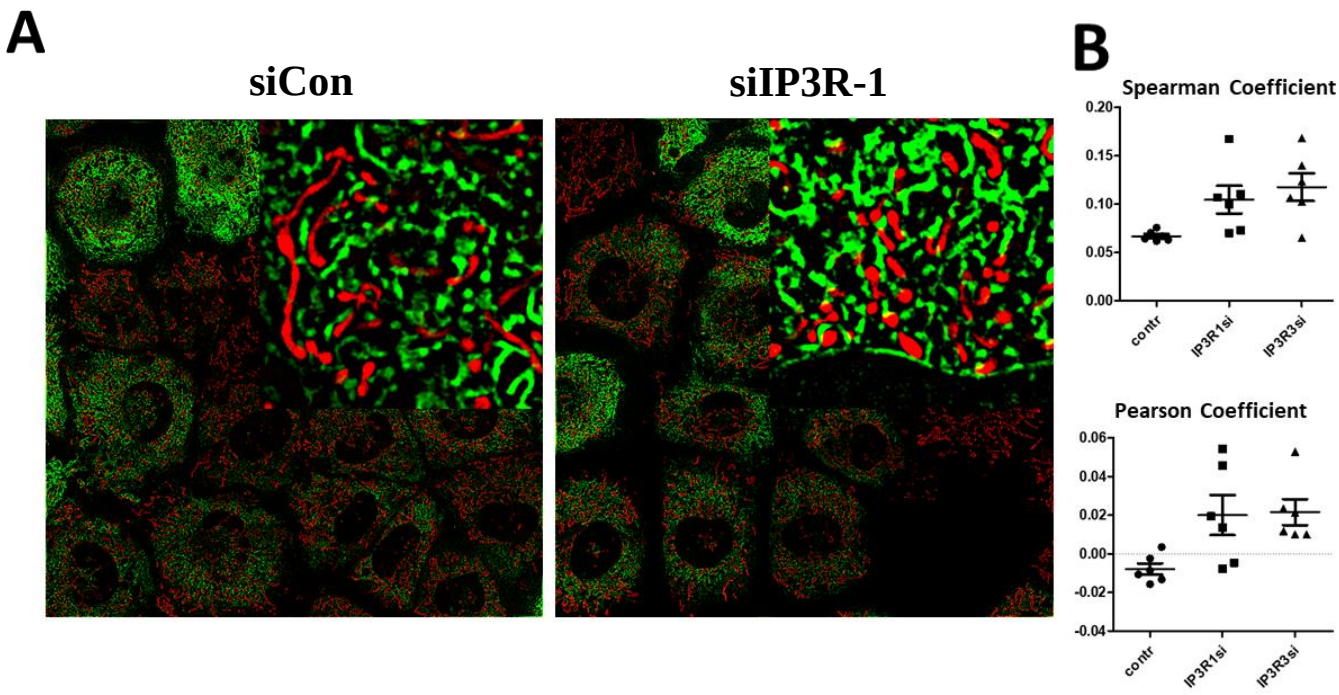

Figure 18. Depletion of either IP3R isoform increases ER-mitochondria membrane apposition. (A) Representative SIM microscopy images of control (left) and siIP3R-1 (right) NRK cells expressing D1ER (green) and stained with MitoTrackerRed® CMXRos (red). (B) Co-localization presented as Spearman (top) and Pearson (bottom) coefficients.

4.2.3 IP3R Depletion Induces Isoform Specific Transcriptional Effects

One could imagine that the decreased ER luminal Ca^{2+} seen in IP3R knockdowns could activate the UPR which can have a range of transcriptional effects. To test this, we examined the expression of a range of relevant genes using qRT-PCR. While many transcripts were unaffected (Figure 19), a number of transcripts were altered upon IP3R depletion (Figure 20).

Bcl-2 expression was decreased in both knockdown conditions. A number of anti-apoptotic Bcl-2 family proteins, including Bcl-2 itself, are known to interact with IP3Rs and suppress Ca^{2+} signaling activity. Theoretically this protects cells from apoptotic stimuli by dampening apoptotic mitochondrial Ca^{2+} overload (Berridge, 2016). Thus, the decrease in Bcl-2 expression may help to explain the hyperactive basal Ca^{2+} signaling described in Chapter 3.

Several transcripts were differentially regulated based on which IP3R isoform was knocked down. Rab32, a GTPase that regulates ER-mitochondria tethering interactions and mitochondrial dynamics (Madreiter-Sokolowski et al., 2019; Saito & Imaizumi, 2018), was downregulated specifically in IP3R-3 depleted cells. This provides yet another indirect indication that MAM functionality may be impaired, or at least altered, upon IP3R-3 depletion. Interestingly, the UPR sensor and signaling protein ATF6 was downregulated in IP3R-1 depleted cells, indicating a potential change in ER stress. Along the same lines, expression of COPII associated proteins Sec16 and Sec24b were also decreased specifically in IP3R-1 depleted cells. Sec16 and Sec24 are both upregulated by the IRE1 arm of the UPR upon ER stress (Farhan et al., 2008). Therefore, their downregulation might indicate an alleviation of ER stress. Decreased expression of COPII components was especially surprising given that IP3R-1 depletion still caused an increase in ER-to-Golgi transport (Figure 15). This provides further evidence that the increased transport seen in each IP3R isoform knockdown has its own isoform specific mechanism, rather than being caused purely by a decreased total IP3R density.

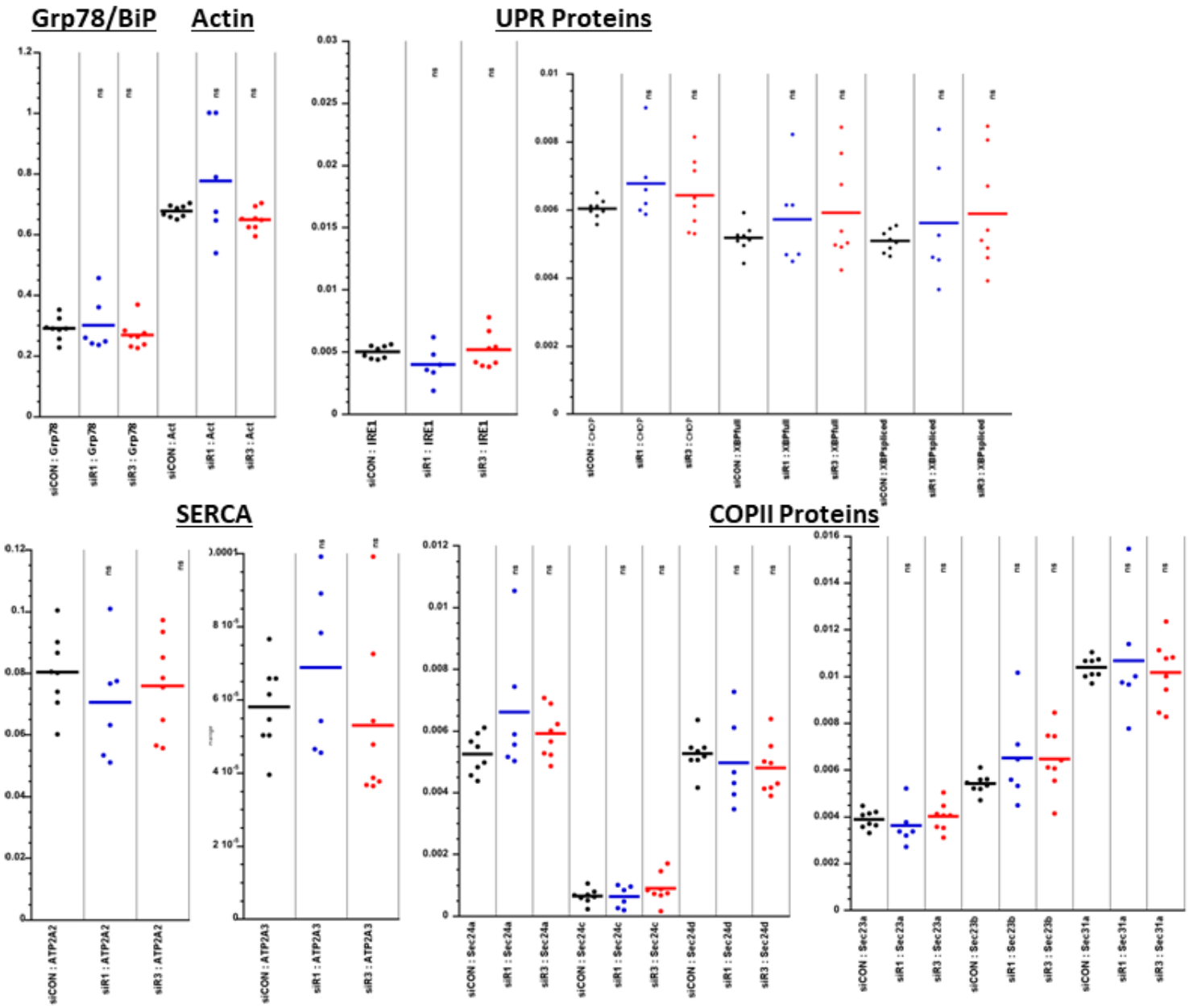

Figure 19. Transcripts unaffected by IP3R depletion. NRK cells were transfected with control (black), IP3R-1 (blue), or IP3R-3 (red) siRNAs, grown for 48 h, lysed, and then mRNA was analyzed by qRT-PCR to detect expression of trafficking and other proteins. The quantity of each target RNA is normalized to that determined for GAPDH in parallel reactions. All differences presented here are non-significant.

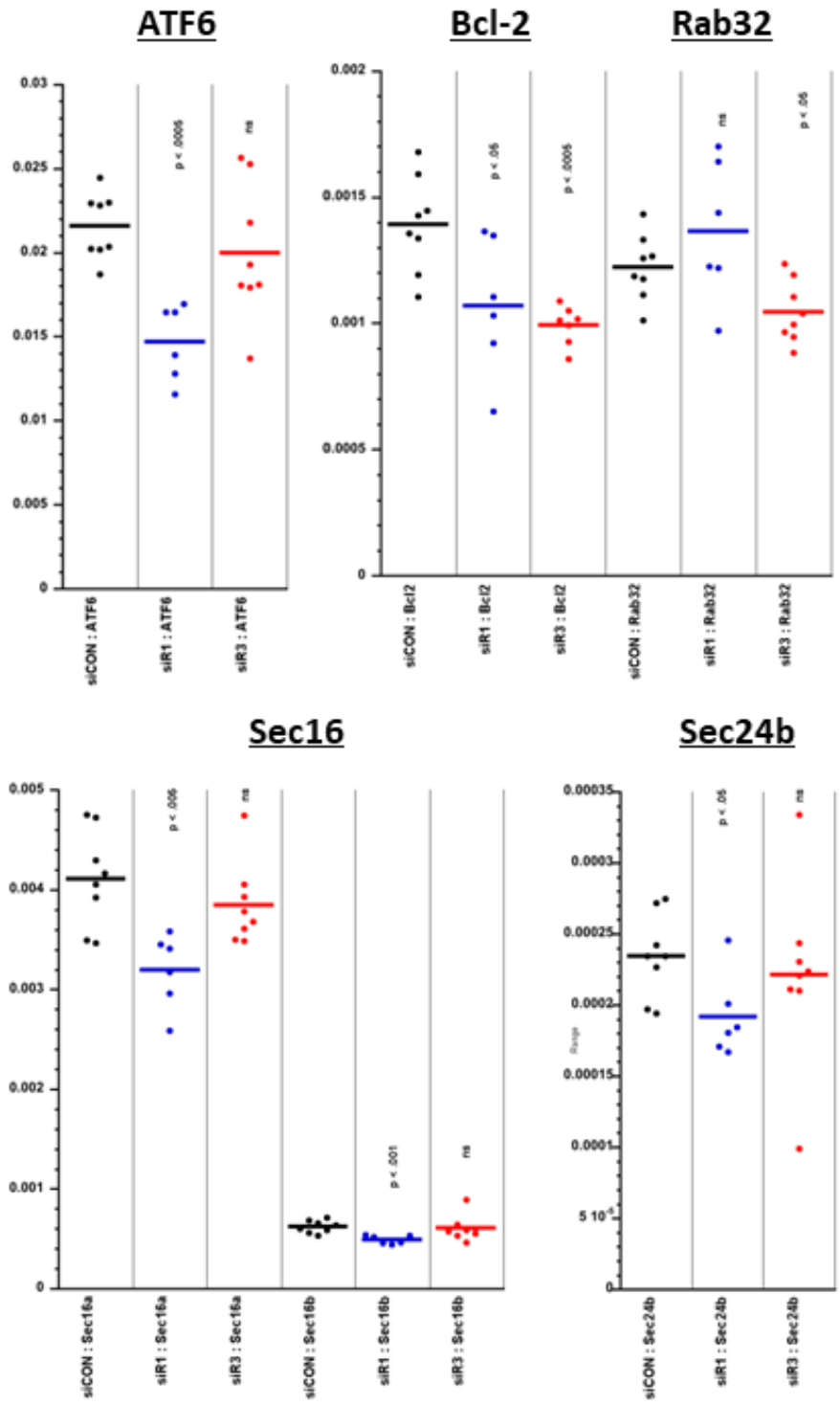

Figure 20. Isoform specific transcriptional effects of IP3R depletion. NRK cells were transfected with control (black), IP3R-1 (blue), or IP3R-3 (red) siRNAs, grown for 48 h, lysed, and then mRNA was analyzed by qRT-PCR to detect expression of trafficking and other proteins. The quantity of each target RNA is normalized to that determined for GAPDH in parallel reactions. Significance of each difference is indicated by a p-value or labeled non-significant (ns).

4.2.4 IP3R-1 Depletion Alters UPR Activity in an Isoform-Specific Manner

To directly examine IP3R knockdown effects on ER protein homeostasis we performed western blot analysis for a number of different UPR effectors (Figure 21). There is a very low level of UPR activity under steady-state conditions, and interestingly, we found a slight decrease in this basal IRE1 activation (phosphorylation) in IP3R-1 depleted cells. To determine the cells' ability to respond to ER stress, we measured UPR activation after 4 hours of Tg exposure. Similar to steady-state conditions, we observed a drastic decrease in IRE1 activation upon ER stress induction specifically in IP3R-1 depleted cells. Though we saw no differences in eIF2 activation, we did see a significant decrease in its downstream effector ATF4 specifically in IP3R-1-depleted cells.

These results, combined with the ATF6 downregulation seen in figure 20, illustrate that all three arms of the UPR are suppressed specifically by IP3R-1 depletion, indicating an improved proteostatic environment despite the decrease in luminal Ca^{2+}.

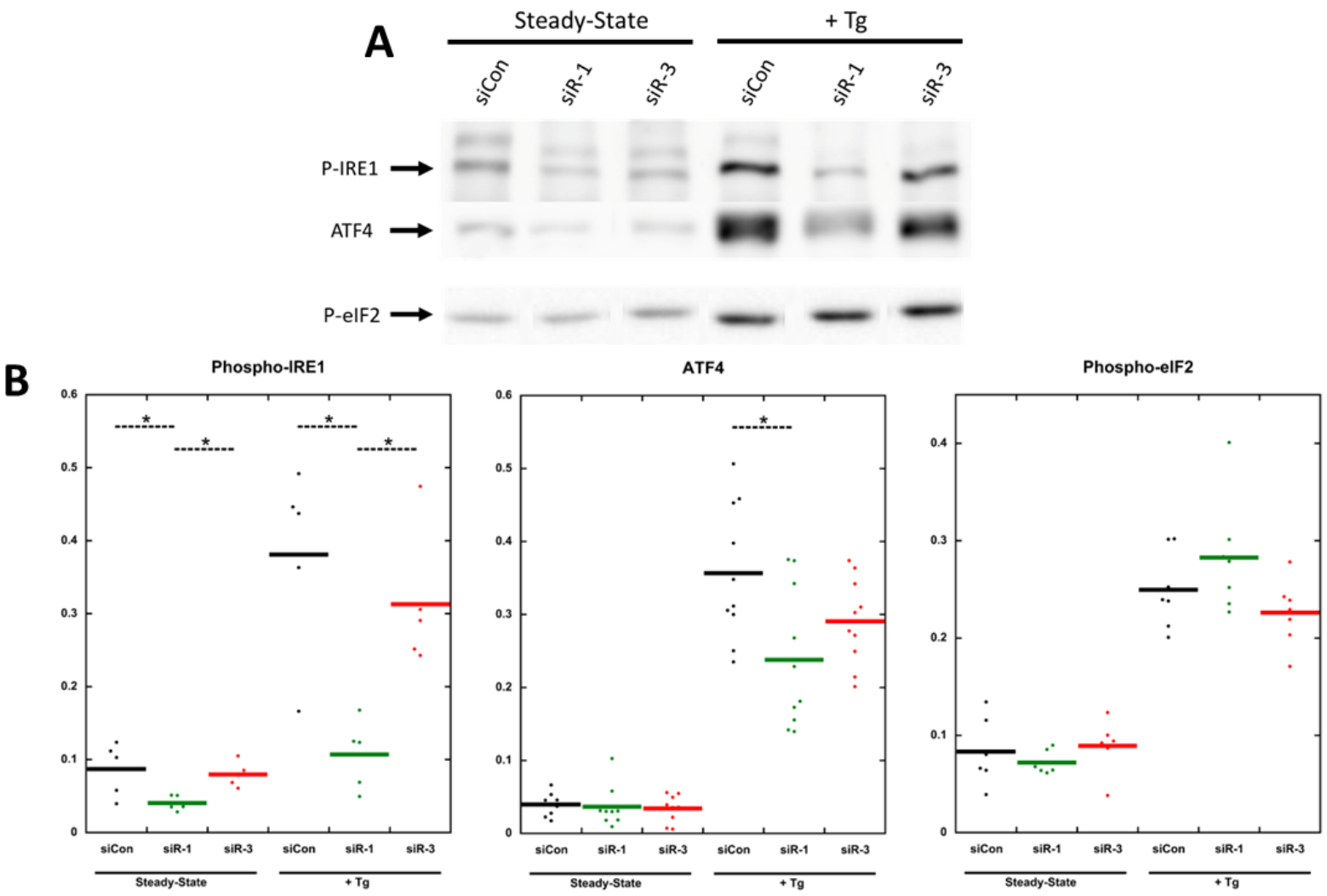

Figure 21. Isoform specific effects on UPR activation. NRK cells were transfected with control, IP3R-1, or IP3R-3 siRNAs and grown for 48 h. Cells were then exposed to 1 µM Tg for 4 h, lysed, and examined via Western blot. (A) Representative immunoblots of phospho-IRE1, ATF4, and phospho-eIF2. (B) Quantitation of multiple technical replicates from several different experiments documenting effects of IP3R depletion on protein abundance.

4.3 DISCUSSION

4.3.1 Mechanism of Effects on ER Protein Homeostasis

The preliminary results detailed here provide interesting insight into the isoform specific effects that IP3R depletion has on NRK cell physiology. Importantly, we found that IP3R-1 depletion seems to improve ER protein homeostasis as indicated by decreased UPR activation. This finding is particularly interesting given the ER luminal Ca^{2+} depletion caused by IP3R-1 knockdown shown in figure 16, because it provides direct evidence against the idea that ER proteostatic environment tracks strictly with Ca^{2+} concentration. Not only did Ca^{2+} depletion not cause ER stress, but ER stress was actually alleviated by IP3R-1 knockdown.

Additionally, we found that the effects on UPR were specific to IP3R-1 knockdown, even though IP3R-3 knockdown resulted in similar Ca^{2+} depletion and mitochondrial membrane localization effects. We therefore propose that the differential effects of IP3R isoform knockdowns are the result of a shift in Ca^{2+} signaling characteristics towards that of the remaining isoform. IP3R-1 is more likely to direct Ca^{2+} signals to the cytosol and has a higher affinity for both IP3 and Ca^{2+} (I. Bezprozvanny, 2005; Iwai et al., 2007). Thus, IP3R-3 knockdown in NRK cells elicits an increase in cytosolic Ca^{2+} signaling, as illustrated in Chapter 3. Alternatively, IP3R-3 is most implicated in Ca^{2+} communication to the mitochondria via MAMs (Kuo et al., 2019; Mendes et al., 2005). Thus, IP3R-1 knockdown in NRK cells may result in more efficient Ca^{2+} communication to the mitochondrial matrix. We therefore propose a model in which IP3R-1 depletion accentuates IP3R-3 function at MAMs, providing efficient Ca^{2+} signaling to the mitochondrial matrix and driving mitochondrial bioenergetics. The ATP produced by this process is then shuttled to the ER lumen via AXER to improve chaperone function and alleviate ER stress, even with the reduced luminal Ca^{2+} concentration. This phenotype thus exemplifies the idea that ER luminal Ca^{2+} is important in protein folding both by acting as a chaperone cofactor and, in this case more prominently, as an exchange currency to provide ER ATP via MAM functionality.

4.3.2 Models of ER ATP Regulation

Since its discovery, two seemingly antagonistic mechanistic models of AXER regulation of ER ATP homeostasis have been proposed. Klein et al. proposed the Ca^{2+}-dependent signaling pathway termed “lowER” in which AXER acts in the vicinity of the Sec61 complex. In high ER ATP conditions, ATP facilitates BiP interaction with Sec61 to decrease Ca^{2+} leak from the channel (Schäuble et al., 2012). In low ER ATP conditions caused by increased protein import or accumulation of unfolded/misfolded proteins, BiP dissociates from Sec61 and increases Ca^{2+} leak to trigger AXER activity and ATP import (Vishnu et al., 2014) and thus a return to baseline (Klein et al., 2018).

An alternative model, termed Ca^{2+} antagonized transport into the ER (CaATiER), was proposed by Yong et al. after additional characterization of AXER functionality. Importantly, they demonstrated that high cytosolic Ca^{2+} inhibits AXER activity. The authors acknowledge the probable role of MAMs in the stimulation of ATP production and subsequent transfer to the ER, but since MAMs create a high Ca^{2+} microdomain and AXER is inhibited by high cytosolic Ca^{2+}, one of two possible scenarios must be true. Either there are two different forms of MAM, one for Ca^{2+} transfer to the mitochondria and one for ATP transfer to the cytosol, or the Ca^{2+} and ATP communication at MAMs are temporally separated (Yong et al., 2019).

The group from Klein et al. has since proposed a unifying model in which a major proteostatic challenge induces “lowER,” while a sustained or major proteostatic challenge induces “CaATiER” (Zimmermann & Lang, 2020). Our findings provide possible evidence for a homeostatic mechanism that provides proactive protection against proteostatic challenges while at steady-state conditions.

4.3.3 Caveats and Alternative Interpretations

As stated in the beginning of this chapter, the results presented here are preliminary. We therefore recognize that there are a number of gaps in our understanding of the mechanism

proposed and that a number of our conclusions require significant caveats. Future directions to fill knowledge gaps and address these caveats will be discussed in Chapter 5.

Throughout this chapter we make numerous assumptions about the enhanced or diminished functionality of MAMs after IP3R-1 or IP3R-3 knockdown, respectively. We provided evidence for changes in ER-mitochondrial membrane contact sites, but noted that this membrane apposition does not necessarily equate to functional MAMs. We noted attempts to measure mitochondrial Ca^{2+} stores, theoretically examining the result of MAM functionality, but these experiments yielded inconsistent results. Additionally, we have not measured mitochondrial bioenergetics directly.

When discussing transcriptional effects of IP3R knockdowns, ATF6, Sec16, and Sec24b downregulation led us to conclude that UPR activity was altered by IP3R-1 depletion. This conclusion has a number of complications. First, ATF6 function in UPR signaling is based on its stress-dependent trafficking to the Golgi where it is cleaved into an active transcription factor (Figure 4). While a reduction in ER stress would likely result in less ATF6 trafficking and transcription factor activity, there is no reason to assume that expression of ATF6 itself would be affected. As stated before, Sec16 and Sec24 are both upregulated by UPR, so their reduced expression could indicate reduced UPR induction. However, it is curious that Sec24b was the only Sec24 paralog effected in this way. Finally, though these transcriptional changes may indicate changes in UPR activity, there are also a number of UPR effectors that we would expect to change with UPR attenuation that were, in fact, unchanged by IP3R depletion, for example Grp78 (BiP) and the spliced form of XBP1 (Figure 19).

A similar critique can be levied against our interpretations of Figure 21. While the effect on IRE1 activation is striking, the decrease in ATF4 expression is more difficult to interpret. ATF4 translation is induced by eIF2 activation (Figure 4); however, eIF2 phosphorylation was unaffected by IP3R-1 depletion. It is therefore unclear if the decrease in ATF4 expression is indicative of reduced ER stress and UPR activation or is the result of a disruption of eIF2 functionality.

There are also a number of UPR proteins that we were unable to obtain quantifiable western images for. Understanding of the entirety of the UPR signaling cascade would strengthen our conclusions significantly. Finally, UPR activation may not be an accurate measurement of the ER luminal folding environment in this context. Inactivation of the UPR inducers by BiP is mediated by BiP's substrate binding affinity (Bertolotti et al., 2000). As discussed previously, BiP's substrate binding affinity is dependent on Ca^{2+}. Therefore, Tg exposure, which induces UPR by drastically reducing ER luminal Ca^{2+}, may induce UPR irrespective of the luminal folding environment. Changes in UPR activity in this context may not accurately reflect changes in the proteostatic environment. In the future, we should address the proteostatic environment directly using sensors of the protein folding environment.

Finally, even if we accept that ER stress is, in fact, attenuated by IP3R-1 depletion, additional studies must be done to definitively conclude that ER ATP provided by MAM functionality is the causative factor. Future directions to address these concerns are discussed in Chapter 5.

CHAPTER 5:
CONCLUSION

5.1 DISCUSSION

Throughout this work we have demonstrated a number of ways in which IP3Rs and PEF proteins regulate the physiology of the ER luminal environment and the efficiency by which proteins are trafficked from the ER to the Golgi. In Chapter 3 we illustrated that IP3R-3 depletion accentuates steady-state cytosolic Ca^{2+} signaling, activating ALG-2 and accelerating COPII client transport by augmenting cargo sorting stringency at ERES. This work provided significant advancements in our understanding of PEF protein functionality, particularly of ALG-2's role in protein sorting at ERES and transport of different types of protein cargos. In addition, it provided the new insight that homeostatic Ca^{2+} oscillations are a rate-limiting feature of the biosynthetic secretory pathway. In Chapter 4 we provided evidence for the idea that IP3R depletion causes differential effects depending on the isoform depleted. Specifically, we found that IP3R-1 depletion suppresses UPR activity, presumably by amplifying the remaining IP3R-3 influence on mitochondrial bioenergetics to enhance ATP communication to the ER and improve the luminal folding environment. This work enhances our understanding of the interplay between ER luminal Ca^{2+} and ATP in the maintenance of ER proteostasis.

As discussed in section 3.3.2, changes in IP3R expression have been observed in a number of different physiological and pathophysiological situations. Additionally, a number of different pathophysiological consequences occur depending on dysfunction or expression changes of specific IP3R isoforms (Kerkhofs et al., 2018). The results presented here indicate that the pathophysiology of these various insults may involve changes in secretory function or ER proteostasis. The differential expression of IP3R isoforms may also play a role in the defining functional characteristics of different cell types such as secretory capacity and resistance to proteostatic stressors. The applicability of the results presented here to alternative cell types is a particularly interesting area for future studies.

5.2 OPEN QUESTIONS AND FUTURE DIRECTIONS

5.2.1 IP3R and PEF Protein Influence on Transport

Though Chapter 3 provided a thorough exploration of the mechanistic details of IP3R and PEF protein control of ER export, a number of open questions remain. Our understanding of the system would be vastly improved by a more comprehensive evaluation of the Ca^{2+} signaling patterns that influence ER-to Golgi transport.

We observed ICWs in NRK cells and posited that IP3R-3 depletion increases the participation rate in these waves. However, we did not attempt to directly quantify these waves. ICWs can be propagated via two mechanisms, either alone or in combination. The first is Ca^{2+} or IP3 communication between cells via gap junctions. This is dependent on cell-cell contact and the formation of functional gap junctions by the oligomerization of connexins in each participating cell. The second mechanism involves paracrine signaling between adjacent cells, allowing for ICW propagation across cell-free zones. This usually involves ATP release through plasma membrane transporters, vesicular discharge, or diffusion though membrane channels. The released ATP then stimulates purinergic receptors on nearby cells to activate the G protein-PLC-IP3 signaling cascade to release Ca^{2+} via IP3Rs (Leybaert & Sanderson, 2012). Which of these two mechanisms is most at play in NRK cells and is this altered upon IP3R-3 depletion? Are the transport effects observed dependent on ICWs specifically, or are intrinsic Ca^{2+} signaling events sufficient? Additionally, do the ICWs trigger secretion changes, or do secretion changes amplify ICWs by more efficiently trafficking ATP-filled vesicles or gap junction components? A number of these questions could be addressed using various established ICW inhibitors that can differentiate between gap-junction-based and paracrine-based propagation (Leybaert & Sanderson, 2012).

Though we established an association between the Ca^{2+} signaling changes and PEF protein activity, the conclusions would be strengthened by a more thorough evaluation of this relationship. Can we reproduce the Ca^{2+} signaling changes without altering IP3R expression? This would require a more intricate understanding of the Ca^{2+} signaling patterns that IP3R-3 depletion produces. If this proves feasible, does that also recreate the transport effects we observed? Our group already has experiments underway trying to explore these ideas.

Finally, we concluded that ALG-2 activation in this context augments COPII cargo sorting stringency at ERES, more efficiently loading client cargos and thus accelerating their transport at the expense of bulk flow cargos. This conclusion would be strengthened by examining a wider array of secretory cargos. Are other COPII client cargos, for example ER/Golgi SNAREs, accumulated at ERES more efficiently as well, or is this effect specific to clients containing a C-terminal DxE export signal such as VSV-G? VSV-G has a Sec24 paralog preference; are these effects specific to cargos utilizing Sec24a and b? Are other bulk flow cargos similarly excluded from ERES? Future studies should examine these questions.

5.2.2 Isoform-Specific IP3R Influence on MAM Activity and Protein Homeostasis

Given the preliminary nature of the results in Chapter 4, a number of open questions remain. If R-1 is more active and the main cytosolic Ca^{2+} signaling isoform, how does R-1 depletion affect cytosolic Ca^{2+} signaling? Do these cells participate in ICWs? Are the PEF proteins similarly affected?

There are a variety of experiments that need to be performed to strengthen the model proposed in Chapter 4. First, more direct characterization of MAM functionality needs to be performed. When we knock down IP3R-1, does the remaining R-3 communicate Ca^{2+} to the mitochondria more effectively? This can be measured using the 4mtD3cpv FRET sensor in conjunction with legitimate IP3R stimulating agonists. Measuring the mitochondrial Ca^{2+} store would provide an indirect look at MAM functionality, and though we attempted experiments examining this metric, these protocols could be improved to elicit more consistent results. If MAM functionality is shown to be enhanced in IP3R-1 depleted cells, it would also be interesting to examine whether these cells are then more susceptible to apoptotic stimuli via mitochondrial Ca^{2+} overload and opening of the permeability transition pore.

Examination of mitochondrial bioenergetics using methodology such as a Seahorse XF analyzer may answer whether the potentially enhanced mitochondrial Ca^{2+} uptake at MAMs is having a functional result to increase ATP production. We then would need to examine how

effectively the ATP is being transmitted to the ER lumen and if that is the cause of the observed UPR effects. This could be examined by knocking down AXER or inhibiting its function.

We also need to further explore the ER luminal environment. Do IP3R-1 depleted cells have more luminal ATP? This can be explored using ER ATP sensors such as that described in (Vishnu et al., 2014). Finally, what is the true state of the proteostatic environment? Chapter 4 described decreased activation of a number of UPR proteins, but others were unaffected by IP3R-1 depletion. A complete examination of all UPR proteins may be required to fully understand how this system is being affected. Additionally, protein folding sensors may be a more direct indicator of the folding environment, rather than the response to said environment.

Though significant further study is needed to make conclusive statements about exact mechanisms, these studies still indicate that IP3Rs can have isoform-specific effects on the proteostatic environment. This finding may have broad implications for a number of proteostatic diseases.

REFERENCES

Alder, N. N., Shen, Y., Brodsky, J. L., Hendershot, L. M., & Johnson, A. E. (2005). The molecular mechanisms underlying BiP-mediated gating of the Sec61 translocon of the endoplasmic reticulum. *Journal of Cell Biology*, *168*(3), 389–399. https://doi.org/10.1083/jcb.200409174

Almirza, W. H. M., Peters, P. H. J., van Meerwijk, W. P. M., van Zoelen, E. J. J., & Theuvenet, A. P. R. (2010). Different roles of inositol 1,4,5-trisphosphate receptor subtypes in prostaglandin F2α-induced calcium oscillations and pacemaking activity of NRK fibroblasts. *Cell Calcium*, *47*(6), 544–553. https://doi.org/10.1016/j.ceca.2010.05.004

Alzayady, K. J., Wang, L., Chandrasekhar, R., Wagner II, L. E., Van Petegem, F., & Yule, D. I. (2016). Defining the stoichiometry of inositol 1,4,5-trisphosphate binding required to initiate Ca2+ release. *Science Signaling*, *9*(422). https://doi.org/10.1126/scisignal.aad6281

Ananthanarayanan, M., Banales, J. M., Guerra, M. T., Spirli, C., Munoz-Garrido, P., Mitchell-Richards, K., Tafur, D., Saez, E., & Nathanson, M. H. (2015). Post-translational regulation of the type III inositol 1,4,5-trisphosphate receptor by miRNA-506. *Journal of Biological Chemistry*, *290*(1), 184–196. https://doi.org/10.1074/jbc.M114.587030

Antonny, B., Madden, D., Hamamoto, S., Orci, L., & Schekman, R. (2001). Dynamics of the COPII coat with GTP and stable analogues. *Nature Cell Biology*, *3*(6), 531–537. https://doi.org/10.1038/35078500

Appenzeller-Herzog, C., & Hauri, H. P. (2006). The ER-Golgi intermediate compartment (ERGIC): In search of its identity and function. *Journal of Cell Science*, *119*(11), 2173–2183. https://doi.org/10.1242/jcs.03019

Appenzeller, C., Andersson, H., Kappeler, F., & Hauri, H. P. (1999). The lectin ERGIC-53 is a cargo transport receptor for glycoproteins. *Nature Cell Biology*, *1*(6), 330–334. https://doi.org/10.1038/14020

Arakel, E. C., & Schwappach, B. (2018). Formation of COPI-coated vesicles at a glance. *Journal of Cell Science*, *131*(7). https://doi.org/10.1242/jcs.218347

Balch, W. E., McCaffery, J. M., Plutner, H., & Farquhar, M. G. (1994). Vesicular stomatitis virus glycoprotein is sorted and concentrated during export from the endoplasmic reticulum. *Cell*, *76*(5), 841–852. https://doi.org/10.1016/0092-8674(94)90359-x

Balch, William E., Morimoto, R. I., Dillin, A., & Kelly, J. W. (2008). Adapting proteostasis for disease intervention. *Science*, *319*(5865), 916–919. https://doi.org/10.1126/science.1141448

Bannykh, S. I., Rowe, T., & Balch, W. E. (1996). The organization of endoplasmic reticulum export complexes. *Journal of Cell Biology*, *135*(1), 19–35. https://doi.org/10.1083/jcb.135.1.19

Barlowe, C., & Helenius, A. (2016). Cargo Capture and Bulk Flow in the Early Secretory Pathway.

Annual Review of Cell and Developmental Biology, *32*, 197–222. https://doi.org/10.1146/annurev-cellbio-111315-125016

Baust, T., Anitei, M., Czupalla, C., Parshyna, I., Bourel, L., Thiele, C., Krause, E., & Hoflack, B. (2008). Protein Networks Supporting AP-3 Function in Targeting Lysosomal Membrane Proteins. *Molecular Biology of the Cell*, *19*(May), 1942–1951. https://doi.org/10.1091/mbc.E08-02-0110

Beck, R., Adolf, F., Weimer, C., Bruegger, B., & Wieland, F. T. (2009). ArfGAP1 activity and COPI vesicle biogenesis. *Traffic*, *10*(3), 307–315. https://doi.org/10.1111/j.1600-0854.2008.00865.x

Beckers, C. J. M., & Balch, W. E. (1989). Calcium and GTP: Essential components in vesicular trafficking between the endoplasmic reticulum and Golgi apparatus. *Journal of Cell Biology*, *108*(4), 1245–1256. https://doi.org/10.1083/jcb.108.4.1245

Bentley, M., Liang, Y., Mullen, K., Xu, D., Sztul, E., & Hay, J. C. (2006). SNARE status regulates tether recruitment and function in homotypic COPII vesicle fusion. *Journal of Biological Chemistry*, *281*(50), 38825–38833. https://doi.org/10.1074/jbc.M606044200

Bentley, M., Nycz, D. C., Joglekar, A., Fertschai, I., Malli, R., Graier, W. F., & Hay, J. C. (2010). Vesicular Calcium Regulates Coat Retention, Fusogenicity, and Size of Pre-Golgi Intermediates. *Molecular Biology of the Cell*, *21*, 1033–1046. https://doi.org/10.1091/mbc.E09-10-0914

Berridge, M. J. (2016). The inositol trisphosphate/calcium signaling pathway in health and disease. *Physiological Reviews*, *96*(4), 1261–1296. https://doi.org/10.1152/physrev.00006.2016

Berridge, M. J., Lipp, P., & Bootman, M. D. (2000). The versatility and universality of calcium signalling. *Nature Reviews*, *1*(October), 11–21.

Bertolotti, A., Zhang, Y., Hendershot, L. M., Harding, H. P., & Ron, D. (2000). Dynamic interaction of BiP and ER stress transducers in the unfolded-protein response. *Nature Cell Biology*, *2*(6), 326–332. https://doi.org/10.1038/35014014

Bezprozvanny, I. (2005). The inositol 1,4,5-trisphosphate receptors. *Cell Calcium*, *38*(3-4 SPEC. ISS.), 261–272. https://doi.org/10.1016/j.ceca.2005.06.030

Bezprozvanny, L., Watras, J., & Ehrlich, B. E. (1992). Bell-shaped calcium-response curves of Ins(1,4,5)P3- and calcium-gated channels from endoplasmic reticulum of cerebellum. *Nature*, *351*(6329), 751–754. https://doi.org/10.1038/351751a0

Bi, X., Corpina, R. A., & Goldberg, J. (2002). Structure of the Sec23/24-Sar1 pre-budding complex of the COPII vesicle coat. *Nature*, *419*(6904), 271–277. https://doi.org/10.1038/nature01040

Bi, X., Mancias, J. D., & Goldberg, J. (2007). Insights into COPII Coat Nucleation from the Structure of Sec23•Sar1 Complexed with the Active Fragment of Sec31. *Developmental*

Cell, *13*(5), 635–645. https://doi.org/10.1016/j.devcel.2007.10.006

Boehning, D., Patterson, R. L., Sedaghat, L., Glebova, N. O., Kurosaki, T., & Snyder, S. H. (2003). Cytochrome c binds to inositol (1,4,5) trisphosphate receptors, amplifying calcium-dependent apoptosis. *Nature Cell Biology*, *5*, 1051–1061. https://doi.org/10.1038/ncb1063

Boncompain, G., Divoux, S., Gareil, N., De Forges, H., Lescure, A., Latreche, L., Mercanti, V., Jollivet, F., Raposo, G., & Perez, F. (2012). Synchronization of secretory protein traffic in populations of cells. *Nature Methods*, *9*(5), 493–498. https://doi.org/10.1038/nmeth.1928

Boncompain, G., & Perez, F. (2013). Fluorescence-based analysis of trafficking in mammalian cells. In *Methods in Cell Biology* (Vol. 118, pp. 179–194). Academic Press. https://doi.org/10.1016/B978-0-12-417164-0.00011-2

Bonifacino, J. S., & Glick, B. S. (2004). The Mechanisms of Vesicle Budding and Fusion. *Cell*, *116*(2), 153–166. https://doi.org/10.1016/S0092-8674(03)01079-1

Bonifacino, J. S., & Lippincott-Schwartz, J. (2003). Coat proteins: shaping membrane transport. *Nature Reviews. Molecular Cell Biology*, *4*(5), 409–414. https://doi.org/10.1038/NRM1099

Bonifacino, J. S., & Rojas, R. (2006). Retrograde transport from endosomes to the trans-Golgi network. *Nature Reviews Molecular Cell Biology*, *7*(8), 568–579. https://doi.org/10.1038/nrm1985

Bonnon, C., Wendeler, M. W., Paccaud, J. P., & Hauri, H. P. (2010). Selective export of human GPI-anchored proteins from the endoplasmic reticulum. *Journal of Cell Science*, *123*(10), 1705–1715. https://doi.org/10.1242/jcs.062950

Bononi, A., Giorgi, C., Patergnani, S., Larson, D., Verbruggen, K., Tanji, M., Pellegrini, L., Signorato, V., Olivetto, F., Pastorino, S., Nasu, M., Napolitano, A., Gaudino, G., Morris, P., Sakamoto, G., Ferris, L. K., Danese, A., Raimondi, A., Tacchetti, C., … Carbone, M. (2017). BAP1 regulates IP3R3-mediated Ca 2+ flux to mitochondria suppressing cell transformation. *Nature*, *546*(7659), 549–553. https://doi.org/10.1038/nature22798

Booth, C., & Koch, G. L. E. (1989). Perturbation of cellular calcium induces secretion of luminal ER proteins. *Cell*, *59*(4), 729–737. https://doi.org/10.1016/0092-8674(89)90019-6

Bravo, R., Vicencio, J. M., Parra, V., Troncoso, R., Munoz, J. P., Bui, M., Quiroga, C., Rodriguez, A. E., Verdejo, H. E., Ferreira, J., Iglewski, M., Chiong, M., Simmen, T., Zorzano, A., Hill, J. A., Rothermel, B. A., Szabadkai, G., & Lavandero, S. (2011). Increased ER-mitochondrial coupling promotes mitochondrial respiration and bioenergetics during early phases of ER stress. *Journal of Cell Science*, *124*(14), 2511. https://doi.org/10.1242/jcs.095455

Burgoyne, R. D., & Clague, M. J. (2003). Calcium and calmodulin in membrane fusion. *Biochimica et Biophysica Acta - Molecular Cell Research*, *1641*(2–3), 137–143. https://doi.org/10.1016/S0167-4889(03)00089-2

Cantero-Recasens, G., Butnaru, C. M., Valverde, M. A., Naranjo, J. R., Brouwers, N., & Malhotra, V. (2018). KChIP3 coupled to ca 2+ oscillations exerts a tonic brake on baseline mucin

release in the colon. *ELife*, *7*. https://doi.org/10.7554/eLife.39729

Cao, Q., Zhong, X. Z., Zou, Y., Murrell-Lagnado, R., Zhu, M. X., & Dong, X. P. (2015). Calcium release through P2X4 activates calmodulin to promote endolysosomal membrane fusion. *Journal of Cell Biology*, *209*(6), 879–894. https://doi.org/10.1083/jcb.201409071

Cárdenas, C., Miller, R. A., Smith, I., Bui, T., Molgó, J., Müller, M., Vais, H., Cheung, K. H., Yang, J., Parker, I., Thompson, C. B., Birnbaum, M. J., Hallows, K. R., & Foskett, J. K. (2010). Essential Regulation of Cell Bioenergetics by Constitutive InsP3 Receptor Ca2+ Transfer to Mitochondria. *Cell*, *142*(2), 270–283. https://doi.org/10.1016/j.cell.2010.06.007

Cárdenas, C., Müller, M., McNeal, A., Lovy, A., Jaňa, F., Bustos, G., Urra, F., Smith, N., Molgó, J., Diehl, J. A., Ridky, T. W., & Foskett, J. K. (2016). Selective Vulnerability of Cancer Cells by Inhibition of Ca2+ Transfer from Endoplasmic Reticulum to Mitochondria. *Cell Reports*, *14*(10), 2313–2324. https://doi.org/10.1016/j.celrep.2016.02.030

Chakraborty, S., Deb, B. K., Chorna, T., Konieczny, V., Taylor, C. W., & Hasan, G. (2016). Mutant IP3 receptors attenuate store-operated Ca2+ entry by destabilizing STIM-Orai interactions in Drosophila neurons. *Journal of Cell Science*, *129*(20), 3903–3910. https://doi.org/10.1242/jcs.191585

Chatterjee, S., Choi, A. J., & Frankel, G. (2021). A systematic review of Sec24 cargo interactome. In *Traffic* (Vol. 22, Issue 12, pp. 412–424). https://doi.org/10.1111/tra.12817

Chemaly, E. R., Troncone, L., & Lebeche, D. (2018). SERCA control of cell death and survival. *Cell Calcium*, *69*, 46–61. https://doi.org/10.1016/j.ceca.2017.07.001

Chen, R., Valencia, I., Zhong, F., McColl, K. S., Roderick, H. L., Bootman, M. D., Berridge, M. J., Conway, S. J., Holmes, A. B., Mignery, G. A., Velez, P., & Distelhorst, C. W. (2004). Bcl-2 functionally interacts with inositol 1,4,5-trisphosphate receptors to regulate calcium release from the ER in response to inositol 1,4,5-trisphosphate. *Journal of Cell Biology*, *166*(2), 193–203. https://doi.org/10.1083/jcb.200309146

Collins, B. M., McCoy, A. J., Kent, H. M., Evans, P. R., & Owen, D. J. (2002). Molecular architecture and functional model of the endocytic AP2 complex. *Cell*, *109*(4), 523–535. https://doi.org/10.1016/S0092-8674(02)00735-3

Cooper, G. R., Brostrom, C. O., & Brostrom, M. A. (1997). Analysis of the endoplasmic reticular Ca2+ requirement for α-antitrypsin processing and transport competence. *Biochemical Journal*, *325*(3), 601–608. https://doi.org/10.1042/bj3250601

Čopič, A., Latham, C. F., Horlbeck, M. A., D'Arcangelo, J. G., & Miller, E. A. (2012). ER cargo properties specify a requirement for COPII coat rigidity mediated by Sec13p. *Science*, *335*(6074), 1359–1362. https://doi.org/10.1126/science.1215909

Csordás, G., Renken, C., Várnai, P., Walter, L., Weaver, D., Buttle, K. F., Balla, T., Mannella, C. A., & Hajnóczky, G. (2006). Structural and functional features and significance of the physical linkage between ER and mitochondria. *Journal of Cell Biology*, *174*(7), 915–921. https://doi.org/10.1083/jcb.200604016

Danoff, S. K., Ferris, C. D., Donath, C., Fischer, G. A., Munemitsu, S., Ullrich, A., Snyder, S. H., & Ross, C. A. (1991). Inositol 1,4,5-trisphosphate receptors: Distinct neuronal and nonneuronal forms derived by alternative splicing differ in phosphorylation. *Proceedings of the National Academy of Sciences of the United States of America*, *88*(7), 2951–2955. https://doi.org/10.1073/pnas.88.7.2951

De Brito, O. M., & Scorrano, L. (2008). Mitofusin 2 tethers endoplasmic reticulum to mitochondria. *Nature*, *456*(7222), 605–610. https://doi.org/10.1038/nature07534

Dell'Angelica, E. C., & Bonifacino, J. S. (2019). Coatopathies: Genetic disorders of protein coats. *Annual Review of Cell and Developmental Biology*, *35*, 131–168. https://doi.org/10.1146/annurev-cellbio-100818-125234

Depaoli, M. R., Hay, J. C., Graier, W. F., & Malli, R. (2019). The enigmatic ATP supply of the endoplasmic reticulum. *Biological Reviews*, *94*(2), 610–628. https://doi.org/10.1111/brv.12469

Dodonova, S. O., Diestelkoetter-Bachert, P., Von Appen, A., Hagen, W. J. H., Beck, R., Beck, M., Wieland, F., & Briggs, J. A. G. (2015). A structure of the COPI coat and the role of coat proteins in membrane vesicle assembly. *Science*, *349*(6244), 195–198. https://doi.org/10.1126/science.aab1121

Doms, R. W., Keller, D. S., Helenius, A., & Balch, W. E. (1987). Role for adenosine triphosphate in regulating the assembly and transport of vesicular stomatitis virus G protein trimers. *Journal of Cell Biology*, *105*(5), 1957–1969. https://doi.org/10.1083/jcb.105.5.1957

Dong, Y., Lee, Y., Cui, K., He, M., Wang, B., Bhattacharjee, S., Zhu, B., Yago, T., Zhang, K., Deng, L., Ouyang, K., Wen, A., Cowan, D. B., Song, K., Yu, L., Brophy, M. L., Liu, X., Wylie-Sears, J., Wu, H., … Chen, H. (2020). Epsin-mediated degradation of IP3R1 fuels atherosclerosis. *Nature Communications*, *11*(1). https://doi.org/10.1038/s41467-020-17848-4

Eckenrode, E. F., Yang, J., Velmurugan, G. V., Kevin Foskett, J., & White, C. (2010). Apoptosis protection by Mcl-1 and Bcl-2 modulation of inositol 1,4,5-trisphosphate receptor-dependent Ca2+ signaling. *Journal of Biological Chemistry*, *285*(18), 13678–13684. https://doi.org/10.1074/jbc.M109.096040

Fan, G., Baker, M. L., Wang, Z., Baker, M. R., Sinyagovskiy, P. A., Chiu, W., Ludtke, S. J., & Serysheva, I. I. (2015). Gating machinery of InsP3R channels revealed by electron cryomicroscopy. *Nature*, *527*(7578), 336–341. https://doi.org/10.1038/nature15249

Farhan, H., Weiss, M., Tani, K., Kaufman, R. J., & Hauri, H. P. (2008). Adaptation of endoplasmic reticulum exit sites to acute and chronic increases in cargo load. *EMBO Journal*, *27*(15), 2043–2054. https://doi.org/10.1038/emboj.2008.136

Fass, D., Blacklow, S., Kim, P. S., & Berger, J. M. (1997). Molecular basis of familial hypercholesterolaemia from structure of LDL receptor module. *Nature*, *388*(6643), 691–693. https://doi.org/10.1038/41798

Fath, S., Mancias, J. D., Bi, X., & Goldberg, J. (2007). Structure and Organization of Coat Proteins

in the COPII Cage. *Cell*, *129*(7), 1325–1336. https://doi.org/10.1016/j.cell.2007.05.036

Feizi, A., Gatto, F., Uhlen, M., & Nielsen, J. (2017). Human protein secretory pathway genes are expressed in a tissue-specific pattern to match processing demands of the secretome. *Npj Systems Biology and Applications*, *3*(1), 1–9. https://doi.org/10.1038/s41540-017-0021-4

Filadi, R., Greotti, E., Turacchio, G., Luini, A., Pozzan, T., & Pizzo, P. (2015). Mitofusin 2 ablation increases endoplasmic reticulum-mitochondria coupling. *Proceedings of the National Academy of Sciences of the United States of America*, *112*(17), E2174–E2181. https://doi.org/10.1073/pnas.1504880112

Fill, M., & Copello, J. A. (2002). Ryanodine Receptor Calcium Release Channels. *Physiological Reviews*, *82*(4), 893–922. https://doi.org/10.1152/physrev.00013.2002

Fontana, J. M., Khodus, G. R., Unnersjö-Jess, D., Blom, H., Aperia, A., & Brismar, H. (2019). Spontaneous calcium activity in metanephric mesenchymal cells regulates branching morphogenesis in the embryonic kidney. *FASEB Journal*, *33*(3), 4089–4096. https://doi.org/10.1096/fj.201802054R

Forster, R., Weiss, M., Simmermann, T., Reynaud, E. G., Verissimo, F., Stephens, D. J., & Pepperkok, R. (2006). Secretory Cargo Regulates the Turnover of COPII Subunits at Single ER Exit Sites. *Current Biology*, *16*(2), 173–179. https://doi.org/10.1016/j.cub.2005.11.076

Foskett, J. K., White, C., Cheung, K. H., & Mak, D. O. D. (2007). Inositol trisphosphate receptor Ca2+ release channels. In *Physiological Reviews* (Vol. 87, Issue 2, pp. 593–658). NIH Public Access. https://doi.org/10.1152/physrev.00035.2006

Fotin, A., Cheng, Y., Sliz, P., Grigorieff, N., Harrison, S. C., Kirchhausen, T., & Walz, T. (2004). Molecular model for a complete clathrin lattice from electron cryomicroscopy. *Nature*, *432*(7017), 573–579. https://doi.org/10.1038/nature03079

Franca, A., Carlos Melo Lima Filho, A., Guerra, M. T., Weerachayaphorn, J., Loiola dos Santos, M., Njei, B., Robert, M., Xavier Lima, C., Vieira Teixeira Vidigal, P., Banales, J. M., Ananthanarayanam, M., Fatima Leite, M., & Nathanson, M. H. (2019). Effects of Endotoxin on Type 3 Inositol 1,4,5-Trisphosphate Receptor in Human Cholangiocytes. *Hepatology*, *69*(2), 817–830. https://doi.org/10.1002/hep.30228

Fujita, M., Watanabe, R., Jaensch, N., Romanova-Michaelides, M., Satoh, T., Kato, M., Riezman, H., Yamaguchi, Y., Maeda, Y., & Kinoshita, T. (2011). Sorting of GPI-anchored proteins into ER exit sites by p24 proteins is dependent on remodeled GPI. *Journal of Cell Biology*, *194*(1), 61–75. https://doi.org/10.1083/jcb.201012074

Gimeno, R. E., Espenshade, P., & Kaiser, C. A. (1996). COPII coat subunit interactions: Sec24p and Sec23p bind to adjacent regions of Sec16p. *Molecular Biology of the Cell*, *7*(11), 1815–1823. https://doi.org/10.1091/mbc.7.11.1815

Gincel, D., Zaid, H., & Shoshan-Barmatz, V. (2001). Calcium binding and translocation by the voltage-dependent anion channel: a possible regulatory mechanism in mitochondrial function. *Biochemical Journal*, *358*(1), 147–155. https://doi.org/10.1042/bj3580147

Gomez-Navarro, N., Boulanger, J., & Miller, E. A. (2020). The Ubp3/Bre5 deubiquitylation complex modulates COPII vesicle formation. *Traffic*, *21*(11), 702–711. https://doi.org/10.1111/tra.12766

Gomez-Navarro, N., Maldutyte, J., Poljak, K., Peak-Chew, S. Y., Orme, J., Bisnett, B. J., Lamb, C. H., Boyce, M., Gianni, D., & Miller, E. A. (2022). Selective inhibition of protein secretion by abrogating receptor-coat interactions during ER export. *Proceedings of the National Academy of Sciences of the United States of America*, *119*(31), e2202080119. https://doi.org/10.1073/PNAS.2202080119/SUPPL_FILE/PNAS.2202080119.SD03.XLSX

Gomez-Navarro, N., Melero, A., Li, X. H., Boulanger, J., Kukulski, W., & Miller, E. A. (2020). Cargo crowding contributes to sorting stringency in COPII vesicles. *Journal of Cell Biology*, *219*(7). https://doi.org/10.1083/JCB.201806038

Graier, W. F., Klec, C., Madreiter-Sokolowski, C. T., Ziomek, G., Stryeck, S., Sachdev, V., Duta-Mare, M., Gottschalk, B., Depaoli, M. R., Rost, R., Hay, J., Waldeck-Weiermair, M., Kratky, D., Madl, T., & Malli, R. (2019). Presenilin-1 established ER-Ca2+ leak: A follow up on its importance for the initial insulin secretion in pancreatic islets and β-cells upon elevated glucose. *Cellular Physiology and Biochemistry*, *53*(3), 573–586. https://doi.org/10.33594/000000158

Guest, P. C., Bailyes, E. M., & Hutton, J. C. (1997). Endoplasmic reticulum Ca2+ is important for the proteolytic processing and intracellular transport of proinsulin in the pancreatic β-cell. *Biochemical Journal*, *323*(2), 445–450. https://doi.org/10.1042/bj3230445

Györke, I., & Györke, S. (1998). Regulation of the cardiac ryanodine receptor channel by luminal Ca2+ involves luminal Ca2+ sensing sites. *Biophysical Journal*, *75*(6), 2801–2810. https://doi.org/10.1016/S0006-3495(98)77723-9

Haigh, N. G., & Johnson, A. E. (2002). A new role for BiP: Closing the aqueous translocon pore during protein integration into the ER membrane. *Journal of Cell Biology*, *156*(2), 261–270. https://doi.org/10.1083/jcb.200110074

Hamada, K., & Mikoshiba, K. (2020). IP3 Receptor Plasticity Underlying Diverse Functions. In *Annual Review of Physiology* (Vol. 82, pp. 151–176). Annual Reviews. https://doi.org/10.1146/annurev-physiol-021119-034433

Hamamori, Y., Hoshijima, M., Ohmori, T., Ueda, T., & Takai, Y. (1988). Serotonin as a major serum factor inducing the phospholipase C-mediated hydrolysis of phosphoinositides in normal rat kidney cells. *Cancer Research*.

Hammadi, M., Oulidi, A., Gackière, F., Katsogiannou, M., Slomianny, C., Roudbaraki, M., Dewailly, E., Delcourt, P., Lepage, G., Lotteau, S., Ducreux, S., Prevarskaya, N., & Van Coppenolle, F. (2013). Modulation of ER stress and apoptosis by endoplasmic reticulum calcium leak via translocon during unfolded protein response: Involvement of GRP78. *FASEB Journal*, *27*(4), 1600–1609. https://doi.org/10.1096/fj.12-218875

Han, J., Back, S. H., Hur, J., Lin, Y. H., Gildersleeve, R., Shan, J., Yuan, C. L., Krokowski, D., Wang,

S., Hatzoglou, M., Kilberg, M. S., Sartor, M. A., & Kaufman, R. J. (2013). ER-stress-induced transcriptional regulation increases protein synthesis leading to cell death. *Nature Cell Biology*, *15*(5), 481–490. https://doi.org/10.1038/ncb2738

Harding, H. P., Zhang, Y., Zeng, H., Novoa, I., Lu, P. D., Calfon, M., Sadri, N., Yun, C., Popko, B., Paules, R., Stojdl, D. F., Bell, J. C., Hettmann, T., Leiden, J. M., & Ron, D. (2003). An integrated stress response regulates amino acid metabolism and resistance to oxidative stress. *Molecular Cell*, *11*(3), 619–633. https://doi.org/10.1016/S1097-2765(03)00105-9

Hattori, M., Suzuki, A. Z., Higo, T., Miyauchi, H., Michikawa, T., Nakamura, T., Inoue, T., & Mikoshiba, K. (2004). Distinct Roles of Inositol 1,4,5-Trisphosphate Receptor Types 1 and 3 in Ca2+ Signaling. *Journal of Biological Chemistry*, *279*(12), 11967–11975. https://doi.org/10.1074/jbc.M311456200

Hay, J. C., Klumperman, J., Oorschot, V., Steegmaier, M., Kuo, C. S., & Scheller, R. H. (1998). Localization, dynamics, and protein interactions reveal distinct roles for ER and Golgi SNAREs. *Journal of Cell Biology*, *141*(7), 1489–1502. https://doi.org/10.1083/jcb.141.7.1489

Haze, K., Yoshida, H., Yanagi, H., Yura, T., & Mori, K. (1999). Mammalian transcription factor ATF6 is synthesized as a transmembrane protein and activated by proteolysis in response to endoplasmic reticulum stress. *Molecular Biology of the Cell*, *10*(11), 3787–3799. https://doi.org/10.1091/mbc.10.11.3787

Helm, J. R., Bentley, M., Thorsen, K. D., Wang, T., Foltz, L., Oorschot, V., Klumperman, J., & Hay, J. C. (2014). Apoptosis-linked gene-2 (ALG-2)/Sec31 interactions regulate endoplasmic reticulum (ER)-to-Golgi transport: A potential effector pathway for luminal calcium. *Journal of Biological Chemistry*, *289*(34), 23609–23628. https://doi.org/10.1074/jbc.M114.561829

Hetz, C., Zhang, K., & Kaufman, R. J. (2020). Mechanisms, regulation and functions of the unfolded protein response. *Nature Reviews Molecular Cell Biology*, *21*(8), 421–438. https://doi.org/10.1038/s41580-020-0250-z

Hirst, J., & Robinson, M. S. (1998). Clathrin and adaptors. *Biochimica et Biophysica Acta - Molecular Cell Research*, *1404*(1–2), 173–193. https://doi.org/10.1016/S0167-4889(98)00056-1

Hollien, J., & Weissman, J. S. (2006). Decay of Endoplasmic Reticulum-Localized mRNAs During the Unfolded Protein Response. *Science*, *313*(July), 104–107. https://doi.org/10.1126/science.1129631

Hughes, H., Budnik, A., Schmidt, K., Palmer, K. J., Mantell, J., Noakes, C., Johnson, A., Carter, D. A., Verkade, P., Watson, P., & Stephens, D. J. (2009). Organisation of human ER-exit sites: Requirements for the localisation of Sec16 to transitional ER. *Journal of Cell Science*, *122*(16), 2924–2934. https://doi.org/10.1242/jcs.044032

Iwai, M., Michikawa, T., Bosanac, I., Ikura, M., & Mikoshiba, K. (2007). Molecular basis of the isoform-specific ligand-binding affinity of inositol 1,4,5-trisphosphate receptors. *Journal of*

Biological Chemistry, *282*(17), 12755–12764. https://doi.org/10.1074/jbc.M609833200

James, G., & Butt, A. M. (2002). P2Y and P2X purinoceptor mediated Ca2+ signalling in glial cell pathology in the central nervous system. *European Journal of Pharmacology*, *447*(2–3), 247–260. https://doi.org/10.1016/S0014-2999(02)01756-9

Jansen, G., Määttänen, P., Denisov, A. Y., Scarffe, L., Schade, B., Balghi, H., Dejgaard, K., Chen, L. Y., Muller, W. J., Gehring, K., & Thomas, D. Y. (2012). An interaction map of endoplasmic reticulum chaperones and foldases. *Molecular and Cellular Proteomics*, *11*(9), 710–723. https://doi.org/10.1074/mcp.M111.016550

Jin, L., Pahuja, K. B., Wickliffe, K. E., Gorur, A., Baumgärtel, C., Schekman, R., & Rape, M. (2012). Ubiquitin-dependent regulation of COPII coat size and function. *Nature*, *482*(7386), 495–500. https://doi.org/10.1038/nature10822

Kanapin, A., Batalov, S., Davis, M. J., Gough, J., Grimmond, S., Kawaji, H., Magrane, M., Matsuda, H., Schönbach, C., Teasdale, R. D., Arakawa, T., Carninci, P., Kawai, J., Hayashizaki, Y., & Yuan, Z. (2003). Mouse proteome analysis. *Genome Research*, *13*(6B), 1335–1344. https://doi.org/10.1101/GR.978703

Kerkhofs, M., Seitaj, B., Ivanova, H., Monaco, G., Bultynck, G., & Parys, J. B. (2018). Pathophysiological consequences of isoform-specific IP 3 receptor mutations. In *Biochimica et Biophysica Acta - Molecular Cell Research*. https://doi.org/10.1016/j.bbamcr.2018.06.004

Kitaura, Y., Matsumoto, S., Satoh, H., Hitomi, K., & Maki, M. (2001). Peflin and ALG-2, Members of the Penta-EF-Hand Protein Family, Form a Heterodimer That Dissociates in a Ca2+-dependent Manner. *Journal of Biological Chemistry*, *276*(17), 14053–14058. https://doi.org/10.1074/jbc.M008649200

Kitaura, Y., Satoh, H., Takahashi, H., Shibata, H., & Maki, M. (2002). Both ALG-2 and peflin, penta-EF-hand (PEF) proteins, are stabilized by dimerization through their fifth EF-hand regions. *Archives of Biochemistry and Biophysics*, *399*(1), 12–18. https://doi.org/10.1006/abbi.2001.2736

Kitaura, Y., Watanabe, M., Satoh, H., Kawai, T., Hitomi, K., & Maki, M. (1999). Peflin, a novel member of the five-EF-hand-protein family, is similar to the apoptosis-linked gene 2 (ALG-2) protein but possesses nonapeptide repeats in the N-terminal hydrophobic region. *Biochemical and Biophysical Research Communications*, *263*(1), 68–75. https://doi.org/10.1006/bbrc.1999.1189

Klein, M. C., Zimmermann, K., Schorr, S., Landini, M., Klemens, P. A. W., Altensell, J., Jung, M., Krause, E., Nguyen, D., Helms, V., Rettig, J., Fecher-Trost, C., Cavalié, A., Hoth, M., Bogeski, I., Neuhaus, H. E., Zimmermann, R., Lang, S., & Haferkamp, I. (2018). AXER is an ATP/ADP exchanger in the membrane of the endoplasmic reticulum. *Nature Communications*, *9*(1), 1–14. https://doi.org/10.1038/s41467-018-06003-9

Klumperman, J., Schweizer, A., Clausen, H., Tang, B. L., Hong, W., Oorschot, V., & Hauri, H. P.

(1998). The recycling pathway of protein ERGIC-53 and dynamics of the ER-Golgi intermediate compartment. *Journal of Cell Science*, *111*(22), 3411–3425. https://doi.org/10.1242/jcs.111.22.3411

Kuchay, S., Giorgi, C., Simoneschi, D., Pagan, J., Missiroli, S., Saraf, A., Florens, L., Washburn, M. P., Collazo-Lorduy, A., Castillo-Martin, M., Cordon-Cardo, C., Sebti, S. M., Pinton, P., & Pagano, M. (2017a). PTEN counteracts FBXL2 to promote IP3R3- and Ca 2+ -mediated apoptosis limiting tumour growth. *Nature*, *546*(7659), 554–558. https://doi.org/10.1038/nature22965

Kuchay, S., Giorgi, C., Simoneschi, D., Pagan, J., Missiroli, S., Saraf, A., Florens, L., Washburn, M. P., Collazo-Lorduy, A., Castillo-Martin, M., Cordon-Cardo, C., Sebti, S. M., Pinton, P., & Pagano, M. (2017b). PTEN counteracts FBXL2 to promote IP3R3- and Ca 2+ -mediated apoptosis limiting tumour growth. *Nature*, *546*(7659), 554–558. https://doi.org/10.1038/nature22965

Kuga, N., Sasaki, T., Takahara, Y., Matsuki, N., & Ikegaya, Y. (2011). Large-scale calcium waves traveling through astrocytic networks in vivo. *Journal of Neuroscience*, *31*(7), 2607–2614. https://doi.org/10.1523/JNEUROSCI.5319-10.2011

Kuo, I. Y., Brill, A. L., Lemos, F. O., Jiang, J. Y., Falcone, J. L., Kimmerling, E. P., Cai, Y., Dong, K., Kaplan, D. L., Wallace, D. P., Hofer, A. M., & Ehrlich, B. E. (2019). Polycystin 2 regulates mitochondrial Ca2+ signaling, bioenergetics, and dynamics through mitofusin 2. *Science Signaling*, *12*(580). https://doi.org/10.1126/scisignal.aat7397

Kuo, I. Y., DesRochers, T. M., Kimmerling, E. P., Nguyen, L., Ehrlich, B. E., & Kaplan, D. L. (2014). Cyst formation following disruption of intracellular calcium signaling. *Proceedings of the National Academy of Sciences of the United States of America*, *111*(39), 14283–14288. https://doi.org/10.1073/pnas.1412323111

Kurth-Nelson, Z. L., Mishra, A., & Newman, E. A. (2009). Spontaneous glial calcium waves in the retina develop over early adulthood. *Journal of Neuroscience*, *29*(36), 11339–11346. https://doi.org/10.1523/JNEUROSCI.2493-09.2009

la Cour, J. M., Mollerup, J., & Berchtold, M. W. (2007). ALG-2 oscillates in subcellular localization, unitemporally with calcium oscillations. *Biochemical and Biophysical Research Communications*, *353*(4), 1063–1067. https://doi.org/10.1016/j.bbrc.2006.12.143

la Cour, J. M., Schindler, A. J., Berchtold, M. W., & Schekman, R. (2013). ALG-2 Attenuates COPII Budding In Vitro and Stabilizes the Sec23/Sec31A Complex. *PLoS ONE*, *8*(9). https://doi.org/10.1371/journal.pone.0075309

La Rovere, R. M. L., Roest, G., Bultynck, G., & Parys, J. B. (2016). Intracellular Ca2+ signaling and Ca2+ microdomains in the control of cell survival, apoptosis and autophagy. *Cell Calcium*, *60*(2), 74–87. https://doi.org/10.1016/j.ceca.2016.04.005

Lamb, H. K., Mee, C., Xu, W., Liu, L., Blond, S., Cooper, A., Charles, I. G., & Hawkins, A. R. (2006). The affinity of a major Ca2+ binding site on GRP78 is differentially enhanced by ADP and

ATP. *Journal of Biological Chemistry*, *281*(13), 8796–8805. https://doi.org/10.1074/jbc.M503964200

Le Corre, S., Eyre, D., & Drummond, I. A. (2014). Modulation of the secretory pathway rescues zebrafish polycystic kidney disease pathology. *Journal of the American Society of Nephrology*, *25*(8), 1749–1759. https://doi.org/10.1681/ASN.2013101060

Lederkremer, G. Z., Cheng, Y., Petre, B. M., Vogan, E., Springer, S., Schekman, R., Walz, T., & Kirchhausen, T. (2001). Structure of the Sec23p/24p and Sec13p/31p complexes of COPII. *Proceedings of the National Academy of Sciences of the United States of America*, *98*(19), 10704–10709. https://doi.org/10.1073/pnas.191359398

Lee, M. C. S., Orci, L., Hamamoto, S., Futai, E., Ravazzola, M., & Schekman, R. (2005). Sar1p N-terminal helix initiates membrane curvature and completes the fission of a COPII vesicle. *Cell*, *122*(4), 605–617. https://doi.org/10.1016/j.cell.2005.07.025

Lefrancois, L., & Lyles, D. S. (1982). The interaction of antibody with the major surface glycoprotein of vesicular stomatitis virus I. Analysis of neutralizing epitopes with monoclonal antibodies. *Virology*, *121*(1), 157–167. https://doi.org/10.1016/0042-6822(82)90125-8

Leybaert, L., & Sanderson, M. J. (2012). Intercellular Ca2+ waves: Mechanisms and function. In *Physiological Reviews* (Vol. 92, Issue 3, pp. 1359–1392). American Physiological Society. https://doi.org/10.1152/physrev.00029.2011

Lo, K. W. H., Zhang, Q., Li, M., & Zhang, M. (1999). Apoptosis-linked gene product ALG-2 is a new member of the Calpain small subunit subfamily of Ca2+-binding proteins. *Biochemistry*, *38*(23), 7498–7508. https://doi.org/10.1021/bi990034n

Lodish, H. F., Kong, N., & Wikstrom, L. (1992). Calcium is required for folding of newly made subunits of the asialoglycoprotein receptor within the endoplasmic reticulum. *Journal of Biological Chemistry*, *267*(18), 12753–12760. https://doi.org/10.1016/s0021-9258(18)42340-x

Lowe, M., & Kreis, T. E. (1995). In vitro assembly and disassembly of coatomer. *Journal of Biological Chemistry*, *270*(52), 31364–31371. https://doi.org/10.1074/jbc.270.52.31364

Lu, P. D., Harding, H. P., & Ron, D. (2004). Translation reinitiation at alternative open reading frames regulates gene expression in an integrated stress response. *Journal of Cell Biology*, *167*(1), 27–33. https://doi.org/10.1083/jcb.200408003

Ma, W., Goldberg, E., & Goldberg, J. (2017). ER retention is imposed by COPII protein sorting and attenuated by 4-phenylbutyrate. *ELife*, *6*, 1–22. https://doi.org/10.7554/eLife.26624

Ma, W., & Goldberg, J. (2013). Rules for the recognition of dilysine retrieval motifs by coatomer. *EMBO Journal*, *32*(7), 926–937. https://doi.org/10.1038/emboj.2013.41

Madreiter-Sokolowski, C. T., Waldeck-Weiermair, M., Bourguignon, M. P., Villeneuve, N., Gottschalk, B., Klec, C., Stryeck, S., Radulovic, S., Parichatikanond, W., Frank, S., Madl, T.,

Malli, R., & Graier, W. F. (2019). Enhanced inter-compartmental Ca 2+ flux modulates mitochondrial metabolism and apoptotic threshold during aging. *Redox Biology*, *20*, 458–466. https://doi.org/10.1016/j.redox.2018.11.003

Maes, K., Missiaen, L., De Smet, P., Vanlingen, S., Callewaert, G., Parys, J. B., & De Smedt, H. (2000). Differential modulation of inositol 1,4,5,-trisphosphate receptor type 1 and type 3 by ATP. *Cell Calcium*, *27*(5), 257–267. https://doi.org/10.1054/ceca.2000.0121

Mahul-Mellier, A. L., Strappazzon, F., Petiot, A., Chatellard-Causse, C., Torch, S., Blot, B., Freeman, K., Kuhn, L., Garin, J., Verna, J. M., Fraboulet, S., & Sadoul, R. (2008). Alix and ALG-2 are involved in tumor necrosis factor receptor 1-induced cell death. *Journal of Biological Chemistry*, *283*(50), 34954–34965. https://doi.org/10.1074/jbc.M803140200

Maki, M., Kitaura, Y., Satoh, H., Ohkouchi, S., & Shibata, H. (2002). Structures, functions and molecular evolution of the penta-EF-hand Ca 2+-binding proteins. *Biochimica et Biophysica Acta - Proteins and Proteomics*, *1600*(1–2), 51–60. https://doi.org/10.1016/S1570-9639(02)00444-2

Maki, M., Takahara, T., & Shibata, H. (2016). Multifaceted roles of ALG-2 in Ca2+-regulated membrane trafficking. *International Journal of Molecular Sciences*, *17*(9), 1–23. https://doi.org/10.3390/ijms17091401

Mancias, J. D., & Goldberg, J. (2008). Structural basis of cargo membrane protein discrimination by the human COPII coat machinery. *EMBO Journal*, *27*(21), 2918–2928. https://doi.org/10.1038/emboj.2008.208

Mangla, A., Guerra, M. T., & Nathanson, M. H. (2020). Type 3 inositol 1,4,5-trisphosphate receptor: A calcium channel for all seasons. In *Cell Calcium* (Vol. 85, p. 102132). Elsevier Ltd. https://doi.org/10.1016/j.ceca.2019.102132

Matsuoka, K., Orci, L., Amherdt, M., Bednarek, S. Y., Hamamoto, S., Schekman, R., & Yeung, T. (1998). COPII-coated vesicle formation reconstituted with purified coat proteins and chemically defined liposomes. *Cell*, *93*(2), 263–275. https://doi.org/10.1016/S0092-8674(00)81577-9

McGourty, C. A., Akopian, D., Walsh, C., Gorur, A., Werner, A., Schekman, R., Bautista, D., & Rape, M. (2016). Regulation of the CUL3 Ubiquitin Ligase by a Calcium-Dependent Co-adaptor. *Cell*, *167*(2), 525-538.e14. https://doi.org/10.1016/j.cell.2016.09.026

Mendes, C. C. P., Gomes, D. A., Thompson, M., Souto, N. C., Goes, T. S., Goes, A. M., Rodrigues, M. A., Gomez, M. V., Nathanson, M. H., & Leite, M. F. (2005). The type III inositol 1,4,5-trisphosphate receptor preferentially transmits apoptotic Ca2+ signals into mitochondria. *Journal of Biological Chemistry*, *280*(49), 40892–40900. https://doi.org/10.1074/jbc.M506623200

Mezzacasa, A., & Helenius, A. (2002). The transitional ER defines a boundary for quality control in the secretion of tsO45 VSV glycoprotein. *Traffic*, *3*(11), 833–849. https://doi.org/10.1034/j.1600-0854.2002.31108.x

Miller, E. A., Beilharz, T. H., Malkus, P. N., Lee, M. C. S., Hamamoto, S., Orci, L., & Schekman, R. (2003). Multiple cargo binding sites on the COPII subunit Sec24p ensure capture of diverse membrane proteins into transport vesicles. *Cell*, *114*(4), 497–509. https://doi.org/10.1016/S0092-8674(03)00609-3

Miller, E. A., Liu, Y., Barlowe, C., & Schekman, R. (2005). ER-Golgi Transport Defects Are Associated with Mutations in the Sed5p-binding Domain of the COPII Coat Subunit, Sec24p. *Molecular Biology of the Cell*, *16*(August), 3719–3726. https://doi.org/10.1091/mbc.E05

Miller, E., Antonny, B., Hamamoto, S., & Schekman, R. (2002). Cargo selection into COPII vesicles is driven by the Sec24p subunit. *EMBO Journal*, *21*(22), 6105–6113. https://doi.org/10.1093/emboj/cdf605

Moravec, R., Conger, K. K., D'Souza, R., Allison, A. B., & Casanova, J. E. (2012). BRAG2/GEP100/IQSec1 interacts with clathrin and regulates α5β1 integrin endocytosis through activation of ADP ribosylation factor 5 (Arf5). *Journal of Biological Chemistry*, *287*(37), 31138–31147. https://doi.org/10.1074/jbc.M112.383117

Morel, J. L., Fritz, N., Lavie, J. L., & Mironneau, J. (2003). Crucial role of type 2 inositol 1,4,5-trisphosphate receptors for acetylcholine-induced Ca2+ oscillations in vascular myocytes. *Arteriosclerosis, Thrombosis, and Vascular Biology*, *23*(9), 1567–1575. https://doi.org/10.1161/01.ATV.0000089013.82552.5D

Moretti, T., Kim, K., Tuladhar, A., & Kim, J. (2023). KLHL12 can form large COPII structures in the absence of CUL3 neddylation. *Molecular Biology of the Cell*, *34*(3), 1–10. https://doi.org/10.1091/mbc.E22-08-0383

Mossessova, E., Bickford, L. C., & Goldberg, J. (2003). SNARE selectivity of the COPII coat. *Cell*, *114*(4), 483–495. https://doi.org/10.1016/S0092-8674(03)00608-1

Mound, A., Vautrin-Glabik, A., Foulon, A., Botia, B., Hague, F., Parys, J. B., Ouadid-Ahidouch, H., & Rodat-Despoix, L. (2017). Downregulation of type 3 inositol (1,4,5)-trisphosphate receptor decreases breast cancer cell migration through an oscillatory Ca2+ signal. *Oncotarget*, *8*(42), 72324–72341. https://doi.org/10.18632/oncotarget.20327

Moussalli, M., Pipe, S. W., Hauri, H. P., Nichols, W. C., Ginsburg, D., & Kaufman, R. J. (1999). Mannose-dependent endoplasmic reticulum (ER)-Golgi intermediate compartment-53-mediated ER to Golgi trafficking of coagulation factors V and VIII. *Journal of Biological Chemistry*, *274*(46), 32539–32542. https://doi.org/10.1074/jbc.274.46.32539

Müller, M., Cheung, K. H., & Foskett, J. K. (2011). Enhanced ROS generation mediated by alzheimer's disease presenilin regulation of InsP3R Ca2+ signaling. *Antioxidants and Redox Signaling*, *14*(7), 1225–1235. https://doi.org/10.1089/ars.2010.3421

Nelson, O., Supnet, C., Tolia, A., Horre, K., De Strooper, B., & Bezprozvanny, I. (2011). Mutagenesis mapping of the presenilin 1 calcium leak conductance pore. *Journal of Biological Chemistry*, *286*(25), 22339–22347. https://doi.org/10.1074/jbc.M111.243063

Noble, A. J., Zhang, Q., O'Donnell, J., Hariri, H., Bhattacharya, N., Marshall, A. G., & Stagg, S. M. (2013). A pseudoatomic model of the COPII cage obtained from cryo-electron microscopy and mass spectrometry. *Nature Structural and Molecular Biology*, *20*(2), 167–173. https://doi.org/10.1038/nsmb.2467

Nyfeler, B., Reiterer, V., Wendeler, M. W., Stefan, E., Zhang, B., Michnick, S. W., & Hauri, H. P. (2008). Identification of ERGIC-53 as an intracellular transport receptor of α1-antitrypsin. *Journal of Cell Biology*, *180*(4), 705–712. https://doi.org/10.1083/jcb.200709100

Nyfeler, B., Zhang, B., Ginsburg, D., Kaufman, R. J., & Hauri, H. P. (2006). Cargo selectivity of the ERGIC-53/MCFD2 transport receptor complex. *Traffic*, *7*(11), 1473–1481. https://doi.org/10.1111/j.1600-0854.2006.00483.x

Omari, S., Makareeva, E., Roberts-Pilgrim, A., Mirigian, L., Jarnik, M., Ott, C., Lippincott-Schwartz, J., & Leikin, S. (2018). Noncanonical autophagy at ER exit sites regulates procollagen turnover. *Proceedings of the National Academy of Sciences*, *115*(43). https://doi.org/10.1073/pnas.1814552115

Ooi, C. E., Dell'Angelica, E. C., & Bonifacino, J. S. (1998). ADP-ribosylation factor 1 (ARF1) regulates recruitment of the AP-3 adaptor complex to membranes. *Journal of Cell Biology*, *142*(2), 391–402. https://doi.org/10.1083/jcb.142.2.391

Padhy, B., Xie, J., Wang, R., Lin, F., & Huang, C. L. (2022). Channel Function of Polycystin-2 in the Endoplasmic Reticulum Protects against Autosomal Dominant Polycystic Kidney Disease. *Journal of the American Society of Nephrology*, *33*(8), 1501–1516. https://doi.org/10.1681/ASN.2022010053

Palmer, A. E., Giacomello, M., Kortemme, T., Hires, S. A., Lev-Ram, V., Baker, D., & Tsien, R. Y. (2006). Ca2+ Indicators Based on Computationally Redesigned Calmodulin-Peptide Pairs. *Chemistry and Biology*, *13*(5), 521–530. https://doi.org/10.1016/j.chembiol.2006.03.007

Palmer, A. E., Jin, C., Reed, J. C., & Tsien, R. Y. (2004). Bcl-2-mediated alterations in endoplasmic reticulum Ca2+ analyzed with an improved genetically encoded fluorescent sensor. *Proceedings of the National Academy of Sciences of the United States of America*, *101*(50), 17404–17409. https://doi.org/10.1073/pnas.0408030101

Palmer, A. E., & Tsien, R. Y. (2006). Measuring calcium signaling using genetically targetable fluorescent indicators. *Nature Protocols*, *1*, 1057–1065. https://doi.org/10.1038/nprot.2006.172

Pantazopoulou, A., & Glick, B. S. (2019). A kinetic view of membrane traffic pathways can transcend the classical view of Golgi compartments. *Frontiers in Cell and Developmental Biology*, *7*(JULY), 1–12. https://doi.org/10.3389/fcell.2019.00153

Pearse, B. M. F. (1975). Coated vesicles from pig brain: Purification and biochemical characterization. *Journal of Molecular Biology*, *97*(1), 93–98. https://doi.org/10.1016/S0022-2836(75)80024-6

Peden, A. A., Oorschot, V., Hesser, B. A., Austin, C. D., Scheller, R. H., & Klumperman, J. (2004).

Localization of the AP-3 adaptor complex defines a novel endosomal exit site for lysosomal membrane proteins. *Journal of Cell Biology*, *164*(7), 1065–1076. https://doi.org/10.1083/jcb.200311064

Periasamy, M., & Kalyanasundaram, A. (2007). SERCA pump isoforms: Their role in calcium transport and disease. *Muscle and Nerve*, *35*(4), 430–442. https://doi.org/10.1002/mus.20745

Phillipson, B. A., Pimpl, P., DaSilva, L. L. P., Crofts, A. J., Taylor, J. P., Movafeghi, A., Robinson, D. G., & Denecke, J. (2001). Secretory bulk flow of soluble proteins is efficient and COPII dependent. *Plant Cell*, *13*(9), 2005–2020. https://doi.org/10.1105/tpc.13.9.2005

Pobre, K. F. R., Poet, G. J., & Hendershot, L. M. (2019). The endoplasmic reticulum (ER) chaperone BiP is a master regulator of ER functions: Getting by with a little help from ERdj friends. *Journal of Biological Chemistry*, *294*(6), 2098–2108. https://doi.org/10.1074/jbc.REV118.002804

Porat, A., & Elazar, Z. (2000). Regulation of intra-Golgi membrane transport by calcium. *Journal of Biological Chemistry*, *275*(38), 29233–29237. https://doi.org/10.1074/jbc.M005316200

Preissler, S., Rato, C., Yan, Y., Perera, L. A., Czako, A., & Ron, D. (2020). Calcium depletion challenges endoplasmic reticulum proteostasis by destabilising bip-substrate complexes. *ELife*, *9*, 1–36. https://doi.org/10.7554/ELIFE.62601

Presley, J. F., Ward, T. H., Pfeifer, A. C., Siggia, E. D., Phair, R. D., & Lippincott-Schwartz, J. (2002). Dissection of COPI and Arf1 dynamics in vivo and role in Golgi membrane transport. *Nature*, *417*(6885), 187–193. https://doi.org/10.1038/417187a

Prole, D. L., & Taylor, C. W. (2016). Inositol 1,4,5-trisphosphate receptors and their protein partners as signalling hubs. *Journal of Physiology*, *594*(11), 2849–2866. https://doi.org/10.1113/JP271139

Rao, R. V., Poksay, K. S., Castro-Obregon, S., Schilling, B., Row, R. H., Del Rio, G., Gibson, B. W., Ellerby, H. M., & Bredesen, D. E. (2004). Molecular Components of a Cell Death Pathway Activated by Endoplasmic Reticulum Stress. *Journal of Biological Chemistry*, *279*(1), 177–187. https://doi.org/10.1074/jbc.M304490200

Rao, Y., Bian, C., Yuan, C., Li, Y., Chen, L., Ye, X., Huang, Z., & Huang, M. (2006). An open conformation of switch I revealed by Sar1-GDP crystal structure at low Mg2+. *Biochemical and Biophysical Research Communications*, *348*(3), 908–915. https://doi.org/10.1016/j.bbrc.2006.07.148

Rayl, M., Truitt, M., Held, A., Sargeant, J., Thorsen, K., & Hay, J. C. (2016). Penta-EF-hand protein peflin is a negative regulator of ER-to-Golgi transport. *PLoS ONE*, *11*(6). https://doi.org/10.1371/journal.pone.0157227

Régimbald-Dumas, Y., Frégeau, M. O., & Guillemette, G. (2011). Mammalian target of rapamycin (mTOR) phosphorylates inositol 1,4,5-trisphosphate receptor type 2 and increases its Ca2+ release activity. *Cellular Signalling*, *23*(1), 71–79.

https://doi.org/10.1016/j.cellsig.2010.08.005

Ren, X., Farías, G. G., Canagarajah, B. J., Bonifacino, J. S., & Hurley, J. H. (2013). Structural basis for recruitment and activation of the AP-1 clathrin adaptor complex by Arf1. *Cell*, *152*(4), 755–767. https://doi.org/10.1016/j.cell.2012.12.042

Rivera, V. M., Wang, X., Wardwell, S., Courage, N. L., Volchuk, A., Keenan, T., Holt, D. A., Gilman, M., Orci, L., Cerasoli, F., Rothman, J. E., & Clackson, T. (2000). Regulation of protein secretion through controlled aggregation in the endoplasmic reticulum. *Science*, *287*(5454), 826–830. https://doi.org/10.1126/science.287.5454.826

Rizzuto, R., De Stefani, D., Raffaello, A., & Mammucari, C. (2012). Mitochondria as sensors and regulators of calcium signalling. *Nature Reviews Molecular Cell Biology*, *13*, 566–578. https://doi.org/10.1038/nrm3412

Ron, D., & Walter, P. (2007). Signal integration in the endoplasmic reticulum unfolded protein response. *Nature Reviews Molecular Cell Biology*, *8*(7), 519–529. https://doi.org/10.1038/nrm2199

Roth, T. F., & Porter, K. R. (1964). Yolk Protein Uptake in the Oocyte of the Mosquito Aedes Aegypti. L. *The Journal of Cell Biology*, *20*, 313–332. https://doi.org/10.1083/jcb.20.2.313

Saito, A., & Imaizumi, K. (2018). Unfolded protein response-dependent communication and contact among endoplasmic reticulum, mitochondria, and plasma membrane. *International Journal of Molecular Sciences*, *19*(10). https://doi.org/10.3390/ijms19103215

Sammels, E., Devogelaere, B., Mekahli, D., Bultynck, G., Missiaen, L., Parys, J. B., Cai, Y., Somlo, S., & De Smedt, H. (2010). Polycystin-2 activation by inositol 1,4,5-trisphosphate-induced Ca 2+ release requires its direct association with the inositol 1,4,5-trisphosphate receptor in a signaling microdomain. *Journal of Biological Chemistry*, *285*(24), 18794–18805. https://doi.org/10.1074/jbc.M109.090662

Sans, M. D., Kimball, S. R., & Williams, J. A. (2002). Effect of CCK and intracellular calcium to regulate eIF2B and protein synthesis in rat pancreatic acinar cells. *American Journal of Physiology - Gastrointestinal and Liver Physiology*, *282*(2 45-2), 267–276. https://doi.org/10.1152/ajpgi.00274.2001

Sargeant, J., & Hay, J. C. (2022). Ca2+ regulation of constitutive vesicle trafficking. *Faculty Reviews*, *11*(6). https://doi.org/10.12703/r/11-6

Sargeant, J., Seiler, D. K., Costain, T., Madreiter-Sokolowski, C. T., Gordon, D. E., Peden, A. A., Malli, R., Graier, W. F., & Hay, J. C. (2021). ALG-2 and peflin regulate COPII targeting and secretion in response to calcium signaling. *Journal of Biological Chemistry*, *297*(6). https://doi.org/10.1016/j.jbc.2021.101393

Sato, K., & Nakano, A. (2005). Dissection of COPII subunit-cargo assembly and disassembly kinetics during Sar1p-GTP hydrolysis. *Nature Structural and Molecular Biology*, *12*(2), 167–174. https://doi.org/10.1038/nsmb893

Schäuble, N., Lang, S., Jung, M., Cappel, S., Schorr, S., Ulucan, Ö., Linxweiler, J., Dudek, J., Blum, R., Helms, V., Paton, A. W., Paton, J. C., Cavalié, A., & Zimmermann, R. (2012). BiP-mediated closing of the Sec61 channel limits Ca 2+ leakage from the ER. *EMBO Journal*, *31*(15), 3282–3296. https://doi.org/10.1038/emboj.2012.189

Seiler, D. K., & Hay, J. C. (2022). Genetically encoded fluorescent tools: Shining a little light on ER-to-Golgi transport. *Free Radical Biology and Medicine*, *183*(December 2021), 14–24. https://doi.org/10.1016/j.freeradbiomed.2022.03.004

Shaywitz, D. A., Espenshade, P. J., Gimeno, R. E., & Kaiser, C. A. (1997). COPII subunit interactions in the assembly of the vesicle coat. *Journal of Biological Chemistry*, *272*(41), 25413–25416. https://doi.org/10.1074/jbc.272.41.25413

Shibao, K., Fiedler, M. J., Nagata, J., Minagawa, N., Hirata, K., Nakayama, Y., Iwakiri, Y., Nathanson, M. H., & Yamaguchi, K. (2010). The type III inositol 1,4,5-trisphosphate receptor is associated with aggressiveness of colorectal carcinoma. *Cell Calcium*, *48*(6), 315–323. https://doi.org/10.1016/j.ceca.2010.09.005

Shibata, H. (2019). Adaptor functions of the Ca2+-binding protein ALG-2 in protein transport from the endoplasmic reticulum. *Bioscience, Biotechnology and Biochemistry*, *83*(1), 20–32. https://doi.org/10.1080/09168451.2018.1525274

Shibata, H., Inuzuka, T., Yoshida, H., Sugiura, H., Wada, D., & Maki, M. (2010). The ALG-2 binding site in Sec31A influences the retention kinetics of Sec31A at the endoplasmic reticulum exit sites as revealed by live-cell time-lapse imaging. *Bioscience, Biotechnology and Biochemistry*, *74*(9), 1819–1826. https://doi.org/10.1271/bbb.100215

Shibata, H., Kanadome, T., Sugiura, H., Yokoyama, T., Yamamuro, M., Moss, S. E., & Maki, M. (2015). A new role for annexin A11 in the early secretory pathway via stabilizing Sec31A protein at the endoplasmic reticulum exit sites (ERES). *Journal of Biological Chemistry*, *290*(8), 4981–4993. https://doi.org/10.1074/jbc.M114.592089

Shibata, H., Suzuki, H., Yoshida, H., & Maki, M. (2007). ALG-2 directly binds Sec31A and localizes at endoplasmic reticulum exit sites in a Ca2+-dependent manner. *Biochemical and Biophysical Research Communications*, *353*(3), 756–763. https://doi.org/10.1016/j.bbrc.2006.12.101

Skowronek, M. H., Hendershot, L. M., & Haas, I. G. (1998). The variable domain of nonassembled Ig light chains determines both their half-life and binding to the chaperone BiP. *Proceedings of the National Academy of Sciences of the United States of America*, *95*(4), 1574–1578. https://doi.org/10.1073/pnas.95.4.1574

Stagg, S. M., Gürkan, C., Fowler, D. M., LaPointe, P., Foss, T. R., Potter, C. S., Carragher, B., & Balch, W. E. (2006). Structure of the Sec13/31 COPII coat cage. *Nature*, *439*(7073), 234–238. https://doi.org/10.1038/nature04339

Stankewich, M. C., Stabach, P. R., & Morrow, J. S. (2006). Human Sec31B: A family of new mammalian orthologues of yeast Sec31p that associate with the COPII coat. *Journal of Cell*

Science, *119*(5), 958–969. https://doi.org/10.1242/jcs.02751

Stutzmann, G. E., & Mattson, M. P. (2011). Endoplasmic reticulum Ca 2+ handling in excitable cells in health and disease. *Pharmacological Reviews*, *63*(3), 700–727. https://doi.org/10.1124/pr.110.003814

Sun, Z., & Brodsky, J. L. (2019). Protein quality control in the secretory pathway. *Journal of Cell Biology*, *218*(10), 3171–3187. https://doi.org/10.1083/jcb.201906047

Suzuki, K., Dashzeveg, N., Lu, Z. G., Taira, N., Miki, Y., & Yoshida, K. (2012). Programmed cell death 6, a novel p53-responsive gene, targets to the nucleus in the apoptotic response to DNA damage. *Cancer Science*, *103*(10), 1788–1794. https://doi.org/10.1111/j.1349-7006.2012.02362.x

Sweadner, K. J., & Donnet, C. (2001). Structural similarities of Na,K-ATPase and SERCA, the Ca2+-ATPase of the sarcoplasmic reticulum. *The Biochemical Journal*, *356*(4), 685–704. https://doi.org/10.1042/0264-6021:3560685

Szabadkai, G., Bianchi, K., Várnai, P., De Stefani, D., Wieckowski, M. R., Cavagna, D., Nagy, A. I., Balla, T., & Rizzuto, R. (2006). Chaperone-mediated coupling of endoplasmic reticulum and mitochondrial Ca2+ channels. *Journal of Cell Biology*, *175*(6), 901–911. https://doi.org/10.1083/jcb.200608073

Szatkowski, C., Parys, J. B., Ouadid-Ahidouch, H., & Matifat, F. (2010). Inositol 1,4,5-trisphosphate-induced Ca2+signalling is involved in estradiol-induced breast cancer epithelial cell growth. *Molecular Cancer*, *9*. https://doi.org/10.1186/1476-4598-9-156

Takada, S. H., Ikebara, J. M., de Sousa, E., Cardoso, D. S., Resende, R. R., Ulrich, H., Rückl, M., Rüdiger, S., & Kihara, A. H. (2017). Determining the Roles of Inositol Trisphosphate Receptors in Neurodegeneration: Interdisciplinary Perspectives on a Complex Topic. In *Molecular Neurobiology* (Vol. 54, Issue 9, pp. 6870–6884). Humana Press Inc. https://doi.org/10.1007/s12035-016-0205-8

Takida, S., Maeda, Y., & Kinoshita, T. (2008). Mammalian GPI-anchored proteins require p24 proteins for their efficient transport from the ER to the plasma membrane. *Biochemical Journal*, *409*(2), 555–562. https://doi.org/10.1042/BJ20070234

Tarabykina, S., Møller, A. L., Durussel, I., Cox, J., & Berchtold, M. W. (2000). Two forms of the apoptosis-linked protein ALG-2 with different Ca2+ affinities and target recognition. *Journal of Biological Chemistry*, *275*(14), 10514–10518. https://doi.org/10.1074/jbc.275.14.10514

Thayanidhi, N., Helm, J. R., Nycz, D. C., Bentley, M., Liang, Y., & Hay, J. C. (2010). α-Synuclein Delays Endoplasmic Reticulum (ER)-to-Golgi Transport in Mammalian Cells by Antagonizing ER/Golgi SNAREs. *Molecular Biology of the Cell*, *21*, 1850–1863. https://doi.org/10.1091/mbc.e09-09-0801

Thillaiappan, N. B., Chakraborty, P., Hasan, G., & Taylor, C. W. (2019). IP3 receptors and Ca2+ entry. In *Biochimica et Biophysica Acta - Molecular Cell Research* (Vol. 1866, Issue 7, pp.

1092–1100). Elsevier B.V. https://doi.org/10.1016/j.bbamcr.2018.11.007

Thor, F., Gautschi, M., Geiger, R., & Helenius, A. (2009). Bulk flow revisited: Transport of a soluble protein in the secretory pathway. *Traffic*, *10*(12), 1819–1830. https://doi.org/10.1111/j.1600-0854.2009.00989.x

Tovey, S. C., De Smet, P., Lipp, P., Thomas, D., Young, K. W., Missiaen, L., De Smedt, H., Parys, J. B., Berridge, M. J., Thuring, J., Holmes, A., & Bootman, D. (2001). Calcium puffs are genetic InsP3-activated elementary calcium signals and are downregulated by prolonged hormonal stimulation to inhibit cellular calcium responses. *Journal of Cell Science*, *114*(22), 3979–3989. https://doi.org/10.1242/jcs.114.22.3979

Townsley, F. M., Wilson, D. W., & Pelham, H. R. B. (1993). Mutational analysis of the human KDEL receptor: Distinct structural requirements for Golgi retention, ligand binding and retrograde transport. *EMBO Journal*, *12*(7), 2821–2829. https://doi.org/10.1002/j.1460-2075.1993.tb05943.x

Van Coppenolle, F., Vanden Abeele, F., Slomianny, C., Flourakis, M., Hesketh, J., Dewailly, E., & Prevarskaya, N. (2004). Ribosome-translocon complex mediates calcium leakage from endoplasmic reticulum stores. *Journal of Cell Science*, *117*(18), 4135–4142. https://doi.org/10.1242/jcs.01274

Vassilakos, A., Michalak, M., Lehrman, M. A., & Williams, D. B. (1998). Oligosaccharide binding characteristics of the molecular chaperones calnexin and calreticulin. *Biochemistry*, *37*(10), 3480–3490. https://doi.org/10.1021/bi972465g

Vishnu, N., Khan, M. J., Karsten, F., Groschner, L. N., Waldeck-Weiermair, M., Rost, R., Hallström, S., Imamura, H., Graier, W. F., & Malli, R. (2014). ATP increases within the lumen of the endoplasmic reticulum upon intracellular Ca2+ release. *Molecular Biology of the Cell*, *25*(3), 368–379. https://doi.org/10.1091/mbc.E13-07-0433

Wang, M., & Kaufman, R. J. (2016). Protein misfolding in the endoplasmic reticulum as a conduit to human disease. In *Nature* (Vol. 529, Issue 7586, pp. 326–335). Nature Publishing Group. https://doi.org/10.1038/nature17041

Wang, T., Grabski, R., Sztul, E., & Hay, J. C. (2015). p115-SNARE Interactions: A Dynamic Cycle of p115 Binding Monomeric SNARE Motifs and Releasing Assembled Bundles. *Traffic*, *16*(2), 148–171. https://doi.org/10.1111/tra.12242

Watson, P., Townley, A. K., Koka, P., Palmer, K. J., & Stephens, D. J. (2006). Sec16 defines endoplasmic reticulum exit sites and is required for secretory cargo export in mammalian cells. *Traffic*, *7*(12), 1678–1687. https://doi.org/10.1111/j.1600-0854.2006.00493.x

Weerachayaphorn, J., Amaya, M. J., Spirli, C., Chansela, P., Mitchell-Richards, K. A., Ananthanarayanan, M., & Nathanson, M. H. (2015). Nuclear Factor, Erythroid 2-Like 2 Regulates Expression of Type 3 Inositol 1,4,5-Trisphosphate Receptor and Calcium Signaling in Cholangiocytes. *Gastroenterology*, *149*(1), 211-222.e10. https://doi.org/10.1053/j.gastro.2015.03.014

Weigel, A. V., Chang, C. L., Shtengel, G., Xu, C. S., Hoffman, D. P., Freeman, M., Iyer, N., Aaron, J., Khuon, S., Bogovic, J., Qiu, W., Hess, H. F., & Lippincott-Schwartz, J. (2021). ER-to-Golgi protein delivery through an interwoven, tubular network extending from ER. *Cell*, *184*(9), 2412-2429.e16. https://doi.org/10.1016/j.cell.2021.03.035

Weissman, J. T., Plutner, H., & Balch, W. E. (2001). The mammalian guanine nucleotide exchange factor mSec12 is essential for activation of the Sar1 GTPase directing endoplasmic reticulum export. *Traffic*, *2*(7), 465–475. https://doi.org/10.1034/j.1600-0854.2001.20704.x

Weissman, T. A., Riquelme, P. A., Ivic, L., Flint, A. C., & Kriegstein, A. R. (2004). Calcium waves propagate through radial glial cells and modulate proliferation in the developing neocortex. *Neuron*, *43*(5), 647–661. https://doi.org/10.1016/j.neuron.2004.08.015

Welch, W. J., Garrels, J. I., Thomas, G. P., Lin, J. J., & Feramisco, J. R. (1983). Biochemical characterization of the mammalian stress proteins and identification of two stress proteins as glucose- and Ca2+-ionophore-regulated proteins. *Journal of Biological Chemistry*, *258*(11), 7102–7111. https://doi.org/10.1016/s0021-9258(18)32338-x

Wiseman, R. L., Mesgarzadeh, J. S., & Hendershot, L. M. (2022). Reshaping endoplasmic reticulum quality control through the unfolded protein response. *Molecular Cell*, *82*(8), 1477–1491. https://doi.org/10.1016/j.molcel.2022.03.025

Wojcikiewicz, R. J. H. (1995). Type I, II, and III inositol 1,4,5-trisphosphate receptors are unequally susceptible to down-regulation and are expressed in markedly different proportions in different cell types. *Journal of Biological Chemistry*, *270*(19), 11678–11683. https://doi.org/10.1074/jbc.270.19.11678

Wong, W. L., Brostrom, M. A., Kuznetsov, G., Gmitter-Yellen, D., & Brostrom, C. O. (1993). Inhibition of protein synthesis and early protein processing by thapsigargin in cultured cells. *Biochemical Journal*, *289*(1), 71–79. https://doi.org/10.1042/bj2890071

Xu, D., & Hay, J. C. (2004). Reconstitution of COPII vesicle fusion to generate a pre-Golgi intermediate compartment. *Journal of Cell Biology*, *167*(6), 997–1003. https://doi.org/10.1083/jcb.200408135

Yamasaki, A., Tani, K., Tmamoto, A., Kitamura, N., Komada, M., Yamamoto, A., Kitamura, N., & Komada, M. (2006). The Ca2+-binding Protein ALG-2 Is Recruited to Endoplasmic Reticulum Exit Sites by Sec31A and Stabilizes the Localization of Sec31A. *Molecular Biology of the Cell*, *17*(11), 4876–4887. https://doi.org/10.1091/mbc.E06

Yarwood, R., Hellicar, J., Woodman, P. G., & Lowe, M. (2020). Membrane trafficking in health and disease. *Disease Models and Mechanisms*, *13*(4). https://doi.org/10.1242/dmm.043448

Yi, M., Weaver, D., & Hajnóczky, G. (2004). Control of mitochondrial motility and distribution by the calcium signal: A homeostatic circuit. *Journal of Cell Biology*, *167*(4), 661–672. https://doi.org/10.1083/jcb.200406038

Yong, J., Bischof, H., Burgstaller, S., Siirin, M., Murphy, A., Malli, R., & Kaufman, R. J. (2019). Mitochondria supply ATP to the ER through a mechanism antagonized by cytosolic Ca2+. *ELife*, *8*. https://doi.org/10.7554/eLife.49682

Yoshihisa, T., Barlowe, C., & Schekman, R. (1993). Requirement for a GTPase-activating protein in vesicle budding from the endoplasmic reticulum. *Science*, *259*(5100), 1466–1468. https://doi.org/10.1126/science.8451644

Yu, X., Breitman, M., & Goldberg, J. (2012). A Structure-based mechanism for Arf1-dependent recruitment of coatomer to membranes. *Cell*, *148*(3), 530–542. https://doi.org/10.1016/j.cell.2012.01.015

Zanetti, G., Pahuja, K. B., Studer, S., Shim, S., & Schekman, R. (2012). COPII and the regulation of protein sorting in mammals. *Nature Cell Biology*, *14*(1), 20–28. https://doi.org/10.1038/ncb2390

Zerangue, N., Schwappach, B., Yuh, N. J., & Lily, Y. J. (1999). A new ER trafficking signal regulates the subunit stoichiometry of plasma membrane K(ATP) channels. *Neuron*, *22*(3), 537–548. https://doi.org/10.1016/S0896-6273(00)80708-4

Zhang, S., Fritz, N., Ibarra, C., & Uhlén, P. (2011a). Inositol 1,4,5-trisphosphate receptor subtype-specific regulation of calcium oscillations. *Neurochemical Research*, *36*(7), 1175–1185. https://doi.org/10.1007/s11064-011-0457-7

Zhang, S., Fritz, N., Ibarra, C., & Uhlén, P. (2011b). Inositol 1,4,5-trisphosphate receptor subtype-specific regulation of calcium oscillations. In *Neurochemical Research* (Vol. 36, Issue 7, pp. 1175–1185). Neurochem Res. https://doi.org/10.1007/s11064-011-0457-7

Zhou, J., Liu, C. Y., Back, S. H., Clark, R. L., Peisach, D., Xu, Z., & Kaufman, R. J. (2006). The crystal structure of human IRE1 luminal domain reveals a conserved dimerization interface required for activation of the unfolded protein response. *Proceedings of the National Academy of Sciences of the United States of America*, *103*(39), 14343–14348. https://doi.org/10.1073/pnas.0606480103

Zimmermann, R., & Lang, S. (2020). A Little AXER ABC: ATP, BiP, and Calcium Form a Triumvirate Orchestrating Energy Homeostasis of the Endoplasmic Reticulum. *Contact*, *3*. https://doi.org/10.1177/2515256420926795

Zlatic, S. A., Grossniklaus, E. J., Ryder, P. V., Salazar, G., Mattheyses, A. L., Peden, A. A., & Faundez, V. (2013). Chemical-genetic disruption of clathrin function spares adaptor complex 3-dependent endosome vesicle biogenesis. *Molecular Biology of the Cell*, *24*(15), 2378–2388. https://doi.org/10.1091/mbc.E12-12-0860